An attempt to study ion outflow in the polar cusp with conjugated measurements from EISCAT and Cluster

Andreas Quamme Nielsen

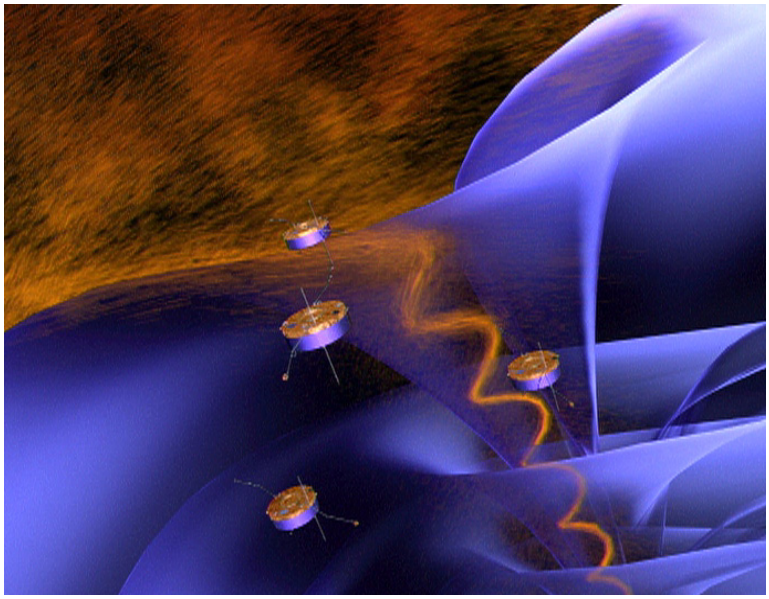

Thesis submitted for the degree of Master of Science
Department of Physics,
University of Oslo
November 2005

Cover picture:
Artist's impression of the Cluster spacecraft crossing the polar cusp
Found at ESA's Cluster web-pages (downloaded the 22. of November):
- http://clusterlaunch.esa.int/science-e/www/object/index.cfm?fobjectid=26142

“The most exciting phrase to hear in science, the one that heralds new discoveries, is not ‘Eureka!’, but ‘That’s funny...’”

Isaac Asimov

Abstract

This thesis sought to find ion outflow as measured by Cluster in the polar cusp, in conjunction with ionospheric upflow events observed by the EISCAT radars outside Longyearbyen on Svalbard (ESR). The constraints placed on the identification of these events proved to narrow the total amount of data. First of all, Cluster's magnetic footprint had to pass close by Svalbard's location. Then, one needed the radars to measure dynamic plasma parameters, which could be interpreted as upflow events. To complete the set, Cluster would also have to observe outflowing O+ particles to confirm that their origin was the ionosphere. After finishing the preliminary search for these data, one pass through the cusp contained data which showed some promise.

The outflow event observed by Cluster, could be traced back to an upflow event seen by the ESR, but with a time delay of about 35 minutes. A possible cause for these incidents was found to be a sudden pressure increase in the solar wind occurring at about 10:00 UT. However, to trace a phenomenon through a turbulent region such as the polar cusp across a time span of uptil 45 minutes, cannot be done without admitting that there might be other factors responsible than the ones specifically studied.

A significant perturbation of the total magnetic field strength was also investigated with the curlometer technique. This yielded magnetic field aligned currents running both parallel and anti-parallel, as one should expect from a flux tube, more specifically a flux transfer event (FTE). The ExB-velocity was used to identify the tube's direction of movement, and some investigation of how this velocity would map to the ionosphere was also performed.

Acknowledgements

I would like to thank my two supervisors, Jøran Moen and Arne Pedersen, for always providing insightful information and useful facts. It has been reassuring to have access to all their technical knowledge throughout this study. So, thank you for always giving me a way out every time I was stuck.

I would also like to thank Bjørn Lybekk. He has always had time to help out with all sorts of computer problems and data acquisition procedures. For other various computer issues, Espen Trondsen has been present to lend a hand. Thank you both.

I have also received technical information and data from the ESR and Cluster satellites from Kjellmar Oksavik and Stein Haaland, respectively, which has proved to be invaluable. Again, thank you both.

If it had not been for Ellen Osmundsen, I would probably still have a hard time understanding any of the MATLAB programming in this thesis. Thank you for always wanting to help out, and for many interesting discussions. Also, I want to thank all the students and employees at the research group for creating such an excellent working environment.

My family has always provided support to my interests, and this has been especially recognized throughout my years at the university. Thank you for always being interested, and for motivating me throughout my studies.

Some people has said that the university can be a lonely place. Fortunately, I cannot relate to that. I would like to thank all my friends here who have set up a social structure which will be missed. I hope to see you all at Helga Eng for many Fridays to come.

To complete this thesis, I have used data from CDAWeb (Geotail and ACE parameters) and Cluster Science Data System site (preliminary magnetic footprint locations, ion- and electron energies, orbital parameters). Thanks to the prime investigators of the respective instruments for providing this. I would also like to thank the ones responsible for the Madrigal Experiment Selector web-pages, for making it easy to investigate EISCAT parameters. EISCAT is an international association supported by Finland (SA), France (CNRS), the Federal Republic of Germany (MPG), Japan (NIPR), Norway (NFR), Sweden (NFR), and the United Kingdom (PPARC). Also, I would like to thank the Orbital Visualization Tool (OVT) team at the Swedish Institute of Space Physics, IRF Uppsala.

Andreas Quamme Nielsen, November 2005

Table Of Contents

Chapter 1

Introduction

Solar- terrestrial physics is a scientific branch that deals with the interaction of the solar wind plasma and the Earth's magnetic field, and subsequently our atmosphere. It evolved and expanded as researchers sought to explain the observed northern lights, fluctuations in the measured geomagnetic field and so on. The Sun's escaping particles and radiation is what drives the systems this branch of physics seeks to explain.

We could have had references to the aurora from very early on, if it hadn't been for the fact that the earliest literate civilizations (for example Egypt) were situated on latitudes too low to be able to observe this phenomenon on a regular basis. There are some examples from the Old Testament that could be interpreted as observations of aurora, but these may be somewhat ambiguous. The earliest rational description is credited to two Greek philosophers from Asia Minor, Anaximenes of Miletus (~585-528 BC) and Xenophanes of Colophon (~570-475 BC). We also have a reference to an observation of aurora on a tablet from Babylon, dated to 567 BC [Hallinan, 1991].

The most commonly used term for the northern lights is Aurora Borealis. It consists of the name of the ancient Greek goddess of dawn Eos (Aurora in Latin), and the word boreios (borealis in Latin) which means northern.

In 1773, Captain Cook reported sightings of the northern lights' counterpart, Aurora Australis. It seemed that the northern skies did not have a monopoly on this phenomenon. Documents from China, reporting observations of northern lights on the same date as Capt. Cook's description, later gave us the first recorded example of conjugate aurora events [Hallinan, 1991].

Toward the end of the 19th century, new theories concerning the origin of the aurora emerged. H. Becquerel suggested in 1878 that the northern lights was produced by particles from the sun, guided by the Earth's magnetic field into the auroral zone. A Norwegian scientist, Kristian O. Birkeland, further developed this theory. On one of his expeditions to northern Norway in 1902-1903, he made measurements of the disturbances in the magnetic field, which led him to conclude that during the auroral events, there were strong currents parallel to the magnetic field lines. Birkeland is also known for producing artificial aurora with his Terella-experiment. He fired an electron beam towards a magnetized "terella" (a sphere), suspended in a vacuum chamber (see Figure 1.1). Birkelands theories was eventually verified by ionospheric and magnetospheric space missions in the 1960's.

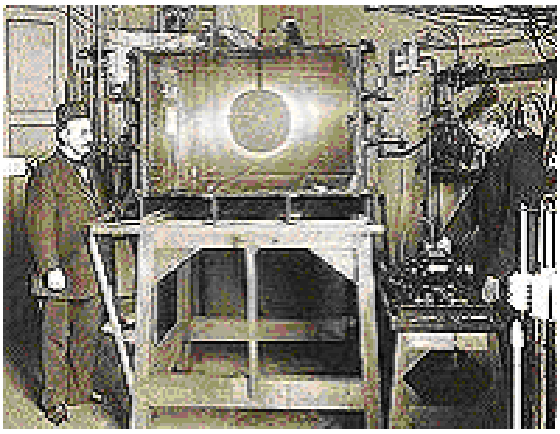

Figure 1.1: *Birkeland and his assistant performing the Terella-experiment.*

Previous to this, several scientists worked with the problem of mapping the geographical distribution of the aurora. During the early 1900's, Carl Størmer determined, by triangulation, that the aurora most frequently occur in an altitude of about 100-300 km [Daglis et al., 2004]. He is also famous for calculating the ions' trajectories in the geomagnetic field.

Today, we know that the aurora most often occurs within the auroral oval, centered on the magnetic pole. The oval exists on the boundary between open and closed magnetic field lines, and its diameter is about 3500 km. Also, its' width is larger on the nightside of the Earth (~600 km) than on the dayside [Daglis et al., 2004].

There are several areas of today's space physics that are, in some way or another, intertwined with the aurora. This is also true for some aspects of ion outflow, or rather, the escaping ions originating in the ionosphere. But, ion outflow dynamics is very intricate and difficult to model (see for example [Bouhram et al., 2003] and [Schunk, 2000]). However, there is one persistent phenomenon, the polar wind, flowing out on open magnetic field lines in the polar region. It was given its name by Axford [1968], because of the way the escaping particles resembled the ones in the solar wind.

The polar wind is a phenomenon whose characteristics have been studied intensely since the 1960s [Gardner et al., 2004]. It consists of thermal ions, mainly H+ and He+, and energetic light and heavy ions, including H+, He+ and O+ [Gardner et al., 2004]. The presence of oxygen ions is important, because they provide evidence that their origin is the ionosphere. For example, solar wind particles (mainly H+ and He+) could enter the magnetosphere, through the process of reconnection (see "Magnetic Reynolds Number and Reconnection of magnetic field lines" on page 11), and move along the geomagnetic field lines towards Earth. Many of these particles would now probably be reflected by the Earth's converging magnetic field, and their signature when measured by satellites could resemble those of outflowing particles from the ionosphere.

Many heating mechanisms have been investigated as the main cause of ion outflow. However, today it is believed that it is more a question of which mechanism contribute the most. Of course, this varies with which region the outflow can be mapped back to

[André et al., 1997]. Different mechanisms seem to dominate in different areas. This thesis will investigate measurements will be made by the Cluster satellites within the cusp region, and many articles report this region as a substantial contributor to outflow ([Lockwood et al., 1985] and [Thelin et al., 1990]). So, it might be instructive to note upon different types of outflowing ions (see “Ionospheric outflow” on page 23).

This paper will examine events where Cluster’s magnetic footprint is situated close to the EISCAT-radars in Longyearbyen on Svalbard. Those events will be further filtered according to days with a lot of activity in the radar data. Finally, the search for oxygen ion outflow will commence in the Cluster CIS-data. Other constraints are that Cluster’s orbit must be favorable for measurements in the cusp (late winter/early spring) and that EISCAT is situated in the cusp (during the winter months -> around 0900 UT). Hopefully, these requirements will still leave enough data sets, so that it is possible to look for events where ion outflow (O+) measured by the satellites, can be related to ground-based measurements by the ESR. If this is indeed so, then it could be interesting to further investigate conditions within the magnetosphere or in the solar wind which might energize particles in the ionosphere. Radar and Cluster conjunctions within the cusp, has not been performed to great lengths in earlier studies. This is because Cluster is still a fairly “young” mission (launched in 2000). Thus, it will be interesting to see whether the constraints set on the gathering of data, will leave us with much data to investigate.

.

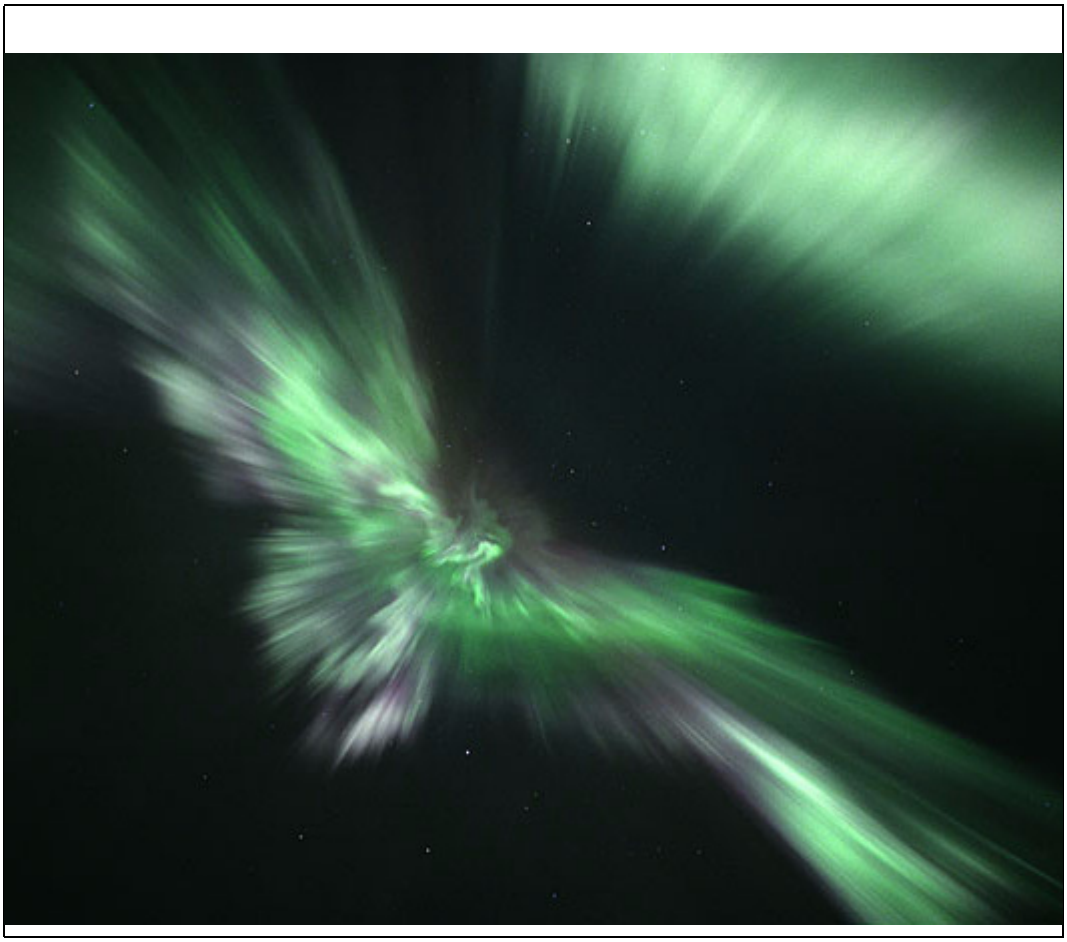

Figure 1.2: Jouni Jussila's picture which was declared Northern Lights Photo of the Year 2003 by www.northern-lights.com (picture taken from that website as well). A terrific example of the many shapes and colors the aurora can take, is displayed in Figure 1.2. It was taken by Jouni Jussila, who is a scientist/ graduate student with the Space Physics Group at the University of Oulu, Finland (more of his pictures can be found on his website: **spaceweb.oulu.fi/ ~jussila/**)

Chapter 2

Space Plasma Physics

In this chapter, I will present some of the theoretical material related to the magnetosphere and the solar wind. But, first one should consider the physics of plasmas, since most of the matter in the solar wind and the magnetosphere can be found in this state.

2. 1. The Physics of Plasmas

One can think of plasma as the fourth state of matter. Matter can exist as a solid, a fluid, a gas or an ionized gas, also referred to as a plasma. In this state, the gas is highly electrically conductive. One approach to describe the physics of a plasma is called ideal MHD (MagnetoHydroDynamics). According to ideal MHD, the conductivity can be infinitely high. This has certain consequences.

2. 1.1. Frozen-in-Field lines and Drift Velocity (E x B)

Ohm's law can be expressed as:

$$\vec{j} = \sigma(\vec{E} + \vec{u} \times \vec{B}) \qquad (2.1)$$

However, MHD also assumes an infinite conductivity, $\sigma \to \infty$, and since we want the possibility of a finite current to exist, this means that:

$$\vec{E} + \vec{u} \times \vec{B} = 0 \qquad (2.2)$$

So, this gives us an expression for the electric field:

$$\vec{E} = -\vec{u} \times \vec{B} \qquad (2.3)$$

If we then take the cross-product of Equation 2.2 and $\vec{B}$, and seek out the solution where $\vec{u}$ is perpendicular to $\vec{B}$, we get:

$$\vec{u} = \frac{\vec{E} \times \vec{B}}{B^2} \qquad (2.4)$$

In this expression, $\vec{u}$ is not the velocity of an individual particle, but the bulk velocity of a plasma element. The expression for this velocity is valid wherever the conductivity can be assumed to be infinite (see "Magnetic Reynolds Number and Reconnection of magnetic field lines" on page 11).

Now, one result that can be derived from MHD's assumption of infinite conductivity (see [Goldston et al., 1997]) is that a plasma element initially bound to a magnetic field line, will stay connected to this field line, even if either the plasma or the field line is displaced spatially. This can be shown by arguing for conservation of magnetic flux in ideal MHD.

The expression for magnetic flux is:

$$\Phi = \int \vec{B} \bullet \vec{dS} \tag{2.5}$$

Now, Faraday's law states that:

$$\frac{\partial}{\partial t}\vec{B} = -\nabla \times \vec{E} \tag{2.6}$$

And, using the result from Equation 2.3, we can express the time-differential of Equation 2.5 as:

$$\frac{\mathrm{d}\Phi}{\mathrm{d}t} = \int \nabla \times (\vec{u} \times \vec{B}) \bullet \vec{dS} + \int \vec{B} \bullet \frac{\mathrm{d}}{\mathrm{d}t}\vec{\Delta S} \tag{2.7}$$

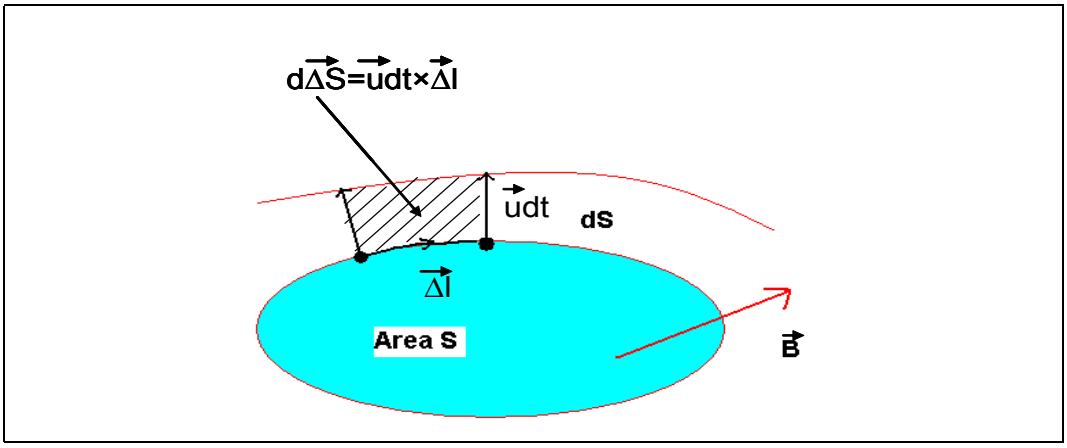

Figure 2.1: *Conservation of magnetic flux according to ideal MHD. Figure adapted from Goldston et al. (1997).*

The first term on the right side in Equation 2.7 can be expressed as a line integral, using Stokes' theorem, namely that $\int \nabla \times (\vec{u} \times \vec{B}) \bullet \vec{dS} = \int (\vec{u} \times \vec{B}) \bullet \vec{\Delta l}$. And, from Figure 2.1, one can see that $\frac{\mathrm{d}}{\mathrm{d}t}\vec{\Delta S} = \vec{u} \times \vec{\Delta l}$. Since, $\vec{B} \bullet (\vec{u} \times \vec{\Delta l}) = -(\vec{u} \times \vec{B}) \bullet \vec{\Delta l}$, we have:

$$\frac{\mathrm{d}\Phi}{\mathrm{d}t} = \int (\vec{u} \times \vec{B}) \bullet \vec{\Delta l} - \int (\vec{u} \times \vec{B}) \bullet \vec{\Delta l} = 0 \tag{2.8}$$

This has an influence of the understanding of the velocity derived in Equation 2.4, since in the event that we have so-called frozen-in-field lines, we must also have that the magnetic field lines themselves are moving with a velocity $\vec{u}$. To check which specimen controls the movement in these situations, the plasma or the magnetic field lines, one can look at the beta-parameter. This is merely the plasma pressure divided by the magnetic-field pressure:

$$\beta = \frac{2\mu_0 p}{B^2} \qquad (2.9)$$

where μ_0 is the permeability of free space. So, if $\beta > 1$, the plasma pressure plays a dominant role in the dynamics of its movements. And, of course the magnetic field dominates when $\beta < 1$.

2. 1.2. Magnetic mirrors

Making a collisionless plasma requires very high temperatures. Heating up a gas within any box wouldn't work, because the box would simply evaporate. However, if you can trap the plasma within a magnetic bottle, see Figure 2.2, you heat the gas sufficiently without doing any damages to yourself or your laboratory.

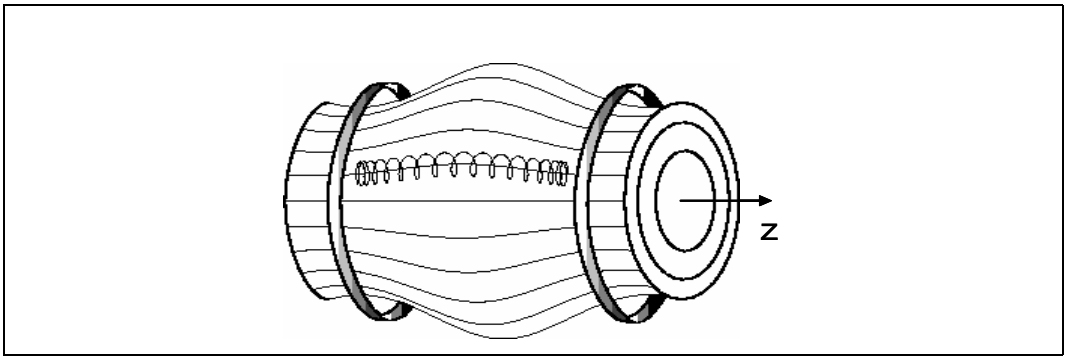

Figure 2.2: *Plasma trapped within magnetic mirrors.*

If we have a magnetic field whose intensity is a function of z, see Figure 2.2, a charged particle within that field will feel a force, averaged over a gyro-period, parallel to the field direction given by:

$$\langle F(par) \rangle = -\frac{W\perp}{B}\frac{dB}{dz} = -\mu\frac{dB}{dz} \qquad (2.10)$$

where $W\perp = \frac{1}{2}mv_\perp^2$ and $v_\perp$ is the particle's velocity perpendicular to the magnetic field.

μ is the gyrating particle's magnetic moment, and one can show that:

$$\frac{d\mu}{dt} = 0 \qquad (2.11)$$

This implies that as a particle moves along a field line into an area where the magnetic field strength increases, its energy perpendicular to the field line must also increase to ensure that $\frac{W\perp}{B} = const$. Since the particle's total energy is also conserved, this means that if a particle's parallel velocity decreases, in a converging magnetic field for example, its perpendicular velocity must increase [Goldston et al., 1997].

Magnetic mirrors aren't just something for the laboratories. They can also exist naturally. The Earth's magnetic field converges at the north and south pole, and particles that doesn't have a large initial parallel velocity component can get trapped, and then oscillate between the poles.

2. 1.3. Particle drifts and their effect on the magnetic field on Earth's surface

Charged particles in inhomogeneous magnetic field, such as the Earth's magnetic field, may acquire additional velocity components which makes them drift perpendicular to the magnetic field lines. Two important drift processes are the curvature drift and the gradient drift. The curvature drift arises when a charged particle has a velocity component parallel to a curved magnetic field line. It is then subjected to a centrifugal force perpendicular to the field line, and this results in a drift velocity given by:

$$\vec{v}_{DC} = -\frac{m v_{par}^2}{qB^2} \cdot \frac{\nabla B \times \vec{B}}{B} \qquad (2.12)$$

where v_{par} is the velocity parallel to the magnetic field, q is the particle charge and m is the particle's mass.

If the magnetic field strength increases in a direction perpendicular to the magnetic field itself, for example in the equatorial plane around the Earth, a charged particle will develop a velocity perpendicular to both the gradient vector and magnetic field direction:

$$\vec{v}_{DG} = -\mu \cdot \frac{\nabla B \times \vec{B}}{qB^2} \qquad (2.13)$$

where μ is the magnetic moment (see Equation 2.10). These velocities play an important role in the movement of charged particles in the equatorial plane at distances of the order of 3-5 R_e [McPherron, 1995].

One can see from these expressions that they will lead to a separation of charges, since q is incorporated. This fact, along with the configuration displayed in Figure 2.3, shows that positively charged particles move toward the west (left in Figure 2.3) and negatively charged particles move toward the east (right in figure). This leads to the formation of the ring current which runs eastward around the Earth. As with all currents, the ring current also induces its own magnetic field. On the Earth's surface, the geomagnetic field points toward the north. However, at the same time the ring current's magnetic field points to the south, when investigated at the surface. So, if one measures the total disturbance of the geomagnetic field at ground-level, one can calculate the kinetic energy stored in the ring current.

Through measurements made by several stations around the world, one can deduce an average value of the disturbance of the geomagnetic field, and this value is referred to as the D_{st} index. It is proportional to the total energy of the drifting particles of the ring current [McPherron, 1995].

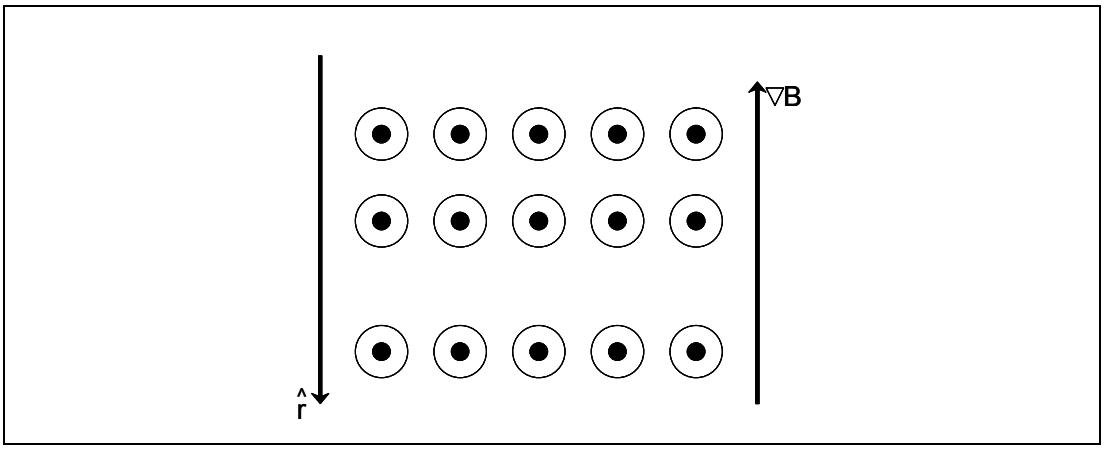

Figure 2.3: *The magnetic field (pointed out of the paper) configuration in the equatorial plane.*

2. 1.4. Magnetic Reynolds Number and Reconnection of magnetic field lines

Ampere's law states that:

$$\vec{j} = \frac{1}{\mu_0}\nabla \times \vec{B} - \varepsilon\frac{\partial}{\partial t}\vec{E} \qquad (2.14)$$

However, it is common to either show that the second term on the right side is much smaller compared to the first term [Kivelson, 1995], or to assume quasi-static state so that $\frac{\partial}{\partial t} \to 0$. Either way, it can usually be neglected. Also, the time variation of the magnetic field is expressed as:

$$\frac{\partial}{\partial t}\vec{B} = -\nabla \times \vec{E} = \nabla \times (\vec{u} \times \vec{B}) - \frac{1}{\sigma}\nabla \times \vec{j} = \nabla \times (\vec{u} \times \vec{B}) + \frac{1}{\sigma\mu_0}\nabla^2\vec{B} \qquad (2.15)$$

when using Ohm's law (Equation 2.1), modified Ampere's law ($\vec{j} = \frac{1}{\mu_0}\nabla \times \vec{B}$) and the vector identity $\nabla \times \nabla \times \vec{B} = \nabla(\nabla \bullet \vec{B}) - \nabla^2\vec{B}$ (remembering that $\nabla \bullet \vec{B} = 0$).

So, it is evident that the temporal variation of the magnetic field can be explained by a convection term (first term on the far right side of Equation 2.15), and a diffusion term (second term). The magnetic Reynolds number is the convection term divided by the diffusion term:

$$\frac{\left|\nabla \times (\vec{u} \times \vec{B})\right|}{\left|\frac{1}{\sigma\mu_0}\nabla^2\vec{B}\right|} \sim \frac{\frac{1}{L}uB}{\frac{1}{\sigma\mu_0 L^2}B} \sim \sigma\mu_0 uL = R_M \qquad (2.16)$$

where L is a typical length scale of the spatial variation of the magnetic field in the region under inspection. So, when $R_M \gg 1$, one can deduce high conductivity and say that the frozen-in-flux condition is valid. If the Reynolds number is close to unity, ideal MHD breaks down [Hughes, 1995]. If one inserts typical magnetospheric values for L (a few R_e) and 100 km/s as the velocity, the Reynolds number turns out to be 10^{11}

[Hughes, 1995]. This is more than high enough for making fairly accurate calculations of magnetospheric parameters using ideal MHD.

Also, the magnetic Reynolds number calculated for solar phenomena on global length scales is very high, $10^6 \sim 10^{12}$ [Priest, 1995]. It is therefore evident that ideal MHD is a good approximation in the solar wind as well, except where we have intense current sheets which can lower the typical length scale L drastically.

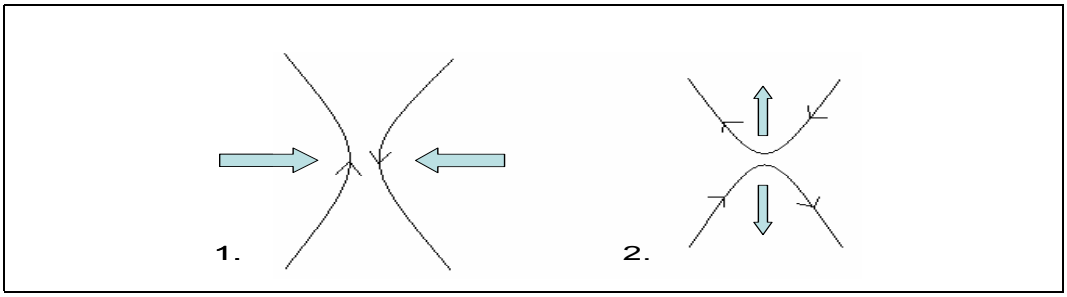

Figure 2.4: *Magnetic field lines reconnect and drift away from each other(2.).*

Reconnection is a process where magnetic field lines with components pointing in opposite directions can reconnect with each other (see Figure 2.4). For this to happen, the frozen-in-flux concept must break down, i.e. the magnetic Reynolds number must approach unity. Right before two magnetic field lines reconnect, they are "pushed" towards each other into an area referred to as the diffusion area. Here, the length scales are so small, that we have $R_M < 1$. After the event of reconnection, the field lines drift out of this area, and the frozen-in-flux is re-established.

After reconnection, the new magnetic field lines are usually very curved. This gives rise to a strong magnetic tension force, which can transfer energy to charged particles lying close to the reconnection area. One can sometimes observe high speed jets which can be traced back to this region.

Events like these provide us with an explanation of how plasma from the Sun can gain access to the Earth's magnetosphere. One might come to the conclusion that the interplanetary magnetic field (IMF) must have a southward (GSE) component for reconnection to happen (because of the terrestrial magnetic field's orientation). But, if the IMF is northward, the reconnection site can be situated at high latitudes, instead of near the ecliptic along the GSE X-axis, and we will then have so-called lobe reconnection.

2. 2. Our Friendly Neighbor, the Sun

It is the Sun that drives most of the dynamics in the terrestrial magnetosphere, and upper atmosphere. It does this by ejecting vast amounts of charged particles, mainly ionized hydrogen and some helium, and electromagnetic radiation.

2. 2.1. Below and above the surface

The Sun's radius, R_S, is about $6,9599 \cdot 10^8$ meters [Carroll et al., 1996]. Its thermonuclear core has a radius of about 0.2 R_S, and the temperature is high enough, around 15 million Kelvin [Priest, 1995], for fusion to occur. Enormous amounts are released as hydrogen atoms are fused together to form helium. The process fuses 4 ionized hydrogen atoms and produces an ionized helium atom. If one calculates the mass before and after the process, one will find that there is some mass missing. Using one of Einstein's most famous equations, $E = mc^2$, one can also calculate the energy released every time this happens.

In the shell that exists from 0.2 to 0.7 R_S , the radiative zone, energy is transported as radiation. However, the gas is extremely dense, so the path that the photon can travel before being scattered is very small. Photons can spend millions of years just traversing this zone.

The convective zone reaches from 0.7 to 1 R_S. In this area energy is transported upwards as bubbles of plasma seek to expand, and moves outwards to do so. The top of the convective zone ends at the bottom of the photosphere, which marks the start of the Sun's atmosphere. The light we can see escaping the Sun originates here. This layer is very thin, only about 500 km deep. Further up, we have the chromosphere, which extends to a height of about 2300 km. Analysis shows that the temperature at the bottom of the chromosphere is about 4400 K, while at the top it is close to 25000 K [Carroll et al., 1996]. From 2300 to 2600 km one can find a transition zone. Above this, we have the corona. The temperatures here are on the scale of several million Kelvin.

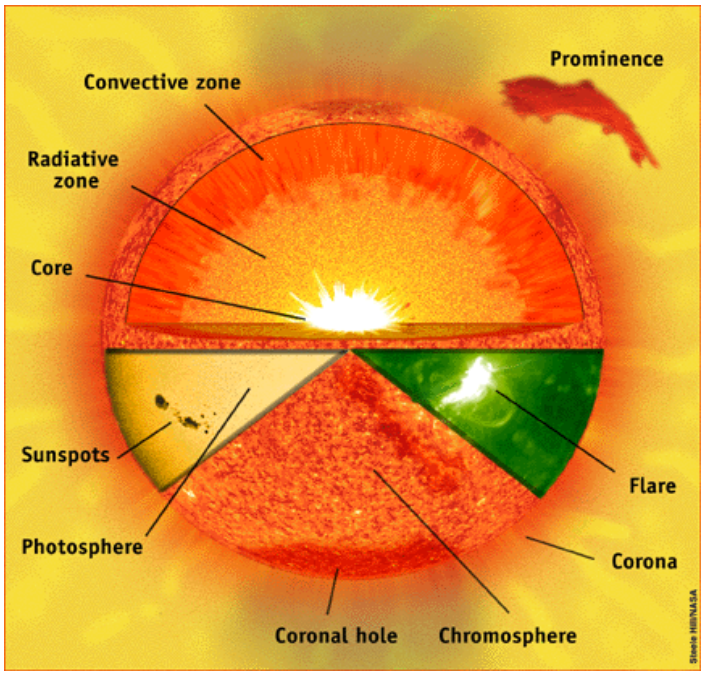

Figure 2.5: *This image taken from http://sohowww.estec.esa.nl, shows the different layers of the Sun.*

2. 2.2. The Sun's magnetic field

The Sun is a ball of gas, and does not rotate around its axis like a rigid body. It has a so-called differential rotation (the gas close to the equator has a shorter rotation period than near the poles), and because of the frozen-in-flux concept, the magnetic field within the Sun gets wound up. They can even appear above the surface in magnetic loops. We can then see them as sunspots. After about 11 years, the magnetic field has been wound up to such a degree that the Sun's magnetic poles suddenly switch places. Right before the dipole axis flips 180 degrees, the Sun's activity is at its peak, with many sunspots which can affect the structure of the corona. The increase, and sudden decrease of the amount of sunspots gives rise to what we call the Sun's 11-year-cycle.

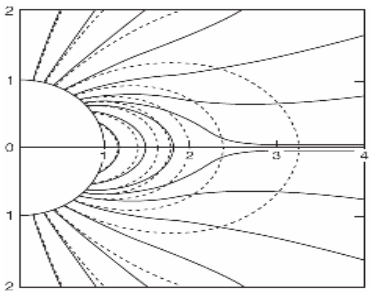

Figure 2.6: *Image displaying the Sun's magnetic field configuration [Russell, 2001] Dashed line indicates the magnetic field of a regular dipole.*

Close to the Sun, the magnetic field resembles that of a regular dipole field (see Figure 2.6). However, as one observes the field further away, it becomes more radially aligned. There is also a drag on the magnetic field which increases with increasing distance from the Sun. As a matter of fact, the angle between a magnetic field line from the Sun, and a line drawn from the Sun's center straight out to the Earth's orbit, is about 45 degrees (both observed and predicted) [Hundhausen, 1995]. Seen from above, the field looks like a twirling skirt, as predicted by Parker (1958). Also, seen in a cross-section from the side, the magnetic field lines have a wave-like structure. The magnetic field's three-dimensional profile is displayed in Figure 2.7.

This magnetic field stretches out to large distances and is referred to as the Interplanetary Magnetic Field (IMF), and its direction at a given position at a given time and position affects the manner in which the solar wind particles interact with the Earth's magnetosphere.

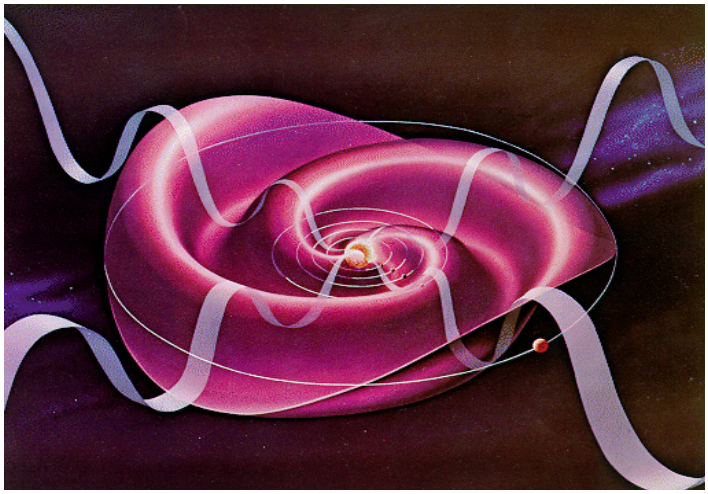

Figure 2.7: *The Parker spiral with its magnetic field lines pointing in opposite directions which keep the current sheet (shown in purple/pink) in place.*

2. 2.3. The Solar Wind

The Sun can lose fractions of its mass in two ways. Mass can be carried away in the solar wind, in other words by outflowing particles, or "lost" in the fusion processes in the Sun's core. However, the mechanism which dominates the Sun's influence on the Earth's magnetosphere, is the solar wind.

If one neglects the solar magnetic field, one can see from the fluid model for the equilibrium of state of the corona, which is believed to be the source of the solar wind, that there has to exist a supersonic flow of particles into interplanetary space. The equations one starts with are quite simple, i.e.:

$$\frac{\partial \rho}{\partial t} + \nabla \bullet \rho \vec{u} = 0 \quad \text{(mass-conservation)} \qquad (2.17)$$

$$\rho\frac{\partial}{\partial t}\vec{u} + \rho\vec{u} \bullet \nabla\vec{u} = -\nabla p + \vec{j} \times \vec{B} + \rho\vec{F}_g \quad \text{(momentum-conservation)} \qquad (2.18)$$

To give us a basic understanding of how the solar-wind can exist, one can use these equations and modify them with a few assumptions (steady-state, spherical symmetry, neglect the magnetic field) [Parker, 1958]. The plasma will stay connected to the magnetic field lines and carry them outwards as they flow with a typical velocity of 400 km per second and a density of about 5 cm^{-3} [Russell, 2001].

If one looks at an X-ray image of the Sun, one may notice some very bright loops, and other areas that are quite dark. The bright areas correspond to closed magnetic field lines in the corona. For an area to appear very bright in an X-ray image, the temperature of the gas there must be several million Kelvin, which you will find in the corona. However, you'll also see dark areas, which signifies open magnetic field lines that stretches out into space. The continuous solar wind flows along these (see Figure 2.8).

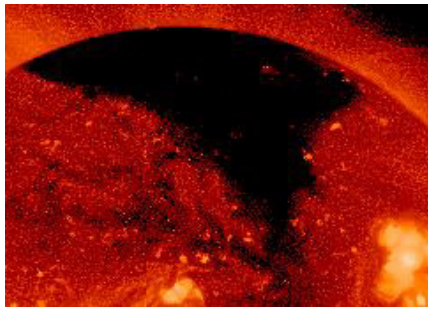

Figure 2.8: *An X-ray image of the Sun showing coronal holes as well as brighter areas which signifies very hot gas in the corona.*

A magnetic cloud is like a large flux rope originating on the Sun. Exactly how these clouds develop, is still being debated. But, it seems that they are formed when coronal magnetic loops rises, aided by reconnection. Inside the cloud, it seems that the magnetic field pressure controls the dynamics, i.e. $\beta < 1$ [Lepping et al., 2000]. If the cloud is to reach equilibrium with the surrounding pressure, it has to expand to beyond the Earth's orbit, at 1 astronomical unit (AU).

At the center of the cloud, the magnetic field is aligned with the parallel axis. Toward the edges, the magnetic field is perpendicular, see Figure 2.9. Because of the distinctive magnetic field structure within a flux rope like this, we can use magnetometers to decide when a cloud crosses the Earth's path, and determine its direction.

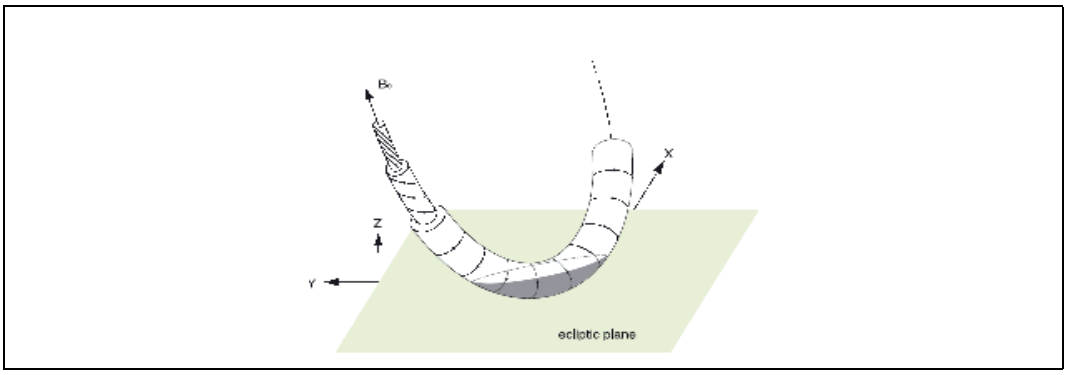

Figure 2.9: *An example of a magnetic cloud (and with GSE coordinates). Picture taken from an article by Ishibashi et al. (2004)*

A solar flare can occur when a magnetic loop, being twisted and turned thereby gathering more energy, suddenly become unstable and erupts, releasing a large amount of energy. It also accelerates electrons and protons into the solar atmosphere. It is referred to as a flare because of the sudden increase in the X-ray wavelength region. As seen in Figure 2.10, a solar flare is closely related to sunspot activity.

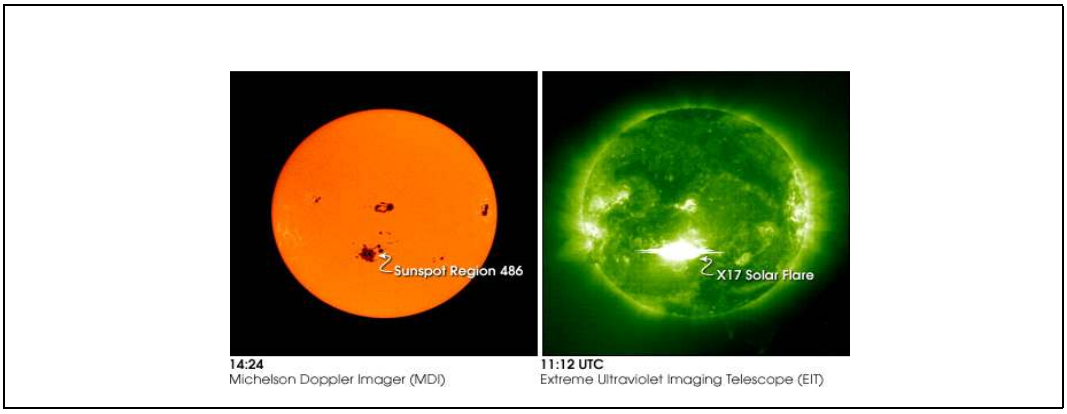

Figure 2.10: *A solar flare, recognized as a sudden brightness in the X-ray image (right).*

However, the amount of energy released during a coronal mass ejection (CME), far surpasses that of a solar flare. One can have coronal plasma contained in equilibrium within a closed magnetic loop. A CME can develop as a result of a violent disruption of these field lines, causing them to become open field lines [Hundhausen, 1995]. This process sends out a huge amount of particles, adding to those within the continuous solar wind. It can hurl plasma into space with a kinetic energy in the order of $10^{24} - 10^{25}$ Joule. The velocity of the particles can reach 1000 km per second [Manchester, 2004]. Thus, a CME like this will compress the Earth's magnetosphere severely. The dynamic pressure of the solar wind can be expressed as [Paschmann, 1991]:

$$P_{SW} = Nm_p u^2 \qquad (2.19)$$

Here, u is the plasma's bulk flow velocity. So, this shows that a large increase in the flow velocity, has a great impact on the pressure exerted on the magnetopause.

A connection between solar flares and CMEs has been investigated, but no conclusive evidence has appeared. CMEs will sometimes follow a flare, but this isn't always the case.

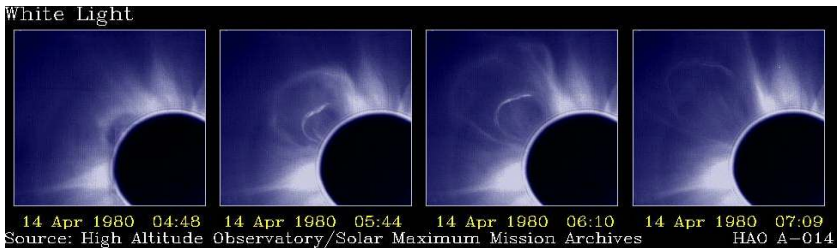

Figure 2.11: *An image sequence of a CME recorded 14 Apr., 1989.*

2. 3. The Magnetosphere

The solar wind consists mainly of ionized matter, i.e. charged particles. Therefore, the terrestrial magnetic field acts as a shield, an obstruction in the path of the flowing plasma from the Sun. The frozen-in-flux concept also acts as an obstacle the plasma has to negotiate to be allowed to enter the magnetosphere. However, this can be done through the process of reconnection. The solar wind can also influence the dynamics of the geomagnetic field by viscous interaction where it exerts a drag on the edges of the magnetosphere [Paschmann, 1991].

2. 3.1. The Shape of the Magnetosphere

The deflection by the magnetosphere of the supersonic flow from the Sun, creates a shock wave that outlines the shape of the sphere. The front of the shock is referred to as the bow shock, the deflected solar particles constitute the magnetosheath, and the border that separates the solar wind from the geomagnetic field is called the magnetopause (MP) see Figure 2.12.

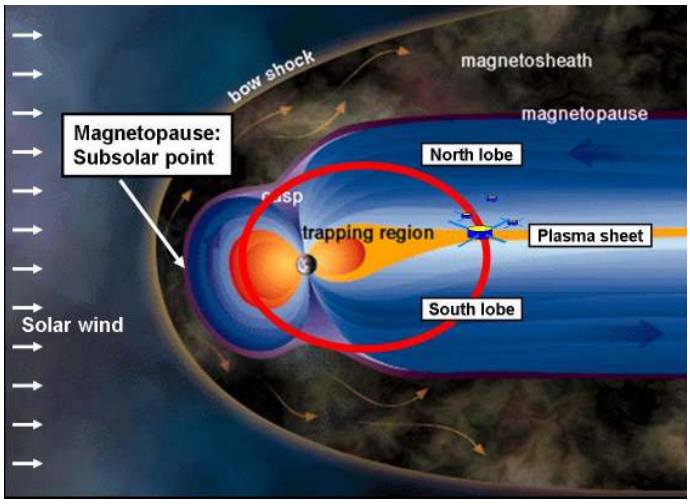

Figure 2.12: *A cross section of the magnetosphere, also showing Cluster's orbit during the summer-fall period.*

The position of the subsolar point (see figure above), can be found by considering the equilibrium between the terrestrial magnetic pressure, and the solar wind's dynamic pressure (for dynamic pressure, see Equation 2.19). In general, the magnetic pressure is given by:

$$P_m = \frac{B^2}{2\mu_0} \qquad (2.20)$$

However, this expression should be modified, since the solar wind's pressure changes can induce currents in the magnetopause, strengthening the geomagnetic field's pressure. Walker and Russell (1995) left those pressure additions to be determined empirically, and found this expression for the position of the subsolar point (given in Earth radii):

$$L_{MP}(R_e) = 107,4 \cdot (n_{SW} \cdot u_{SW}^2)^{-\frac{1}{6}} \qquad (2.21)$$

Under normal conditions, the magnetopause is observed to lie at a distance of about 10 R_e [Walker and Russell, 1995]. However, this distance is greatly influenced by solar wind bulk velocity u_{SW}(km per second) and its density n_{SW} as seen in Equation 2.21.

Several models representing the structure of the geomagnetic field has been suggested. In 1930, Chapman and Ferraro approximated the solar wind as an infinitely conducting sheet pressing on a magnetic dipole. Today, we rely on an empirical model, presented in Figure 2.13, which resembles a magnetic dipole out to a distance of about 5-8 Re and then being distorted, due to being compressed on the dayside, and stretched on the nightside.

It is common to use the Tsyganenko magnetic field models when one wishes to predict the position of certain features within the magnetosphere, or mapping a satellite's magnetic footprint to the Earth's surface from its position inside the magnetopause. The models are corrected every now and then, for example in 1987, 1989, 1996 and 2001. In

some cases, one might as well use an older model of the magnetic field, such as the T-87 model (Tsyganenko's 1987 model), but this might not always give accurate results. For example, Zhou et al. (1997) reports that the T-96 model overestimates the magnetic field surrounding the polar cusp. This is something one has to consider when investigating the magnetic field lines in certain regions of the magnetosphere.

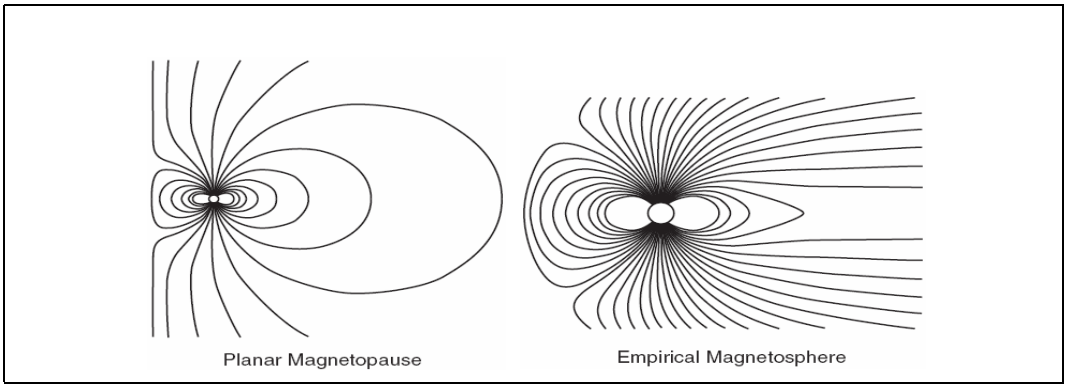

Figure 2.13: *Chapman-Ferraro's model of the Earth's magnetic field (left), and the empirical model (right) [Russell, 2000]*

2. 3.2. Convection and IMF dependence

Some of the Earth's magnetic field lines are what we refer to as open field lines. They connect with the interplanetary magnetic field lines. The border between these and the ones that are closed, constitutes the auroral zone. So, equator ward of this zone, we have closed magnetic loops, and across the polar caps the field lines are open.

This paper will deal with, among other things, a part of the atmosphere which is called the ionosphere. This region starts along with the mesosphere at an altitude of 50 km, and stretches upward for several hundred kilometers. What signifies this region is that its particles can be ionized to the extent that it influences the propagation of radio waves. It can for example reflect and scatter these waves back toward the ground, so that radio signals can be sent to places which are not visible from the source, because of the planet's curvature. Within the ionosphere, there are three major layers identified by the difference in the electron-density profile. One usually divide the ionosphere into the D-layer (in the altitude-interval of approximately 50-90 km), the E-layer (90-150 km) and the F-layer (150-500 km) [Landmark, 1973].

Fifty years ago, one measured plasma flows in the ionosphere, and understood that these must be a result of interaction with the solar wind. In 1961, Dungey proposed a solution by considering reconnection at the sub-solar point and mapping the movement of the reconnected field lines to the ionosphere. However, he pointed out that the IMF Bz component has to dominate and be southward. This model has since been modified after investigating the convection patterns across the polar cap with ground-based measurements, and later with satellites. It later appeared that only parts of the IMF has to be anti-parallel with geomagnetic field lines, allowing reconnection also at the magnetopause near the lobes.

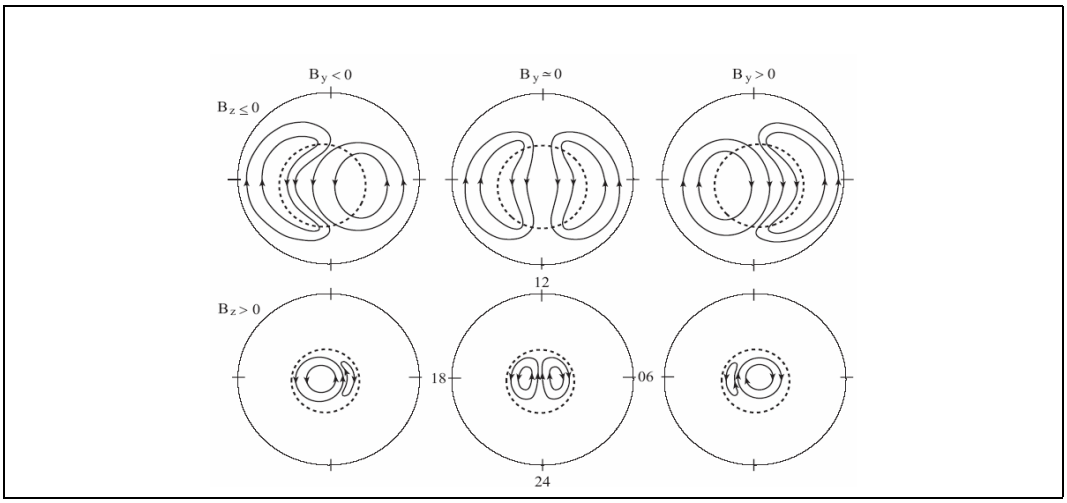

Figure 2.14: *The convection patterns' IMF dependence [Cowley and Lockwood, 1992].*

The idea of solar wind particles penetrating the magnetosphere by the process of reconnection is the most accepted theory today. But, the concept of anti-parallel component reconnection, that the IMF doesn't have to be exactly southward, implies that there are some events when the momentum- and energy transfer from the solar wind is more effective than others. Akasofu derived one of the most well-known expressions for the energy-coupling between the magnetosphere and the solar wind [Akasofu, 1981], the epsilon (ε) parameter.

$$\varepsilon = vB^2 \sin\left(\frac{\theta_C}{2}\right)^4 l_0^2 \qquad (2.22)$$

Here, v is the solar wind bulk speed, B is the magnitude of the IMF, θ_C is the clock angle, which is the projection of the IMF-vector onto the GSE Y-Z plane, and l_0 is a typical size of the merging region at the subsolar magnetopause, empirically determined to be of the order of 7 R_e [Østgaard et al., 2002]. The clock angle is in the range of 0^o (northward IMF) to 180^o (southward IMF). So, this again implies that when the IMF is directly northward, there is no energy transfer, according to the epsilon parameter. However, you might in this case have lobe reconnection, and sunward convection across the polar cap (see Figure 2.14), so it is not a complete solution to the rather complicated problem of energy coupling, which might also include viscous interaction independent of the IMF.

However, it might give us an idea of the order of energy transfer as a function of IMF conditions and solar wind speed. For example, during the passage of a CME, the energy transfer can be huge, since the velocities are large. If also the IMF is predominantly southward, the magnetosphere will shield the Earth less efficiently, and the effects in the ionosphere and even at the surface can be severe.

2. 4. The Polar Cusps

2. 4.1. Position

The magnetic field emanating from a regular dipole, for example a bar-magnet, converges at the southern- and northern magnetic pole. So, since the geomagnetic field is roughly similar to that of a dipole magnetic field, at least within a suitable altitude interval, one should be able to find two areas where the Earth's magnetic field converges. These areas are referred to as the polar cusps. In these areas, the magnetic field is weaker than the surrounding regions, and the plasma density increases as one enters the cusp. This is because the solar wind particles have more or less direct access all the way down to the Earth's ionosphere. The cusps are thus viewed as injection sites for the particles within the solar wind and the magnetosheath.

On a bar magnet, the "cusp"-areas will be found centered on the north and south magnetic poles. But, because of the distortion of the geomagnetic field, the cusps' position is altered, see Figure 2.13. Also, convection expands the footpoint of the cusp to an area, rather than a single point. So, it is apparent that the polar cusps are affected by changes in the IMF [Russell, 2000].

Although the cusps had been a feature in the magnetospheric models for quite some time, their existence was not verified until 1971 [Russell, 2000]. Since then, the cusps have been investigated at both high and low altitudes by such satellites as for example POLAR (high altitude) and the Defense Meteorological Satellite Program (DMSP) satellites (low altitude). But, since the cusp reaches all the way down through the ionosphere, there is also the opportunity to use measurements made by ground-based radars, as has been attempted in this thesis. From here on, the focus will be on the northern cusp, which has been the most investigated. But, the southern cusp is thought to have the same characteristics.

The difficulty of using ground-based instruments is that the cusp region must be situated right within the field-of-view of the instrument. So, to determine the shape of the cusp, and where the footpoint is situated, a good model of the magnetic field is required. Tsyganenko's vacuum model (1989), predicts the location fairly well, and places the cusp at 81^{o} invariant latitude [Russell, 2000]. However, after investigating the northern cusp with the POLAR satellite, Russell [Russell, 2000] found a relation between the latitudinal position of the center of the cusp and the IMF Bz-component, for both northward (positive) and southward (negative) values of Bz (adapted from [Russell, 2000]):

$$\text{Northward IMF Bz: } 80.7 - 0.027\left|B_Z\right| \qquad (2.23)$$

$$\text{Southward IMF Bz: } 81.3 - 0.98\left|B_Z\right| \qquad (2.24)$$

It is thus apparent that the movement of the cusp is dominated by negative values of the IMF Bz, and moves equator ward when the absolute value of Bz increases.

DMSP-data suggests that the latitudinal width of the cusp at low altitudes (800-900 km) is about $7\text{-}8^{o}$ when $Bz \sim 0$ [Russell, 2000]. The longitudinal width is more difficult to establish, since most satellites that pass through the polar regions has an orbit in the

north-south plane. However, the cusp should be centered around 12 MLT (see Appendix A.3), but its longitudinal position is affected by the IMF By component. For large positive values of By (> 6 nT), the cusp is displaced towards the afternoon region. The opposite is evident for large negative values [Russell, 2000]. In Figure 2.15, it is evident that the cusp's position, seen as increased intensity of aurora, moves as the By-component changes from positive (left) to negative (right).

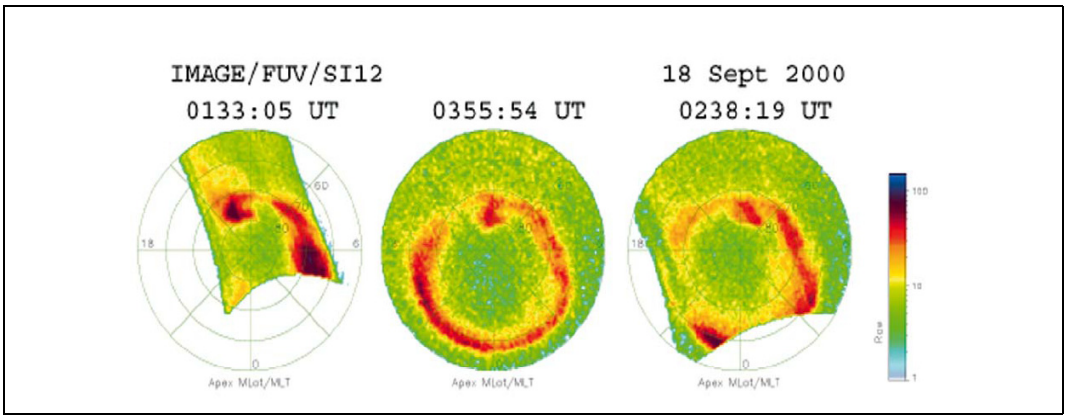

Figure 2.15: *An example of the movement of the cusp hotspot according to changes in the IMF By-component (left: By positive, right: By negative). (Figure taken from [Fuselier et al., 2003])*

Finally, it's worth mentioning that the overall width of the cusp is affected by the dynamic solar wind pressure.

2. 4.2. Ionospheric outflow

In the polar region, there is a continuous outward flow of ions along the open geomagnetic field lines. The flow resembles that of plasma escaping from the sun, and is therefore referred to as the "polar wind" [Gardner et al., 2004]. The main ion populations of the polar wind are H+, He+ and O+ [Ogawa, 2002].

In the cusp there is outflow of several different types. Typically, one has two categories of outflow. The first one includes flows where all the ions acquire a bulk velocity with energies up to a few eV, as in the polar wind for example. The other category includes processes where only a fraction of the ions are accelerated often up to energies much higher than in the first [Yau et al., 1997]. There are several types of ion outflow in the latter group, for example ion beams, Transversely Accelerated Ions (TAIs), ion conics and UpWelling Ions (UWIs). These have been classified according to their different velocity and energy properties by sounding rockets, satellites and ground based instruments.

Ion beams are most often observed above 5000 km [Yau and André, 1997], and the peak flux of particles is parallel to the magnetic field line. Ion conics have a peak flux directed at an angle to the field line, and they have been observed at an altitude between 1000 km and several Earth radii. TAI's are considered to be a special case of ion conics,

and they have pitch-angles close to 90^{o}. They have been found in different altitudes in the dayside and nightside with satellites, 3000 km and 1400 km respectively, and even down to ~400 km with sounding rockets during auroral events [Yau et al., 1997, and references therein]. These three types have energies ranging from 10 eV to a few keV.

During a UWI-event, a larger bulk of ions are energized compared to the ion conic events. One can have UWIs if there is an increase in the plasma pressure in the ionospheric F-region, [Schunk, 2000]. This could be a result from an increase in the ion- or electron temperature, or a sudden elevation of the solar wind dynamic pressure [Fuselier, 2002]. Also, in sunlit areas, escaping photoelectrons can drag the ions along and cause further outflow. It is believed that UWI is a regular phenomenon in the cleft region, surrounding the polar cusp [Yau et al., 1997].

Evidently, a UWI-event can evolve into an ion conic because of convection, see Figure 2.16. Along with UWIs, wave-particle interactions are the most prominent features regarding outflow in the cusp/cleft region ([Yau et al., 1997], [Schunk, 2000]). Wave-particle interactions can heat the ions perpendicularly, and cause them to flow outwards influenced by the magnetic mirror force.

The EISCAT radars can measure ionospheric properties up to a height of about 600 km. So, when they see an upward component in the plasma velocity, the event is usually referred to as upflow, not outflow. After an upflow event, many of the ions may fall back towards the Earth. If properly energized, they can develop into outflowing particles. This is why it could be helpful to use both radar and satellite data to give a more comprehensive picture of the acceleration region. Knowledge about this region is necessary to calculate the time delay of particles travelling from the ionosphere to a satellite.

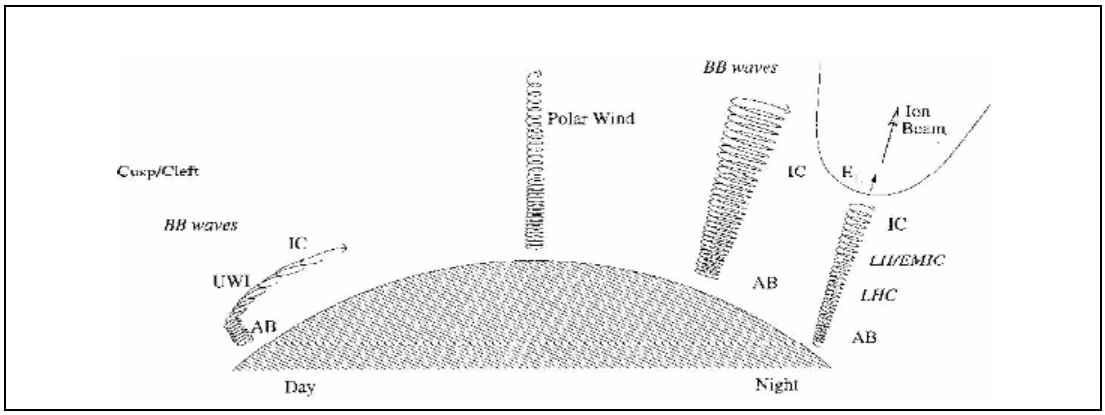

Figure 2.16: *Outflow types in the different regions, broadband low-frequency waves (BB), auroral bulk outflow (AB), ion conics (IC), upwelling ions (UWI), lower hybrid frequency waves (LH) in density cavities (LHC) and electromagnetic ion cyclotron waves (EMIC). (Figure taken from article [André and Yau, 1997])*

Bouhram et al. (2004) used Cluster data to examine dayside outflow of oxygen ions. They found that local variations in O+ fluxes didn't correlate with the total outflow rate. However, they did find that, in accordance to Cully et al. (2003), that the global outflow depended mainly on the dynamic solar wind pressure. So, this illustrates that on small spatial and temporal scales the outflow rates are difficult to predict.

Fuselier et al. (2002) found that the ionospheric response time to a sudden disruption, i.e. a pressure pulse, was very short, if not nearly non-existent. So, any measurable time-delay would consist of the travel time of the perturbation and the particle.

2. 4.3. Other observable features in the polar cusp

Reconnection on the dayside of the magnetosphere, rather than in the tail-like nightside (see right side of Figure 2.13), is usually described to be either continuous or pulsed [Oksavik et al., 2004]. Pulsed reconnection is thought to be the main contributor of transferring mass and momentum from the solar wind to the magnetosphere. This process will create magnetic flux tubes which are connected to the geomagnetic field and closes in the solar wind. However, geomagnetic field lines that are connected to the IMF are usually considered to be "open" field lines. These events are called Flux Transfer Events (FTEs).

A newly reconnected flux tube will be bent (see Figure 2.17), so it will experience a tension force when it seeks to straighten out. One can consider this tension force to be similar to the force acting on a curved string when it is released. This flux tube will then follow the direction of the convection within the magnetosphere, and along with the solar wind it will be dragged toward the magnetospheric nightside.

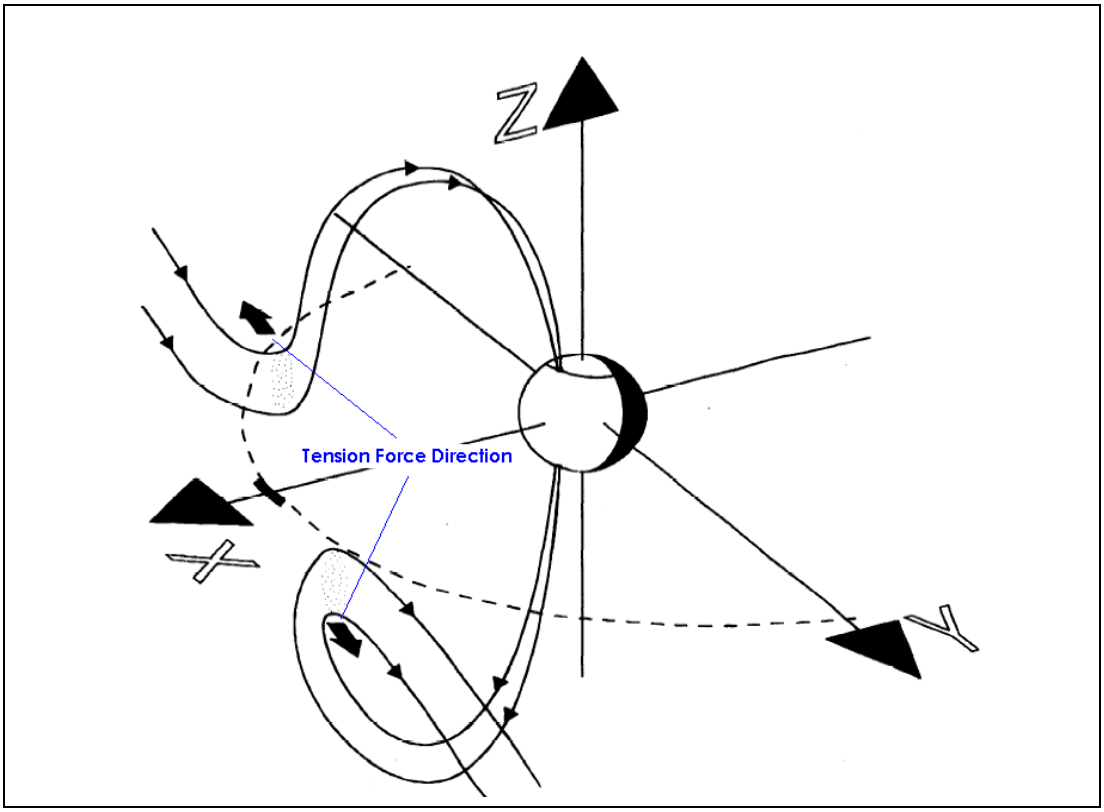

Figure 2.17: *Newly reconnected flux tubes (modified picture taken from Lockwood and Hapgood (1998)). The configuration is shown in GSM-coordinates. The dashed line indicates the magnetopause in the equatorial plane, and the reconnection site is shown on as a thick line on the X-axis.*

Southwood (1987) suggested what the ionospheric signature of an FTE would look like. A flux tube moving across the polar cap, would cause currents and twin-vortices to flow in the ionosphere. This is illustrated in Figure 2.18, where the flux tube is moving toward the left.

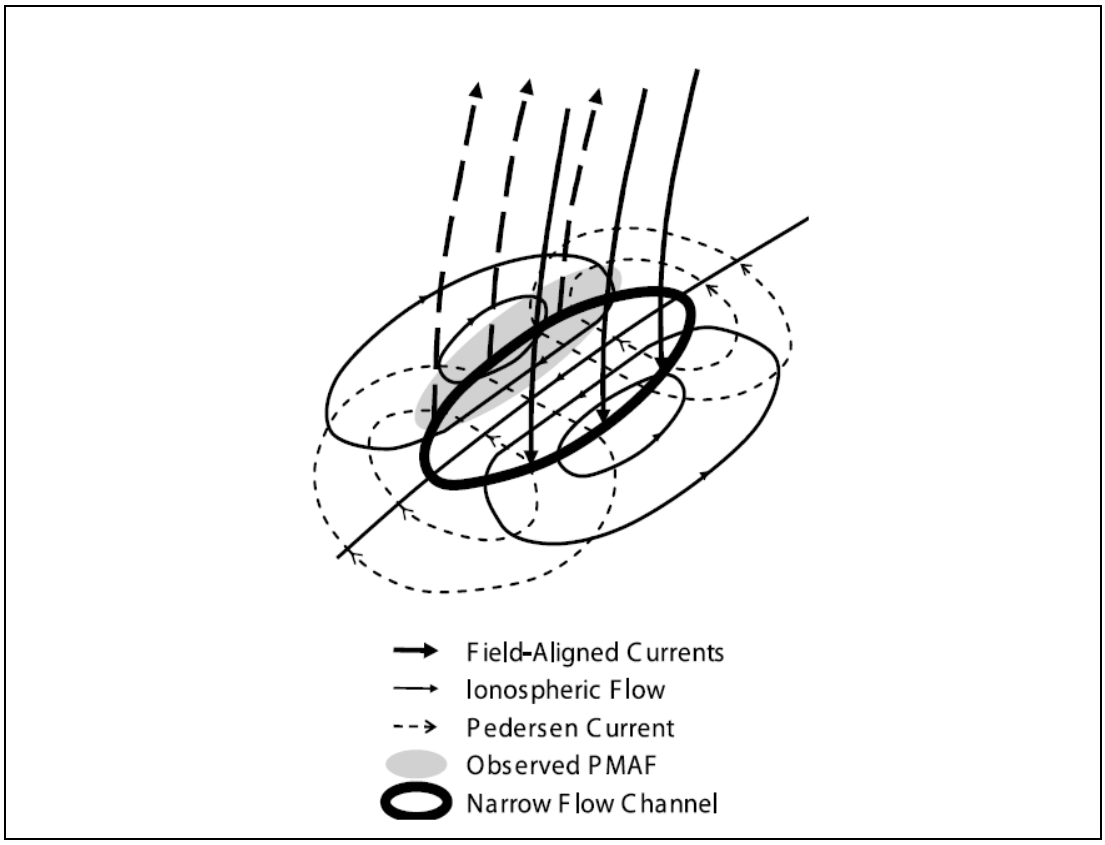

Figure 2.18: *The ionospheric signature of an isolated flux tube convecting across the polar cap (picture taken from Oksavik et al. (2004)). The flux tube's motion toward the left induces currents and plasma flows in the ionosphere.*

If one has a current running out of the ionosphere, one must have electrons precipitating downwards. This causes observable aurora. Looking at Figure 2.18, it is clear that aurora follows the flux tube's motion towards the pole, and this is therefore called a Poleward Moving Auroral Form (PMAF) [Oksavik et al., 2004]. Conclusively, it is interesting to note that an FTE has associated currents running parallel and anti-parallel to the magnetic field line that is surrounded by the flux tube.

Chapter 3

Instrumentation

This thesis deals with the series of events occurring in the northern polar cusp on February 11th, 2004, from about 09:00-11:20 UT. The main data is gathered from the EISCAT radars just outside Longyearbyen on Svalbard, and from the Cluster-satellites orbiting Earth in an elliptic polar orbit. The Geotail satellite was at this time situated in the solar wind, right outside the bow shock. The IMF-data will provide a better understanding of the interaction between the solar wind plasma and processes within the magnetospheric cavity.

3. 1. The CLUSTER Missions

In November, 1982, the concept of the Cluster mission was proposed. The idea was to have four satellites in a polar orbit, studying the Earth's magnetotail and the polar cusps. After 14 years, the Cluster satellites were ready for lift-off with ESA's new Ariane-5 booster. On June 4th, 1996, the rocket was launched on its maiden voyage from French Guiana. However, problems arose after just 37 seconds, and the rocket's automatic self destruct system was activated.

A month later, it was clear that some of the unique science equipment from the mission could be salvaged. So, ESA decided to build a fifth Cluster satellite, named Phoenix, from prototypes and spare parts from the original mission. However, one of Cluster's great advantages is that there are four identical satellites, flying in a tetrahedron configuration. This makes it possible to separate time and space variations and to deduce velocities and directions of any boundary layers that Cluster might encounter. This fact was also recognized by ESA, so instead of just building a fifth satellite, they built a total of four.

These satellites constituted the Cluster II mission. The satellites were similar to those of the first mission, but with certain improvements to both the software and the hardware components. The most important improvement was to change data storage systems on board from tape recorders to modern solid state memories.

The Ariane-5 rocket was now considered to be too expensive by the Science Programme Committee, so they turned to the Russian Soyuz rocket. The performance of this rocket was perfect for launching the Cluster II mission. The two first satellites of the Cluster II mission were launched into orbit on the 9th of August, 2000, followed by the launch of the last two satellites.

As mentioned earlier, Cluster has a elliptic polar orbit, with a perigee of about 4 Re, and an apogee of 19.6 Re [Escoubet et al., 1997]. During the summer months, its perigee is on the dayside of the magnetosphere. And, during the winter months, the orbit will have rotated compared with the Sun-Earth line so that its perigee is on the nightside. This orbit makes it possible for Cluster to measure parameters in many different regions of the magnetosphere.

So far, the data provided by Cluster has shown us the dynamics of both large- and small-scale phenomena within the magnetosphere. The mission has indeed proven to be a large success, and the data collected so far, will keep the researchers busy for many years to come.

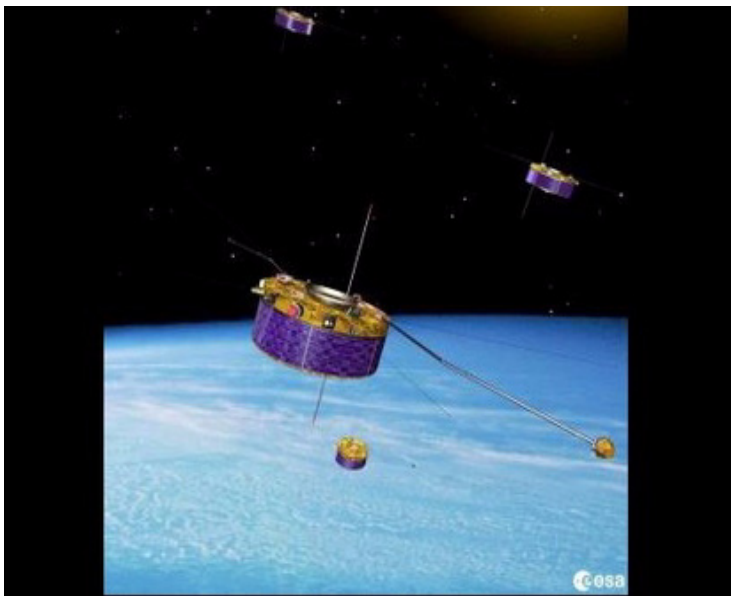

Figure 3.1: *An artists impression of the four Cluster satellites.*

3. 1.1. The Cluster Ion Spectrometry (CIS) experiment

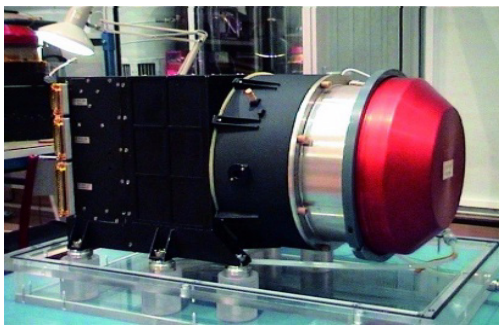

Figure 3.2: *One of the four CIS-experiments developed for the Cluster mission.*

The CIS-experiment was included on the Cluster satellites because of its abilities to measure the three-dimensional distributions of the major ion populations found within the magnetospheric cavity and the solar wind. The experiment includes two instruments, which combined, give a good coverage of ion energies from 0.02 keV/e to about 40 keV/e [Reme et al., 2001]. The two instruments are the COmposition and DIstribution Function analyzer (CODIF) and the Hot Ion Analyzer (HIA). The time resolution of these instruments (when considering the 3-dimensional distributions) is about 4 seconds, the same as the spin-period of the satellites.

Two instruments were included to accommodate all the requirements that were set by the Cluster science objectives [Escoubet and Schmidt, 1997]. The experiment had to be versatile in order to cover large energy ranges, differentiate several ion populations (H+, He+, He++ and O+) and provide good angular sampling resolution, just to mention a few [Reme et al., 2001].

HIA has three concentric symmetric hemispheres, an inner hemisphere, an outer hemisphere with a circular opening and a small cap which holds the entrance aperture [Reme et al., 2001] (see Figure 3.3). Across the inner and outer hemispheres, there is a potential which causes only particles with a limited energy range and azimuth angle to enter (where the azimuth angle is the angle about the spin axis). This instrument has very good angular resolution, 5.6^{o} x 5.6^{o}, and measures particles within a fairly good energy range, about 5 eV/e to 32 keV/e [Reme et al., 2001]. It does not, however, differentiate between the different ion species.

CODIF's cross-section, as seen in Figure 3.3, is similar to that of HIA. However, it offers, among other things, a complete 3-dimensional distribution of the major ion populations, and it measures particles with energies in the interval of about 0.02 keV/e to 38 keV/e. Its angular resolution is 11.2^{o} x 22.5^{o}. This means that if one combines the measurements from HIA with those from CODIF, one will have very good coverage of all the different ion populations in the varied regions along Cluster's orbit.

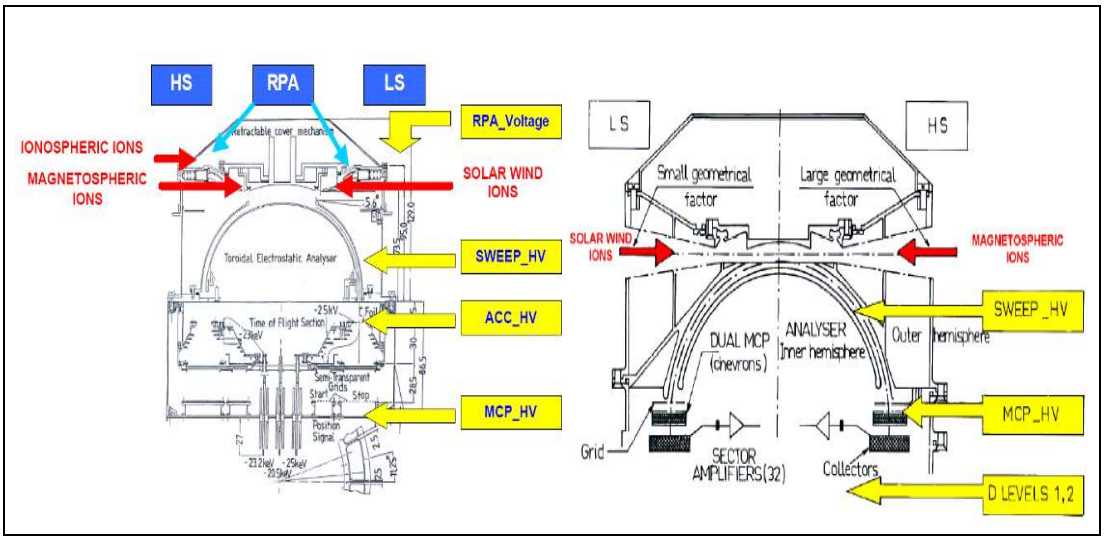

Figure 3.3: *Schematics of the two instruments within the CIS experiment: CODIF (left) and HIA (right) [Reme et al., 2001].*

3. 1.2. The Cluster Electric Field and Wave (EFW) instrument

The EFW instrument consists of 4 spherical probes, with a diameter of 8 cm placed onto wire booms. Two probes on opposite sides, are separated by 88 meters, see Figure 3.4.

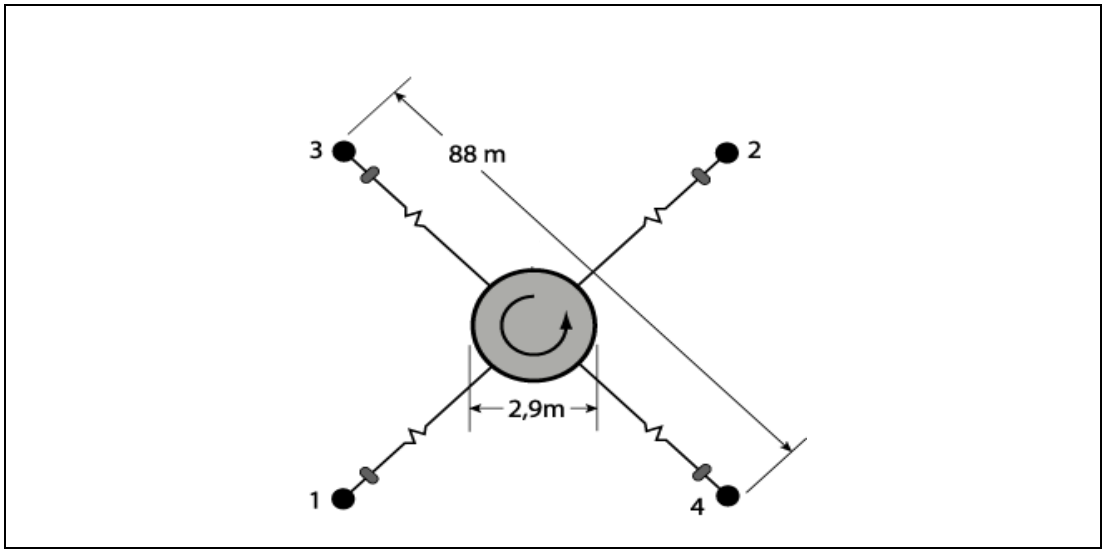

Figure 3.4: *The configuration of the EFW-probes.*

The instrument can operate in different modes, and thus measure several quantities. If the probes are given a bias current, they can give information about the electric field and the satellite potential. Since the satellite potential is affected by the plasma density, it can give a density estimate of the tenuous plasma [Pedersen et al., 2001].

If the probes are given a bias voltage, they can operate as current-collecting Langmuir probes, and measure plasma density and electron temperature [Gustafsson et al., 2001]. However, this mode is sensitive toward escaping photoelectrons, so it proves to be most reliable in dense plasmas.

Most of the measurements made by the EFW experiment have very good time resolutions. Electric field components can be measured with a resolution down to 0.1 ms, and the spacecraft potential can be gathered with a resolution down to 0.2 s [Gustafsson et al., 1997].

3. 1.3. The FluxGate Magnetometers (FGM) onboard the Cluster spacecraft

The FGM instrument is a vital part required to fulfill the objectives formulated in the Master Science Plan. It contributes to analyze the crossing of boundaries, investigate magnetic waves and identify the regions the satellites pass through.

Each FGM instrument consists of two triaxial fluxgate magnetic field sensors positioned on one out of two radial booms on the spacecraft, along with an electronic component on the satellite body. It can operate within different ranges, and with several sampling rates. The different ranges, along with their respective resolutions, are displayed in

Figure 3.5. However, range number 7 was only used initially for ground testing [Balogh et al., 2001]. The time resolution for the measured magnetic vectors, in three dimensions, is 201.75 Hz, but the data is filtered to match the telemetry transmission rate. The transmission rate can vary from 15.519 to 67.249 Hz [Balogh et al., 2001].

Range No.	Range	Resolution
2	−64 nT to +63.97 nT	7.8×10^{-3} nT
3	−256 nT to +255.87 nT	3.1×10^{-2} nT
4	−1024 nT to +1023.5 nT	0.125 nT
5	−4096 nT to +4094 nT	0.5 nT
7	−65536 nT to +65504 nT	8 nT

Figure 3.5: *Different operative ranges for the FGM instrument. Table taken from Balogh et al., 2001.*

The fluxgate magnetometer has been used since World War II. Basically, it consists of a current carrying coil wrapped around a ferrite core. When the current through the coil increases, the core "adds" to the magnetic field up to a certain level, until it reaches its saturation level. If the magnetometer is placed in an external magnetic field parallel to the field set up by the coil and core, the saturation level will be reached faster than normal. If the current polarity changes, so that the external field opposes the induced one, the saturation level will occur at a later time. With the modern version of this technique on Cluster, the geomagnetic field, for example, can be measured with an accuracy better than 1 nT.

3. 2. The European Incoherent SCATter (EISCAT) Svalbard Radar (ESR)

By using RAdio Detection And Ranging (RADAR) it is possible to investigate ionospheric properties like for example electron and positive ion density, velocity and temperature. This is done by sending a radio wave pulse in a certain direction, and then studying the reflected/scattered signal. The shape and strength of the signal that is received contains information about these parameters.

Referring to Figure 3.6, assuming a Maxwellian distribution, one can deduce positive ion temperature from the width of the Doppler spectrum. Also, the electron temperature is revealed by looking at the height of the "shoulders". The frequency shift, f_o, from the transmitted frequency yields the velocity of the scattering components. Finally, the number density is proportional to the power of the returning signal (area underneath the curve).

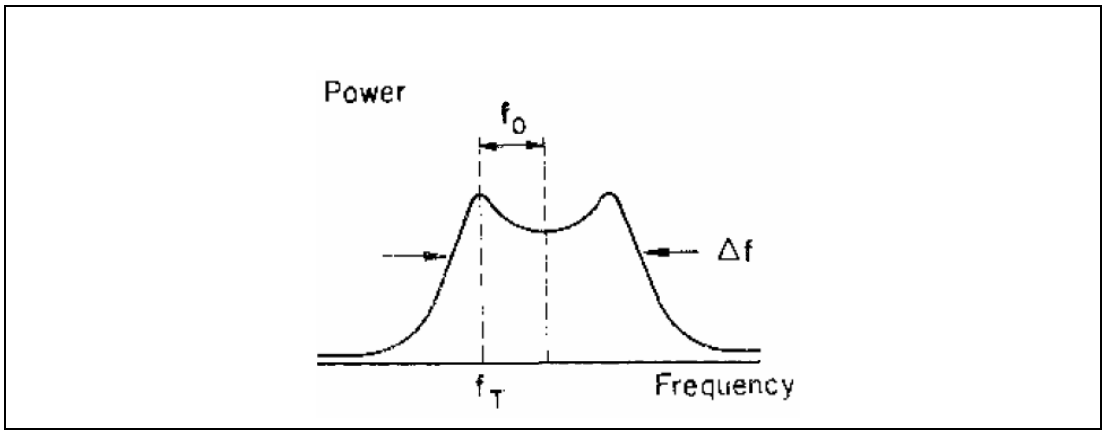

Figure 3.6: *An example of the Doppler spectrum of a backscattered pulse, received by EISCAT.*

The EISCAT Scientific Association operates the ESR, which consist of two parabolic dish antennas, with diameters of 32 and 42 meters, situated outside Longyearbyen on Svalbard (at approximately 78^o N, 16^o E). The 32m dish was operational in 1994, while the other was added in 1999. Having the two radars at the given location was recognized as being an important step towards understanding the dynamics within the polar cusp and across the polar cap. This is because Svalbard passes right beneath the dayside auroral region and the northern polar cusp as its location approaches 12 MLT (approximately 08:50 UT) (see Appendix A.3).

The 42m dish has a field-of-view parallel with the local magnetic field line, and is fixed in this position. The 32m antenna, however, is fully steerable. Both of the radars operate in the Ultra High Frequency region (UHF), transmitting within the frequency band 498-502 megahertz (MHz) and receiving at 485-515 MHz. The pulse length of their signals can vary from 1 microsecond to 0.2 milliseconds.

Figure 3.7: *The 32m and 42m parabolic dish situated outside Longyearbyen, Svalbard (photographed by Tony Van Eyken).*

3. 3. Geotail

The Geotail spacecraft was built by the Institute of Space and Astronautical Science (ISAS), in a collaboration with National Aeronautics and Space Administration (NASA). Its primary purpose is to study the dynamics of the magnetotail region, and it was launched on July 24, 1992. Together with the Wind, POLAR, SOHO and Cluster projects, it constitutes International Solar-Terrestrial Physics (ISTP) program.

Its orbit started out with a maximum apogee of about 200 Re in the magnetosphere's nightside, and a period ranging from one to four months. In 1995, the apogee value was reduced to 30 Re.

Its instruments can measure several quantities, including electron- and ion-velocity distributions (LEP-instrument), the solar wind dynamic pressure (CPI-instrument) and magnetic field variations (MGF-instrument), to name a few parameters which have been used in this paper.

Geotail's orbit will sometimes bring the spacecraft out into the solar wind for shorter periods. It will not drift far beyond the bow shock. So, when using its data, the time it takes for the solar wind conditions, measured by Geotail, to reach the bow shock, will be rather short, if not practically non-existent.

3. 4. The spacecraft potential - an aspect to consider

When applying satellites to make measurements in, or in the vicinity of, the magnetosphere, one often uses the plasma density to classify which region the satellite is situated in (i.e. the magnetosheath, the solar wind, the cusp and so forth). However, instruments which are designed to investigate the properties of the plasma, may not always quantify the exact parameters. This occurs because a sunlit spacecraft within a plasma, is subjected to several processes that can change its electric potential.

For example, in a tenuous plasma, such as the plasma "attached" to the open magnetic field lines across the polar cap, a spacecraft tends to acquire a significant positive potential, because incident photons will cause the emission of photoelectrons. Therefore, the potential of the spacecraft will be determined by the balance between collected electrons and emitted photoelectrons. This potential can be found by measuring the potential between the spacecraft and the EFW-probes (on board Cluster), located close to the plasma potential. It has been demonstrated that this parameter is related to the electron density and can be used for high time-resolution information.

To reduce the effects of having a satellite with a large positive potential, several space crafts are equipped with an ion emitter, for example Geotail and the Cluster satellites. Each of the Cluster spacecraft is fitted with the Active Spacecraft POtential Control (ASPOC) instrument. This instrument will then reduce the positive potential of the spacecraft and serve to make measurements more accurate [Torkar et al., 2001]. However, the information about the electron density as described in the paragraph above, will be lost when an ion emitter is activated.

Chapter 4

EISCAT-Cluster Conjunctions

To find data suited for this study, the predicted magnetic footprints of the Cluster satellites were investigated for the time interval from around mid-January to mid-April. If the footprint was at a given time located close to Svalbard, the next step was to see whether the EISCAT radars outside Longyearbyen was running at the time in question. Often, the radars were, in fact, activated, but only for short time periods. This made it difficult to investigate any large scale events closely. And, sometimes the radars had made long measurement sequences, without yielding much activity. In conclusion, having access to IMF and other solar wind parameters was recognized as an important factor, since this would affect position of the cusp and the dynamics within the magnetospheric cavity.

Table 4.1: Conjugated events with data from both ESR and Cluster

Date	Comments
2001-02-14	Found no data containing the O+ parameters
2001-02-21	Had gaps in ESR data, made it difficult to identify specific events
2002-02-13	Found little data from Cluster
2002-02-25	Cluster crosses MP ~09:25 UT + little activity in ESR data
2002-03-04	Cluster crosses MP fairly early + gaps in the ESR data
2002-03-16	Very little activity in the ion data from ESR
2002-03-23	Very little activity in the ion data from ESR
2002-04-04	Very little activity in the ion data from ESR
2003-03-27	Very little activity and much noise in the ion data from ESR
2004-02-11	Good data coverage from ground based and satellite instruments
2004-02-23	A lot of noise in the ESR data
2004-03-01	No obvious events in ESR data, especially after Cluster enters cusp
2004-03-13	Very little activity in the ion data from ESR
2004-04-13	Very little activity in the ion data from ESR
2004-04-20	Very little activity in the ion data from ESR

The dates where the magnetic footprint of Cluster seemed to pass close to Svalbard, during the time interval 08:00-12:00 UT, and when ESR at this time was making measurements, are included in Table 4.1. The reason why most of these dates were not further investigated is also commented. The searches performed to rule out any dates with little promising data, were done at the Cluster CSDSweb Quicklook Plot site and the Madrigal Experiment Selector (see Appendix B). There were several other incidents where the satellites' magnetic footprint could be found in the vicinity of Svalbard, but unfortunately the radars were not activated.

After searching the winter seasons of 2001 through 2004 for material, only one day was left, the 11. February, 2004. This date showed much promise when investigated at first. However, what originally was set up as the main focus of study was of course oxygen ion outflow. This chapter will uncover what eventually was found.

4. 1. Location of Cluster's magnetic footprint on 11. February, 2004

The EISCAT radars outside Longyearbyen on Svalbard can make reliable measurements of plasma parameters in the ionosphere up to heights of about 600 km. So, when the radars observe large vertical ion velocities, directed upwards, these events are classified as upflow events, not outflow events. This is because some, or possibly all of these ions may not have enough energy to escape the Earth's gravitational pull, or they may be decelerated by electric field parallel to the magnetic field. One can use the CIS experiment onboard the Cluster satellites to investigate the outflowing particles.

During late winter/early spring (mid-February through early April), the perigee of Cluster's orbit lies on the nightside, with an GSE X-component (see Appendix A.2) of about 4-6 R_e. The satellites then pass over the northern polar cap, where their configuration approach a tetrahedron. This is an optimal configuration to study small scale variations in the plasma.

When Cluster passes through the mantle and cusp region, the instruments may register outflowing particles several times. However, these events may be the result of solar wind particles, caught in the geomagnetic field, being mirrored further down in the ionosphere. So, to make sure that the outflowing particles originate in the ionosphere, one can look at the velocity of the oxygen ions.

The most difficult part of this operation is finding a close conjunction between the EISCAT and Cluster data. The first step is finding a date when one has satisfying measurements from both the radar and the satellites during the same time period. There were several examples where this was the case, but the very best day turned out to be the 11. February, 2004. Cluster's magnetic footprint passes just south of Svalbard around 10-11 UT, and both the radar and satellite data showed several events of increasing velocities and densities. So, initially this looked like a very interesting incident.

In Figure 4.1, the Orbital Visualization Tool 2.3 was used to plot Cluster's magnetic footprint. For the external magnetic field, Tsyganenko's 2001 model was used, corrected with D_{st}- (1 hr. resolution) and IMF-data (30 min. resolution)(right image). The

conditions in the solar wind were not extreme at any point during the interesting time interval, 08-12 UT, so the corrections to the footprint were rather small. The time interval was chosen to encompass 09:00 UT, since that correlates to 12 MLT for the location of the radars outside Longyearbyen.

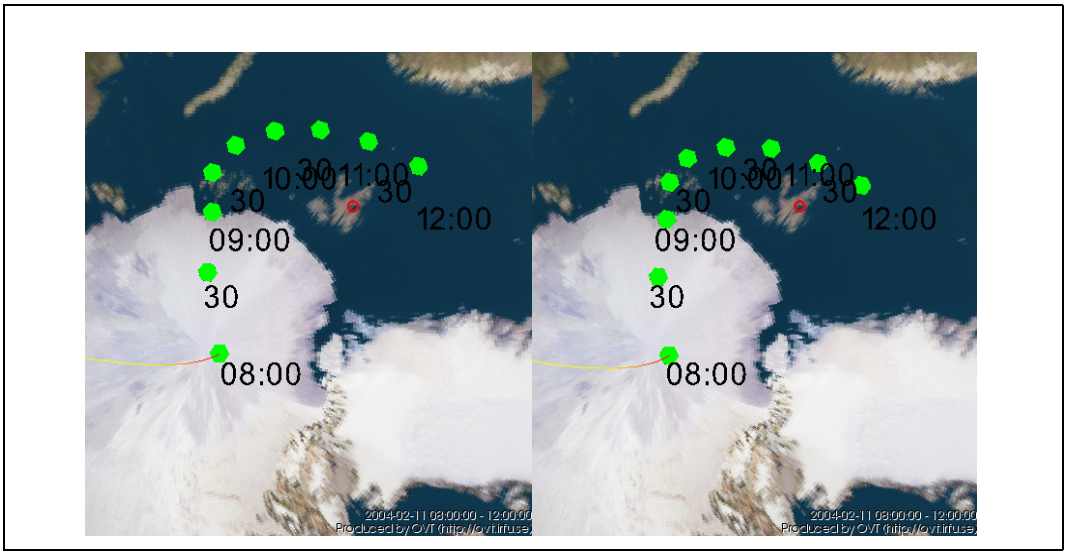

Figure 4.1: *Magnetic footprint of Cluster made with OVT 2.3,calculated with the Tsyganenko 2001 magnetic field model (left image) corrected with IMF- and Dst-data (right image). The red circles indicate the ESR's approximate position. The GSE X-axis points straight upwards.*

In Figure 4.1, the magnetic footprint locations predicted with the Tsyganenko 2001 magnetic field model with and without external correction parameters are presented. It is easy to see that the IMF and D_{st} conditions indeed make a difference. This, and the choice of which of the magnetic field models to use, play an important role in defining which magnetic field lines map out to a given satellite. The change in location of the footprint might not be huge, but it still gives us an idea of probable conjugate sites. In this case, the external parameters correcting the magnetic footprints, serve to bring these closer to Svalbard during the time interval 09:00-11:30 UT.

This image might represent an additional problem. From the observations made by the radars, one cannot simply assume that the structures in the plasma are large enough to cover the spatial interval in latitude and longitude between Longyearbyen and Cluster's footprint projected to a certain altitude. So, since one cannot postulate that the footprints pass exactly over the radar site, one can only hope to find similar events at Cluster and EISCAT, with a suitable time delay. One can also look for incidents where sudden changes in solar wind parameters reach Cluster, and then propagate down into the ionosphere, and then see whether those changes trigger outflow events.

The EISCAT's geographic coordinates are approximately 78^{o}N, and 16^{o}E. The latitudinal separation between these coordinates and the Cluster footprints' coordinates varies from 0^{o} to ~8^{o} during the time period 08:30-11:30 UT. However, during most of the same interval, it is apparent that the distance in longitudinal direction is quite large.

For example, at 09:30 UT, Cluster's footprint's coordinates are 80.88^{o}N, 55.91^{o}E. The longitudinal distance between the EISCAT location, 16^{o}E, and the footprint, if one assume an average latitudinal position of 80^{o}N, will then be:

$$d = R_e \cdot \cos\left(\frac{2\pi \cdot 80°}{360°}\right) \cdot \frac{2\pi \cdot (55,91° - 16°)}{360°} \approx 770km \quad (4.1)$$

where R_e is the Earth's radius, ~6378 km.

An hour later, at 10:30 UT, this distance has decreased to about 500 km. So, this distance makes it impossible to simply assume a one-to-one correspondence between events measured by Cluster, and those measured by the EISCAT radars. However, the data may yet provide us with information about time-delays, and reactions to sudden changes in the solar wind (IMF, dynamic pressure etc.).

As mentioned above, the location of the footprints are based on a model which may not yield exact solutions in areas where electric fields, parallel to the magnetic field, are present. Also, field aligned currents could also influence the shape of the magnetic field lines. In Figure 4.5, one can see that there is a high plasma density, mainly because of the fact that the polar cusp is an area where solar wind particles are injected into the magnetosphere and ionosphere. Therefore, the mapping of the footprints can only serve as an approximate location.

4. 2. Cluster Boundary Crossings

Svalbard's longitudinal location is such that there is about a three hour difference between the time given in UT, compared to the magnetic local time (MLT) at the date in question (11. Feb., 2004). So, at 0900 UT, the EISCAT radar is located at noon MLT. Thus, to consider whether the radars are making measurements in the polar cusp at 1000-1100 UT, is a matter of defining the width of the cusp. This is not an easy task. The data from Cluster compared with its footprints may reveal a solution.

The cusp is a region where one should expect the plasma density to increase, because of the plasma in the solar wind and magnetosheath being injected in this region. This change can be seen in Cluster data from the CIS- and EFW-instruments. The latter plotting the satellite potential. Another parameter that is influenced by a transition into the cusp, is the total magnetic field strength. It should experience a decrease as it crosses the cusp boundary [Fuselier et al., 2003][Russell, 2000].

So, entering the cusp, one should see an increase in electron and ion energy levels. This is quite clearly evident in Figure 4.2, where a boundary is evident first at 09:00 UT and then again at about 09:05 UT. Therefore, these plots suggest that Cluster enters the cusp at about 09:05 UT, and traverses the magnetopause at about 11:20 UT, as can be seen from the elevated flux of electrons with high energies. Another feature evident in the electron spectrogram below, is the pulsed injection typical of the polar cusp. The cusp transition will be further investigated below.

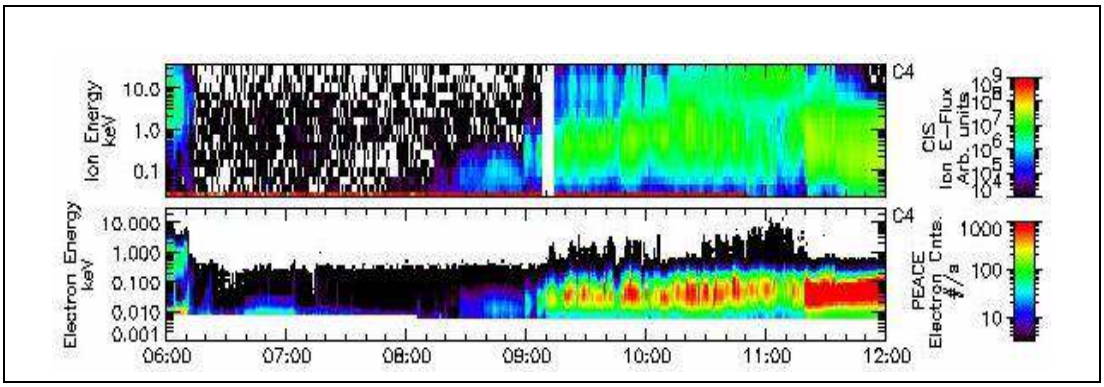

Figure 4.2: *Ion and electron energy spectrograms for Cluster (SC4).Result downloaded from Cluster Quicklook plots (see Appendix B).*

If one assumes that entering the cusp is like traversing a plane, then the analysis method described in Appendix A.5 can be used. The technique applied in Figure 4.3 for finding the time delay between the perturbation in the magnetic field data from the different satellites is not accurate. But, it will be sufficient for determining the approximate direction of the plane's movement. All that is needed in addition to this, is the distances between the satellites, see Table 4.2.

Table 4.2: The position of the Cluster satellites at 09:04:30 UT

SC	GSE-X (km)	GSE-Y (km)	GSE-Z (km)
1	4560.922	19163.314	39262.292
2	4230.992	18868.006	39102.081
3	4592.813	19034.347	39137.742
4	4229.931	18879.219	38929.938

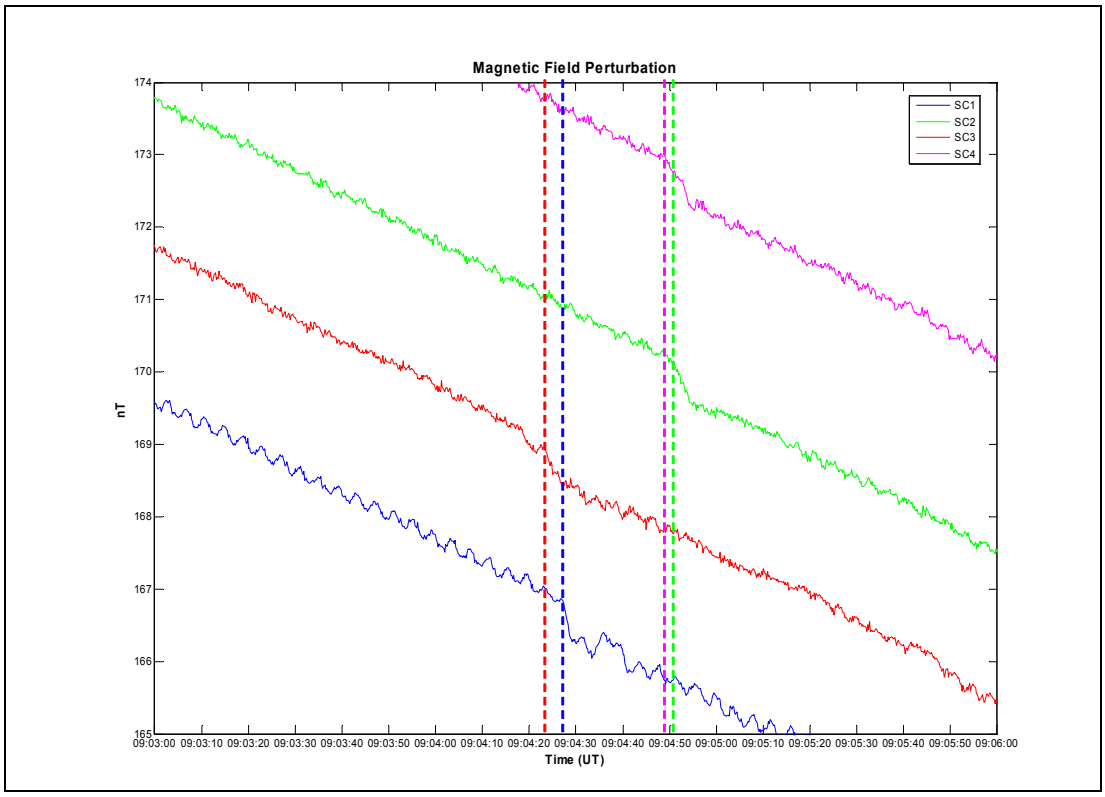

Figure 4.3: *Decrease of magnetic field strength at cusp entry.*

The plane's velocity along the normal vector in the satellites' rest frame can now readily be calculated. This yields $\vec{V} = [-12438, -14, 1916]\frac{m}{s}$, in coordinates parallel to their respective GSE-axes. The velocity component in the anti-sunward direction clearly dominates. However, since $\vec{V}$ is expressed in a coordinate system moving along with the satellites, one must add the velocity vector of the reference satellite (given in GSE-coordinates) to get an estimate of the plane's velocity in pure GSE-coordinates. The velocity vector of the reference satellite is approximately $\vec{V}_{ref} = [3000, 1700, 1100]\frac{m}{s}$. Thus, we get $\vec{V}_{plane} = \vec{V} + \vec{V}_{ref} = [-9438, 1686, 3016]\frac{m}{s}$.

Now, it is clear that the X-component dominates, but there is also a small Y-component. If one examines the convection pattern in the ionosphere at 09:00-09:02 UT, as seen in Figure 4.4, it is evident that one has convection velocities mainly in the negative X-direction, but also in the positive Y-direction. This is in agreement with the calculated $\vec{V}_{plane}$.

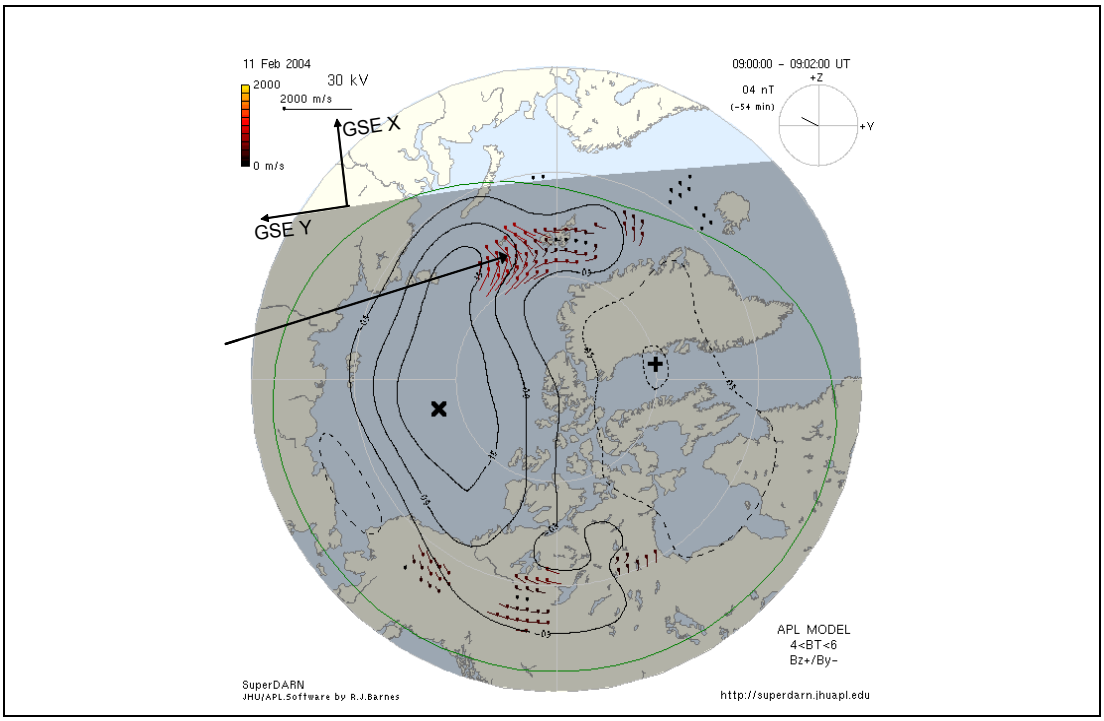

Figure 4.4: *Convection plot of the northern polar ionosphere. The arrow indicates Cluster's magnetic footprint's approximate position at 09:00 UT, and the GSE X- and Y-axis are also shown.*

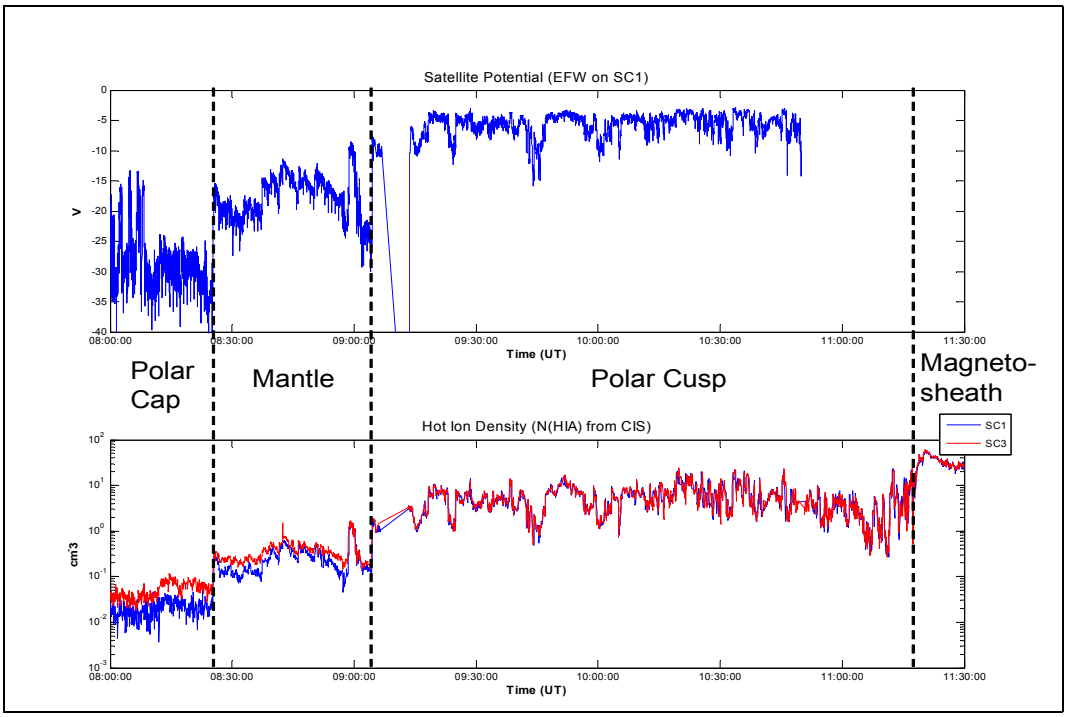

Figure 4.5: *Satellite potential measured by the EFW-instrument onboard SC1 (top), and ion-densities measured by CIS (HIA) onboard SC1 (green) and SC3 (red). The different regimes that the satellites encounter, are also indicated (vertical dotted lines).*

In Figure 4.5, one region indicated is the mantle, also called plasma mantle. This is a region lying on the immediate poleward side of the polar cusps, and on the inside of the magnetopause as one moves tailwards. The plasma flow within this region is mainly directed toward the nightside of the magnetosphere, with typical velocities of 100 km/s [Rosenbauer et al., 1975]. Compared to the plasma across the polar cap, one could expect to find increased plasma density and temperature in the mantle.

From looking at Figure 4.5 it is apparent that although Cluster measures an increase in density parameters right before 0900 UT, the satellites enter the cusp fully around 0904-0905 UT. So, the magnetic footprints from this point and onwards, to about 1120 UT, corresponds to locations where one will be able to observe the polar cusp.

From Figure 4.4, it is clear the Cluster maps down to the ionospheric cusp inflow region. At the same time, this figure shows that EISCAT is located west of this inflow region. If one considers the latitudinal and longitudinal position of Cluster's footprints, it is obvious that they are located east of Svalbard until the satellites enter the magnetosheath (~1120 UT). During the time interval 0900-1130 UT, the footprints move from north to south of Svalbard. Cluster does not leave the cusp region within this time period, and since the solar wind conditions are not extreme, it's fairly safe to say that the radars are not located outside the cusp on either the southern or the northern side.

The orbit of the Cluster spacecraft will not lead them through the middle of the cusp region, at least not at the date in question. Cluster's position at the dayside is at the afternoon flank, see Figure 4.6.

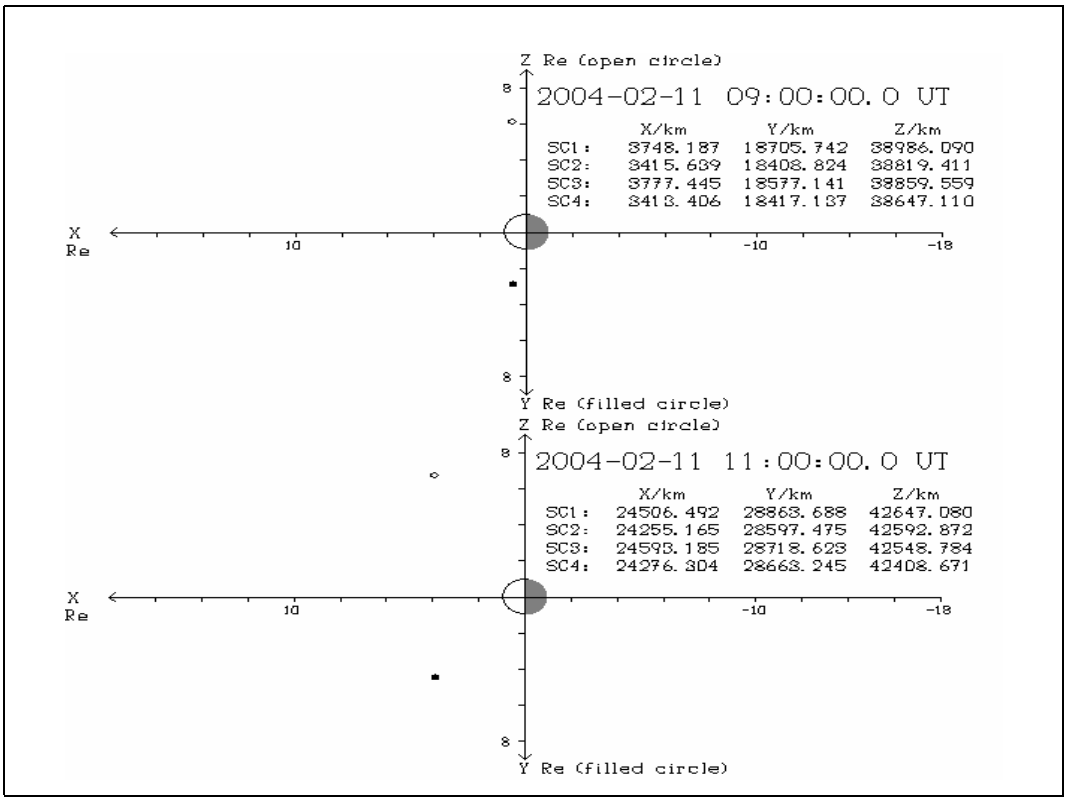

Figure 4.6: *Cluster's position at 09:00 UT and 11:00 UT, both in the GSE X-Z plane (open circle) and the GSE X-Y plane (filled circle).*

In Figure 4.6, the open and filled circles show the position of the reference satellite, which is SC3. In the tables included, one can see the GSE coordinates of all the four satellites.

At the center of the cusp, the magnetic field strength is expected to reach a minimum. However, Cluster's orbit during this period of the year, brings the satellites out into the afternoon sector, so this may not distinctly show up in the magnetic field data. The steady decrease in the total magnetic field strength in Figure 4.7 can probably be attributed to the increase in the radial distance of the satellites from the Earth. The geomagnetic field strength is proportional to r^{-3}, where r is the distance from the Earth's center. So, one can clearly see a reduction in the field strength up until around 10:15 UT. After this, the field fluctuates, but stays fairly constant.

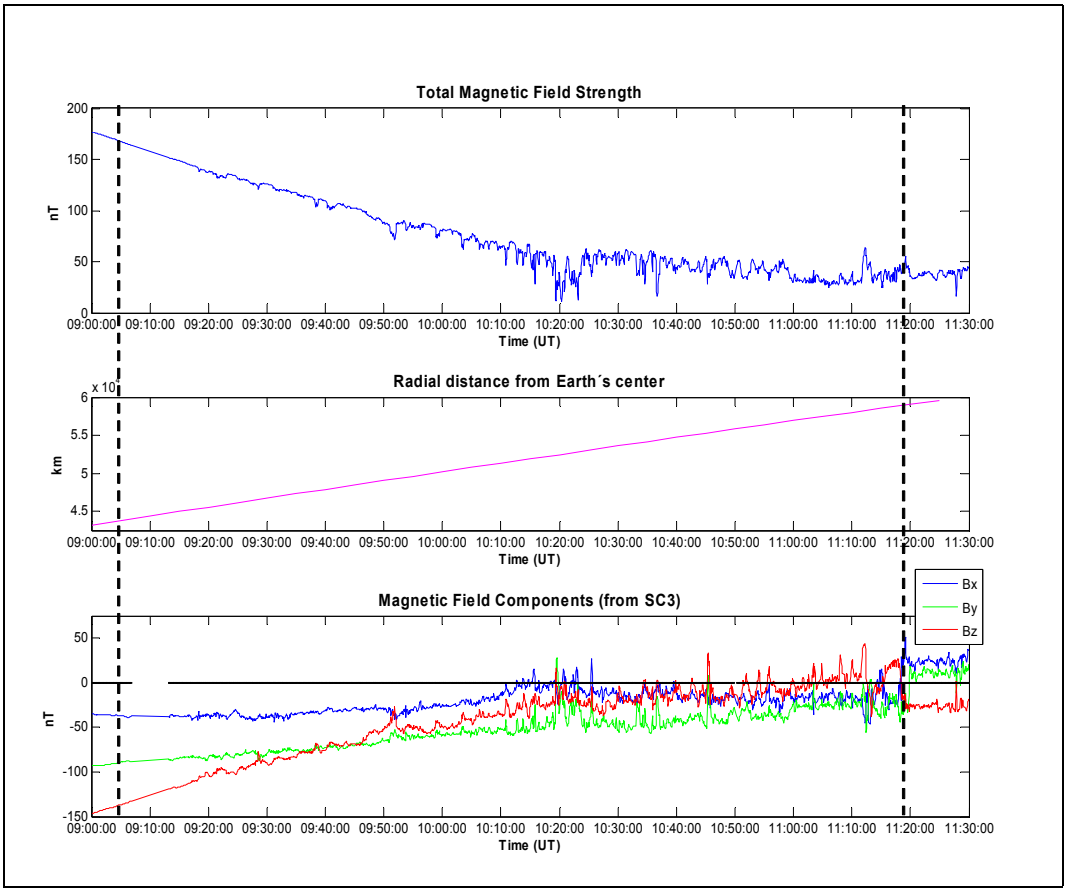

Figure 4.7: *Total magnetic field strength, and its three components in GSE-coordinates, measured by the FGM-instrument onboard SC3. The two vertical purple lines indicate cusp entry (left) and magnetopause crossing (right).*

Figure 4.7 further indicates that the By-component is negative, for the time period the spacecraft spend in the cusp. This is expected, since their location is in the afternoon sector. In Figure 4.8, one can see how Cluster could have moved through the cusp region. The star in this figure marks the most likely position of the satellites, based on the Bz measurements in Figure 4.7. It shows that Bz turns from negative to positive a couple of minutes past 11 o'clock. The Bx-component stays negative until Cluster enters the magnetosheath.

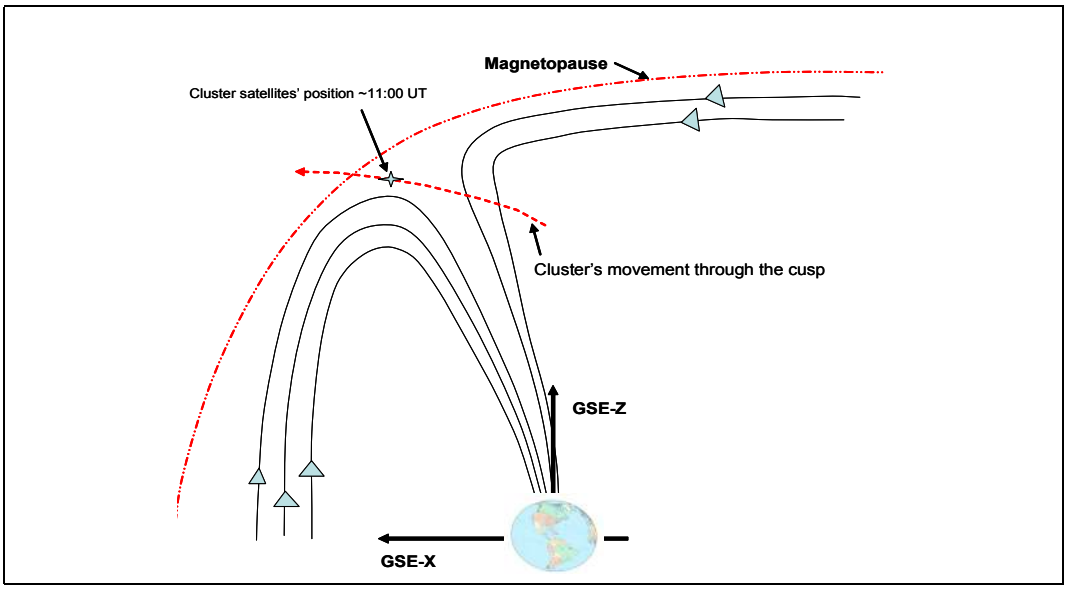

Figure 4.8: *An image of how Cluster could pass through the cusp region on 11th of February, 2004 (not to scale).*

4. 3. IMF data from Geotail

Several researchers have dealt with the problem of the time delay between particles escaping the ionosphere, and the ones picked up by instruments in satellites ([Fuselier et al., 2001],[Bouhram et al., 2003]). Cluster orbits the Earth with an altitude of 5-7 R_e (see Figure 4.6) during the time interval 09:00-11:00 UT (Feb. 11th, 2004). Since the acceleration mechanisms causing ions to flow out of the ionosphere have yet to be defined, it is difficult to estimate the time it will take for an oxygen ion to move from an altitude of 400-600 km up to 5-7 R_e. In addition, the ions do not travel in straight lines, but follow the curved magnetic field lines. But, the plasma particles convect perpendicularly to the magnetic field lines within the magnetosphere because of interactions with the solar wind and the interplanetary magnetic field (IMF). So, a good oversight of sudden changes in the these conditions is required. The Geotail satellite can provide this.

The measured plasma densities and especially high particle velocities indicate that the Geotail satellite was in the solar wind, and not within the magnetosheath region. This could be further verified by comparing IMF measurements from Geotail with measurements made by another satellite positioned in the solar wind. The Advanced Composition Explorer (ACE) satellite has a GSE X-coordinate of approximately 220 R_e during the time interval in question, and orbits one of the Lagrange points, where the gravitational pull from the Sun and the Earth is equal. Since the solar plasma flows basically radially away from the Sun, carrying with it the IMF, the two satellites should, despite their spatial separation, measure similar parameters concerning the magnetic field. In Figure 4.9, the ACE and Geotail IMF-measurements are presented. The ACE data has been shifted 52 minutes, which seemed to make the two sets of data match fairly well.

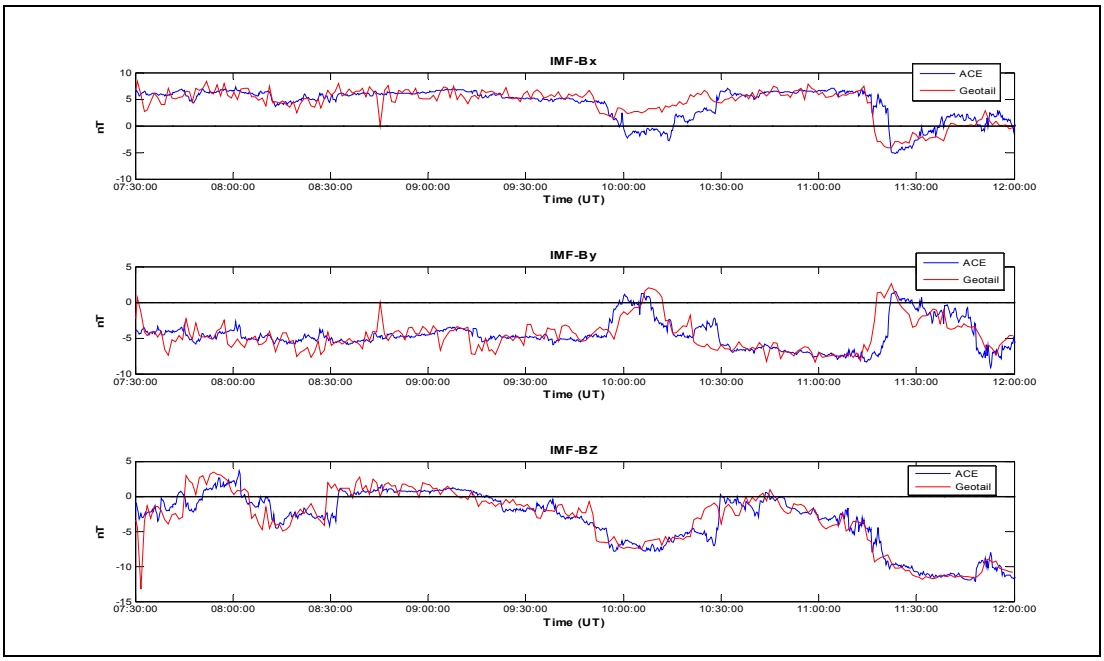

Figure 4.9: *Comparison of the IMF measured by the ACE and Geotail spacecraft (a 52 minute delay has been inferred on the ACE-data).*

As can be seen, the data in Figure 4.9 do not match perfectly. This is because the velocity of the solar wind plasma changes. Therefore, the 52 minute delay may only be accurate in some short intervals. But, it illustrates that the large scale variations of the IMF as observed by ACE, are "reproduced" by Geotail's magnetometer (MGF). And, it is fortunate that Geotail has an orbit that allows it to spend fairly large temporal intervals within the solar wind, since the parameters measured so close to the magnetopause are indeed more reliable than the ones taken so far upstream as ACE's location.

The solar wind particle density and its velocity vectors can be found in Figure 4.10. The SW Theta, describes the angle between the velocity-vector and the ecliptic, and the SW Phi describes the angle between the GSE-X direction and the velocity-vector. These parameters show that the solar wind flows almost parallel to the ecliptic, and that, in GSE-coordinates, the X-component clearly dominates.

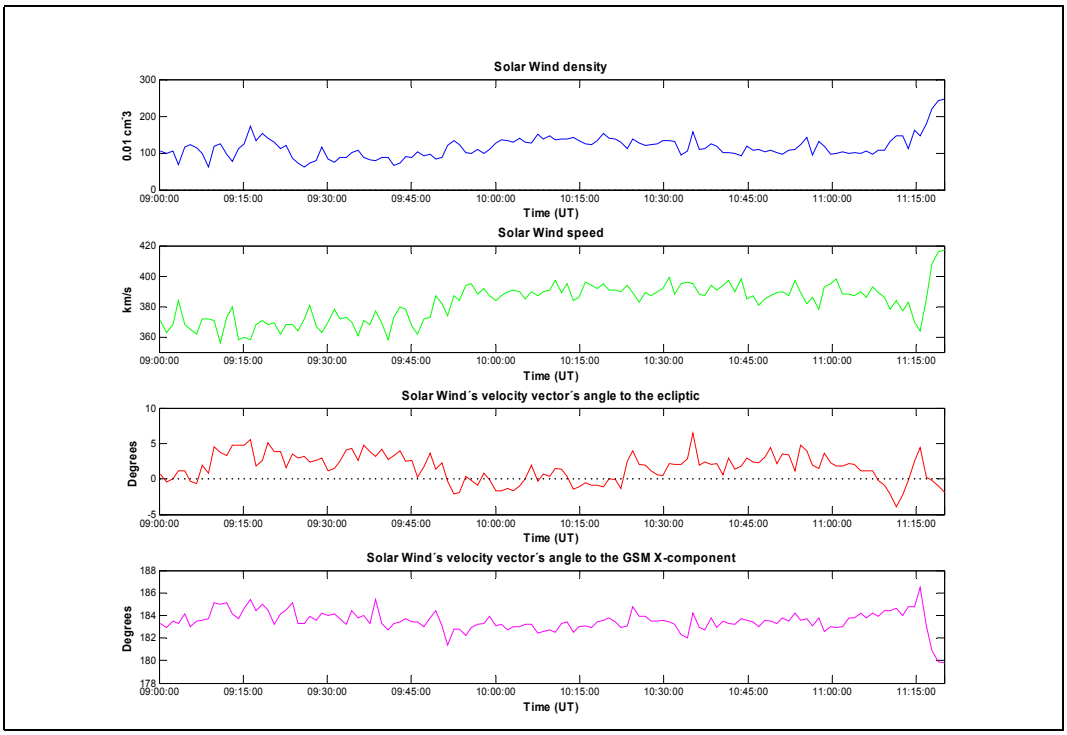

Figure 4.10: *Plasma density and solar wind velocity, measured by Geotail. The parameters were downloaded from http://cdaweb.gsfc.nasa.gov/cdaweb/istp_public/.*

The position of the satellite is shown in Figure 4.11, along with an average position of the magnetosheath. The satellite is close enough to the bowshock that the time it takes for the solar wind plasma to move from Geotail's position to the bowshock is practically negligible.

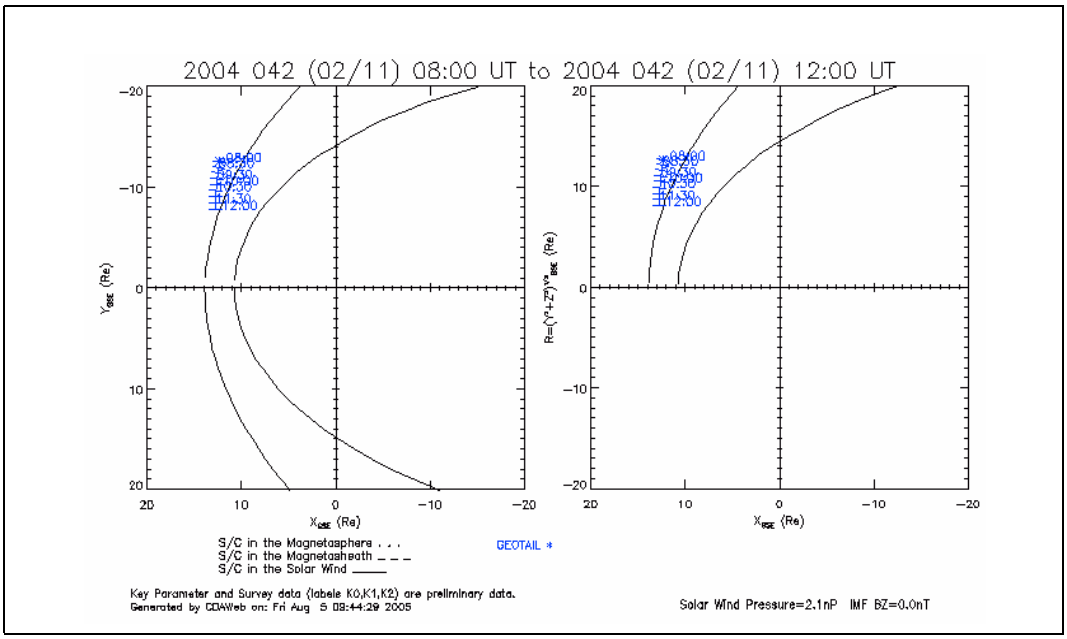

Figure 4.11: *The position of the Geotail satellite in GSE coordinates, plotted every 30 minutes from 08:00 UT (top) to 12:00 UT (bottom).*

As mentioned earlier, the IMF dictates to a large degree the convection patterns within the magnetosphere. It is therefore important to have an oversight of the sudden changes in solar wind conditions, so that one can take this into consideration when looking at data gathered by satellites close to the Earth.

Looking at Geotail's IMF-data in Figure 4.9 (red line), one can see that the IMF Bx-component is mainly positive during the interval 09:00-11:00 UT. This component doesn't influence the convection patterns to a large degree. The By-component is predominantly negative, except a positive bay a few minutes past 10:00 UT. This could cause the center of the cusp to move from the morning side (when By<0), to the afternoon side (when By>0).

The Bz-component makes a negative dip right before 10:00 UT, which probably enhances the anti-sunward convection velocity within the magnetosphere. Also, the By-component experiences a fairly abrupt positive turning right before 10:00 UT. This correlates with the enhanced anti-sunward convection measured by the EISCAT-radar (32m) as seen in Figure 4.12, as the entry region of the convecting plasma across the polar cap shifts to match the MLT sector (see Appendix A.3) of Svalbard.

The ExB-velocity in Figure 4.12, is averaged a bit to remove what can be mistaken as noise in the data. It is averaged over 9 measurement-points to smooth the graph. When comparing this parameter to the convection velocity picked up by the 32m EISCAT radar, one can neglect the high frequency fluctuations in the electric field data measured by a satellite at a high altitude (such as Cluster at this time). Previous studies, using two satellites at different altitudes but at conjugated magnetic field lines, has indicated that the mapping factor of the electric field from high to low altitudes is dependent on the wavelength of the variations [Weimer et al., 1985]. Weimer et al. (1985) found that this effect was effective especially in the auroral zone, which of course includes the cusp. This means that if one measures the electric field at successively decreasing altitude, one will experience a filtering of the high frequency oscillations, leaving only the more large-scale electric fields.

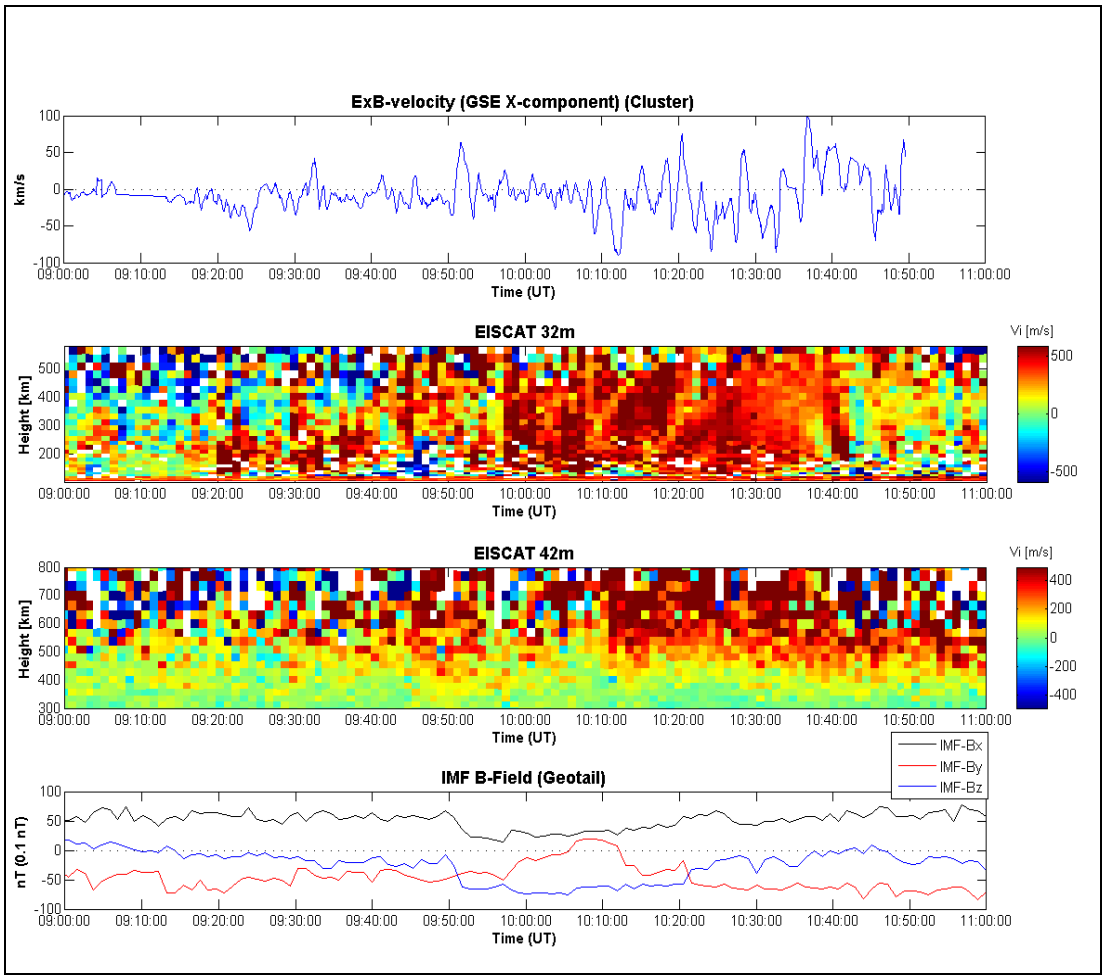

Figure 4.12: *EISCAT-data showing ionospheric plasma velocities (positive -> away from radar) across the polar region and parallel to the local magnetic field line, convection velocity (GSE-X component) from Cluster and IMF-data from Geotail.*

In the figure above, the interval has been chosen to be 09:00 to 11:00 UT. It appears that before 09:00 UT, there is not any conjunction with the Cluster measurements (Cluster is situated in the cusp from 09:04 to 11:20 UT). If there is an event measured by EISCAT after 11:00 UT, it probably would not have time to reach the satellites until they cross the magnetopause.

The IMF By-component can change the symmetry of convection across the pole. So, when By turns from about -5 nT right before 10:00 UT to weakly positive between 10:00 and 10:10 UT, the plasma entry region, and the cusp, will move towards the afternoon sector, as mentioned earlier. This could explain why the radar, which is about an hour past 12 MLT, can suddenly experience a large increase in ionospheric velocities.

Also, looking at the ExB-velocity's X-component displayed in Figure 4.12, it is evident that this parameter oscillates quite a bit. However, from about 10:08 UT to 10:32 UT there is larger variability in this component, but it is negative on average. This corresponds well with the fact that the 32m radar observes bursts of enhanced convection poleward into the polar cap. Due to large spatial and temporal variation in

cusp dynamics and the time delays of momentum transfer, a one-to-one correlation of the plasma flow measured by the radar and the satellites cannot be expected.

4. 4. Upflow versus outflow

The positive ions' velocities, parallel to the magnetic field, are plotted in Figure 4.13. The velocities, from the CIS instrument, are presented in GSE coordinates. To obtain the velocities parallel to the magnetic field, Equation (4.2) can be used. The negative sign just ensures that positive values of v_{par} denote particles travelling outbound, away from Earth's atmosphere, in the northern hemisphere.

$$v_{par} = -\frac{\vec{v} \cdot \vec{B}}{|B|} \tag{4.2}$$

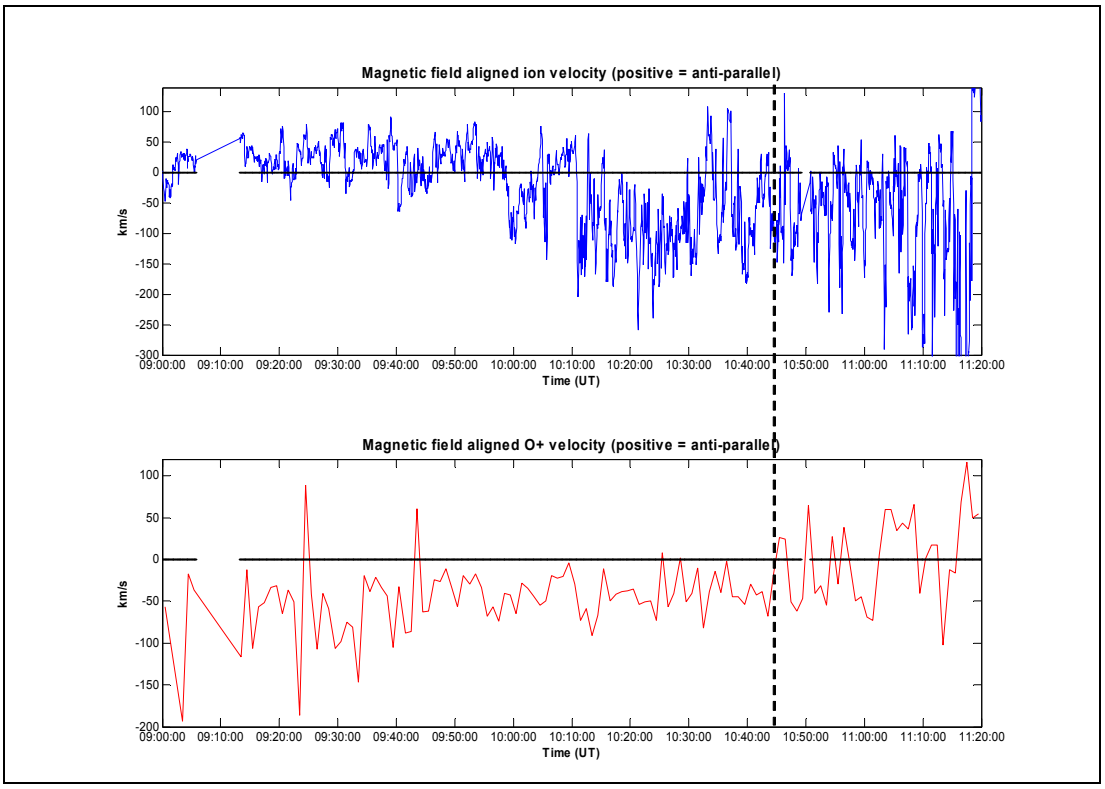

Figure 4.13: *Velocities for both oxygen-ions and ions in general (H+, He+, He++ and O+) parallel to the magnetic field line. Both parameters taken from SC3. The vertical dashed line indicates the start of a series of outflows.*

At 10:45 UT (see Figure 4.13) a series of outflow events commence. There does not seem to be a strong correlation between outflowing positive ions in general, and the outflowing O+ particles. The reason for focusing on this event, is simply that the EISCAT 42m radar does not observe stable intervals of upflowing particles until about 10:10 UT (see Figure 4.12), and that this may be caused by something that is also responsible for the measurable change made by Cluster some 35 minutes later.

As mentioned in "Ionospheric outflow" on page 23, global outflow rates can vary with sudden changes in the solar wind dynamic pressure. In Figure 4.14, the dynamic pressure within the solar wind is plotted. The expression for this pressure is given by Equation (2.19). However, in the plot below, the mass contribution from alpha-particles (double ionized helium) has been included. They constitute about 20 percent of the solar wind [Walker and Russell, 1995].

The pressure oscillates quite a bit, but at 10:00 UT it goes through a rapid increase. After this, it is further strengthened, which probably causes the magnetopause subsolar point to move towards the Earth (the MP subsolar point is the MP's position along the Sun-Earth line).

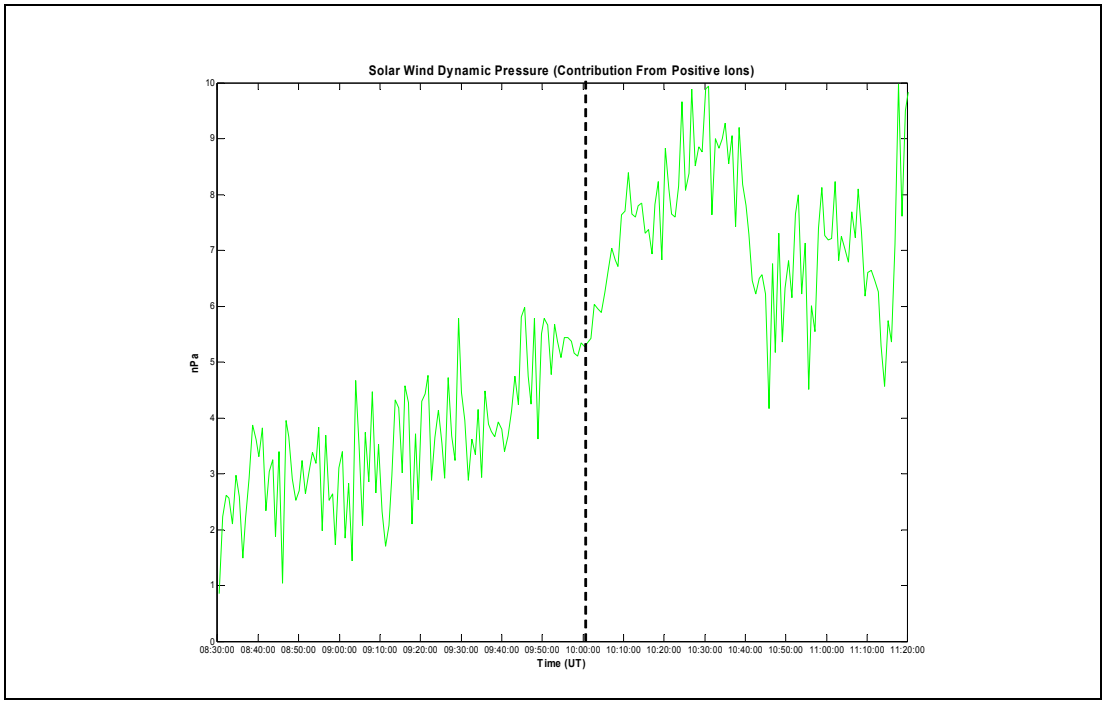

Figure 4.14: *Dynamic Solar Wind Pressure. The dashed vertical line indicates the pressure pulse which may have caused an acceleration of ionospheric particles.*

This pressure perturbation needs some time to manifest itself throughout the magnetospheric cavity. It has to traverse the magnetosheath and propagate to the ionosphere, before it could cause any particles to escape. Fuselier et al. (2002) suggest that the ionospheric response to such a perturbation is prompt. Furthermore, as can be seen from Figure 4.11, the Geotail satellite is in such a position that the time it takes for the solar wind to close the gap between the satellite and the bow shock is negligible. So, the total time delay between the point when the pressure pulse is measured and when Cluster can "see" its effect, consists of three parts: the time it takes for the disturbance to traverse the magnetosheath, the interval where it propagates to the ionosphere, and finally the travel-time for the particle flowing from the ionosphere to the satellite.

Lockwood et. al (1989) provide an approximate expression for the time a perturbation needs to propagate through the magnetosheath:

$$T_{bm} = \frac{(X_b - X_m)}{\langle V_{sh} \rangle} \tag{4.3}$$

where X_b and X_m is the X coordinate (GSE) of the bow shock and magnetopause, respectively. To continue, one assumes that $X_b \approx \frac{4}{3} X_m$ and that $\langle V_{sh} \rangle = \frac{u_{sw}}{8}$, where u_{sw} is the solar wind speed [Lockwood et. al, 1989]. For the time interval given in Figure 4.10, a reasonable average value of this speed would be 380 $\frac{km}{s}$. In Figure 4.15, Equation (2.21) was used with Geotail data to plot the distance, L_{mp} (in Earth radii), from the Earth's center to the magnetopause along the Sun-Earth line. An average value for L_{mp} during this time-interval was approximately 9.86 Re, so having $X_m = 10Re = 63780km$ seems valid.

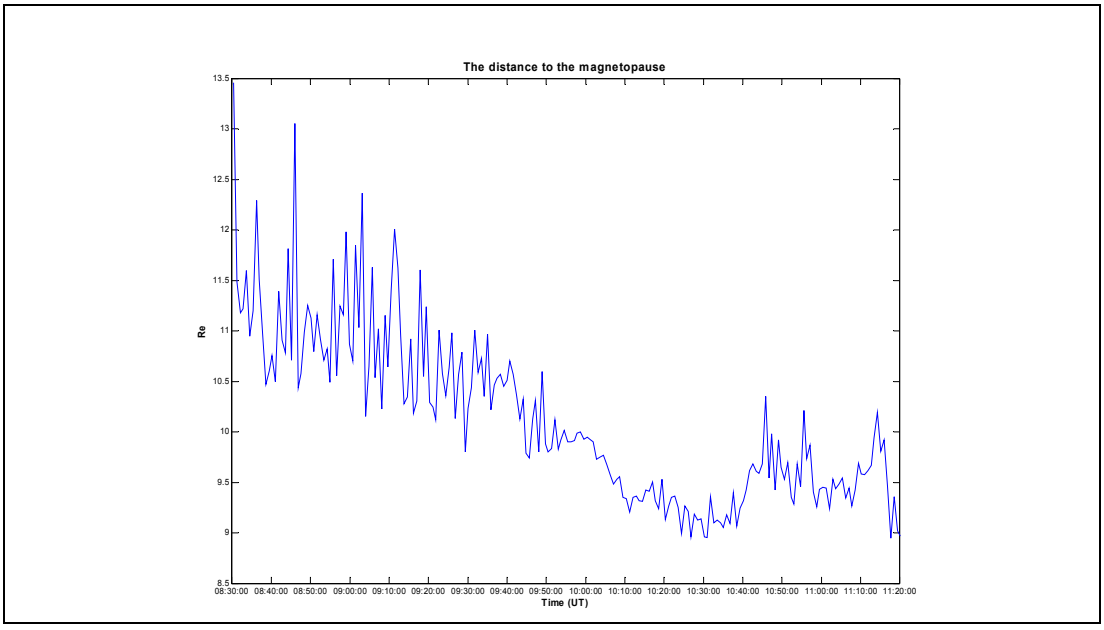

Figure 4.15: *The distance from the Earth's center to the magnetopause along the Sun-Earth line.*

The assumptions above yield $T_{bm} = \frac{8}{3} \cdot \frac{X_m}{u_{sw}} \approx 448s$, which is about 7.5 minutes.

Furthermore, one can assume a disturbance within the magnetosphere to travel parallel the magnetic field lines as an Alfvén wave. A wave of this type displaces the magnetic field line perpendicularly, while propagating with the Alfvén velocity, $v_A = \frac{B}{\sqrt{\mu_0 \rho_0}}$, where μ_0 is the permeability of free space and ρ_0 is the density of the unperturbed plasma. Lockwood et. al (1989) could reveal a travel time from the magnetopause to the ionosphere of about 2 minutes.

So, the sudden density increase measured by Geotail at 10:00 UT would reach the ionosphere around 10:10 UT according to these parameters. This fits well with the sudden enhancement of upflowing ions, measured by the EISCAT 42m radar (see Figure 4.12).

At approximately 10:45 UT, Cluster measures O+ particles flowing outwards along the magnetic field lines, indicating a mass ejection from the ionosphere. If these particles are ejected because of the pressure increase measured by Geotail at 10:00 UT, this implicates a travel time for the oxygen ions of about 35 minutes. At this time, the GSE coordinates of the Cluster reference satellite, SC3, is [3.472, 4.341, 6.660] in units of Earth radii. If one assumes that the particles travelling from the ionosphere and to the Cluster satellites move along approximately straight lines, instead of the slightly curved magnetic field lines, the distance they would have to traverse from an altitude of 500 km is $d = R_e \cdot \sqrt{X^2 + Y^2 + Z^2} - R_e - 500km \approx 48500km$. A particle with a velocity of 25 km/s, as seen at 10:45 UT in Figure 4.13, would cover this distance in about 32 minutes. This, of course, implies that the particle is energized instantly. However, the acceleration region, in which the particle receives its outflow velocity, may reach all the way up to an altitude of more than 20000 km [Bouhram et al., 2003]. This fact adds more time to the total evaluation. But, at least it does not rule out the idea that the increased oxygen ion flux measured by Cluster was energized by the same process that caused enhanced upward ion velocities in the ionosphere, namely the pressure pulse from the solar wind striking the magnetosphere at 10:00 UT.

The convection of plasma further complicates the situation. If one had observed sunward convection across the polar cap, the chance that Cluster could observe particles first measured by EISCAT would exist. However, this is not the case. In Figure 4.16, convection plots from the SuperDARN radars are presented. SuperDARN consists of a series of radar facilities that can monitor plasma parameters within the ionosphere. They make certain measurements, and then apply a model to describe the total plasma convection across the polar cap.

Figure 4.16 cover the time interval 10:10-10:42 UT with a plot every 10 minutes. They also include the IMF-vector superimposed on the Y-Z plane. The large arrows have just been put there to show the approximate position of the magnetic footprint of Cluster.

From the images below, it is apparent that any particles with an ionospheric origin measured by the Cluster satellites, could not belong to magnetic field lines convecting from the EISCAT-radar's (42m) field of view towards Cluster's magnetic footprint. But, it definitely seems as though the upflow, maybe outflow, event commencing after the solar wind pressure increase is a significant event, covering large spatial areas, as already suggested ([Cully et al., 2003], [Bouhram et al., 2004]).

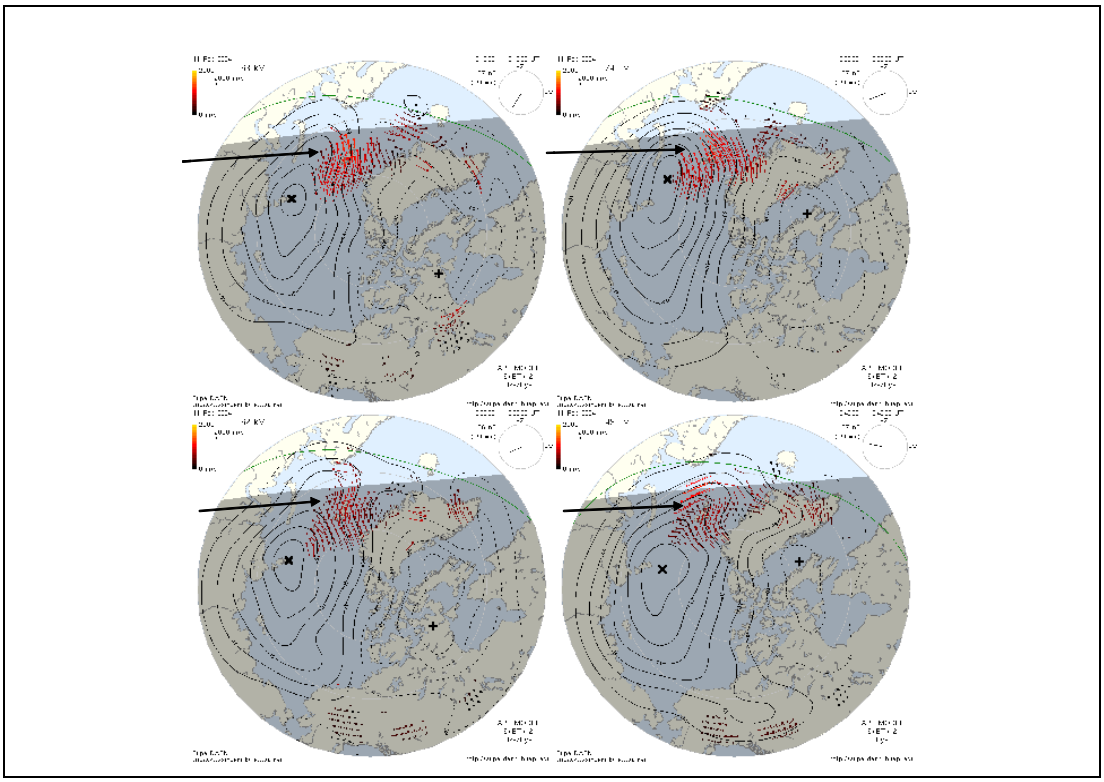

Figure 4.16: *SuperDARN data with an adapted field model.*

One thing worth some attention in the figure above, is the increased ionospheric velocities registered by the SuperDARN radars right above Svalbard. In Figure 4.12, EISCAT observed enhanced poleward convection at about 10:08 UT to 10:42 UT. This fits well with the data presented in Figure 4.16. Cluster's magnetic footprint is also clearly in the vicinity of this dynamic region, so it is clear that conjugated measurements between the radar and satellites are possible, however, only applied to large-scale phenomena which has the ability to cover the spatial distance between the satellites' magnetic footprints and the ESR.

4. 5. A possible FTE-passage

Above, in Figure 4.7, one can see a perturbation in the magnetic field, as measured on board SC3. This disturbance proved to be a suitable event to use the curlometer method described in Appendix A.4. The resulting current density and high temporal resolution measurements of the magnetic field strength from all the Cluster spacecraft can be found in Figure 4.17, along with the calculated ExB-velocity from SC3. A fairly broad time interval is presented to make the dipolar signature of the current density more apparent.

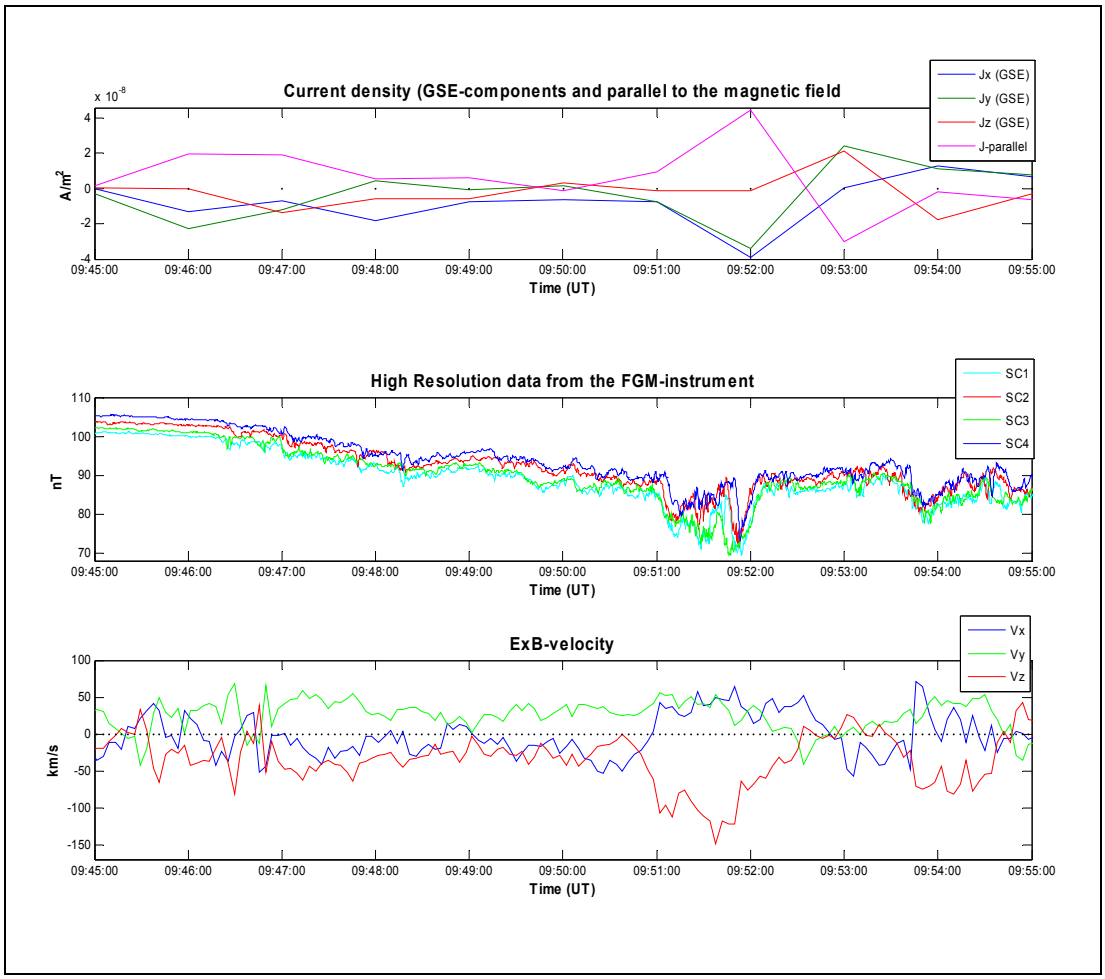

Figure 4.17: *The current density, the magnetic field strength obtained from all 4 satellites and the ExB-velocity (from SC3).*

It is clear from the figure above that some kind of current system passes over the satellites at about 09:51 UT. This also weakens the magnetic field twice, once right after 09:51 UT, and again right before 09:54 UT. One can explain this by looking at how the ionospheric footprint of a flux tube, or an FTE would look like. Referring to Figure 2.18, it is clear that currents, aligned with the magnetic field vector, run both parallel and anti-parallel to this vector on each side of the tube. Thus, if a satellite passes through this system in a certain orientation, it would be able to measure a directional switch of the currents, as shown in Figure 4.17. Also, these currents would contribute with their own induced magnetic field. A system with these specifications is presented below, in Figure 4.18.

The two magnetic disturbances on each flank, as seen on the left and right side of Figure 4.18, can readily be found in Figure 4.17, as mentioned in the paragraph above. However, a decrease of the magnetic field strength does not occur between these two perturbations, as one should expect. This could be because the magnetic field strength in the center of the tube is very strong in comparison with the current induced field. One could calculate this field by using the current density with Ampère's law as given in Equation (A.2), but then one would have to know the dimensions of the flux tube, such as the area which carries the current in each direction. It has been suggested that such a

flux tube has on average a cross section of about an Earth radii squared close to the magnetopause [Southwood, 1987]. This correlates with a circular tube with a diameter of about 7200 km. However, applying any of this to the event in question will be very difficult. It would require a better knowledge of the specific morphology of the flux tube, such as how its thickness changes as the distance from the magnetopause increases, and how large the current carrying areas of its cross section are. Also, the current density might vary within these areas.

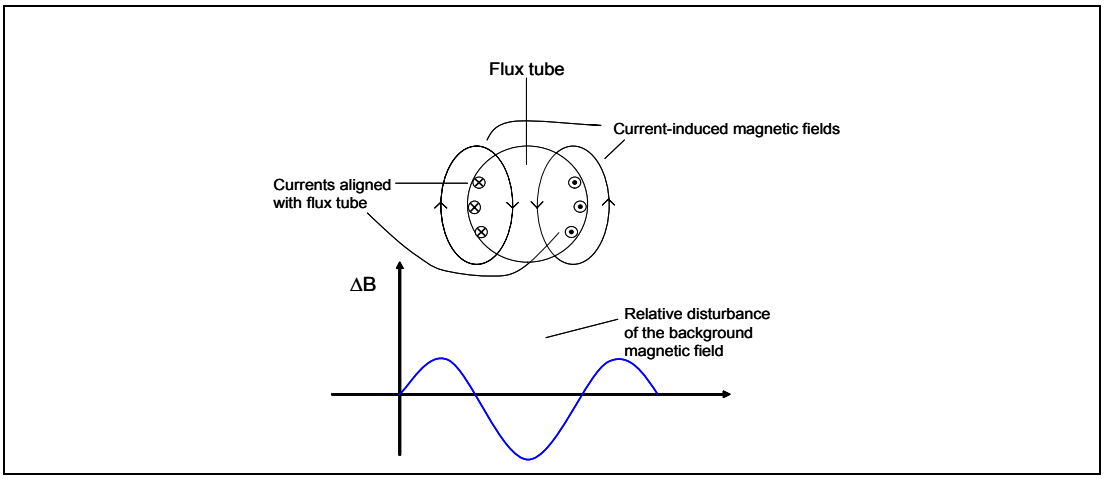

Figure 4.18: *Field-aligned currents within a magnetic flux tube, and their induced magnetic field configuration.*

At the location of the flux tube's footpoint in the ionosphere, currents which run perpendicular to the magnetic field, so called Pedersen currents, will arise. So, one must have an electric field within the flux tube, as indicated in Figure 4.19. This electric field will manifest itself throughout the flux tube. In Figure 4.19, the green arrow shows the direction of the ExB-velocity.

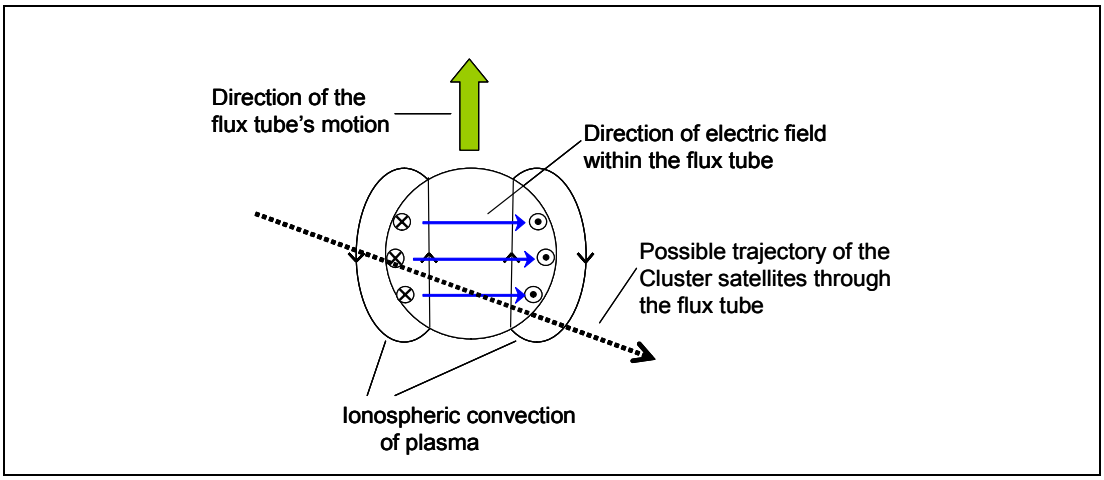

Figure 4.19: *The electric field within the flux tube originating in the ionosphere. A possible Cluster trajectory is superposed onto this image from the satellites' orbit further out in the magnetosphere.*

We already know that the Cluster satellites visit both of the current systems within the flux tube, because of the dipolar signature of the current density (see Figure 4.17). Thus,

when the current density parallel to the magnetic field changes its sign, from positive to negative, the ExB-velocity that Cluster measure should be in the same direction as the convection at the location of Cluster's magnetic footprint in the ionosphere. The switch occurs at approximately 09:52:36 UT and at this time the ExB velocity vector is $[41550, -32350, 8150]\frac{m}{s}$. It is apparent that the dominating convection direction is along the positive GSE-X axis, and negative GSE-Y axis. Comparing this result with the ionospheric convection plots acquired from the SuperDARN radars supports this to a certain degree although in the convection plot, the Y-component seems to be the largest, see Figure 4.20. This could be a result of the currents running along the magnetic field lines, so that they are a bit distorted. Also, there may also be inaccuracies in the mapping of Cluster's magnetic footprint from its position in the magnetosphere into the ionosphere.

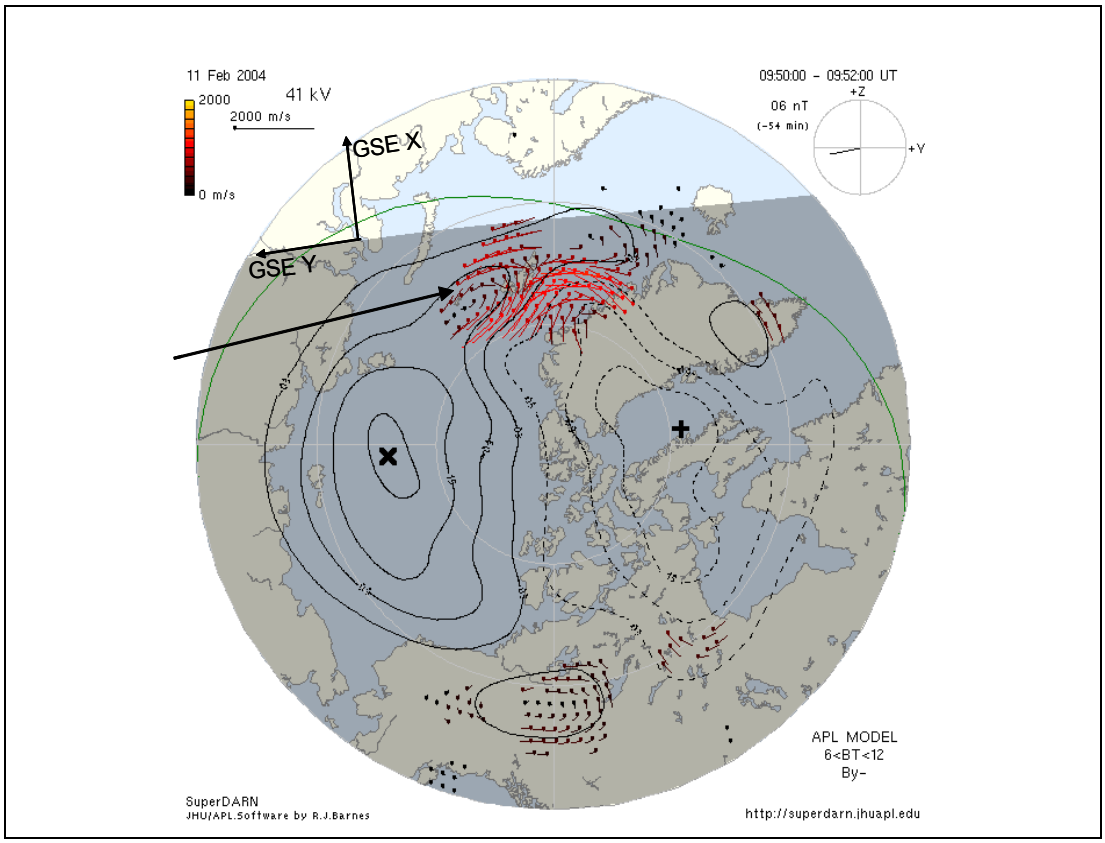

Figure 4.20: *Ionospheric convection measurements made by the SuperDARN radars. The long black arrow indicates Cluster's approximate magnetic footprint position. The GSE X- and Y-axis are also shown.*

One can further investigate the plausible area on the magnetopause where one would reconnection. This would occur where the geomagnetic field and the IMF is the most anti-parallel. Using the IMF Y and Z components (in GSE coordinates), one can plot the angle between the GSE Z axis and this IMF vector. The angle will have a range of $0^o < 360^o$ and increase clockwise (0^o is due north (GSE)). It is presented below in Figure 4.21. It's worth noting that this angle is not the same as the clock angle

mentioned in “2. 3.2.Convection and IMF dependence” on page 20, which is always positive and has a range of $0^o \leq 180^o$.

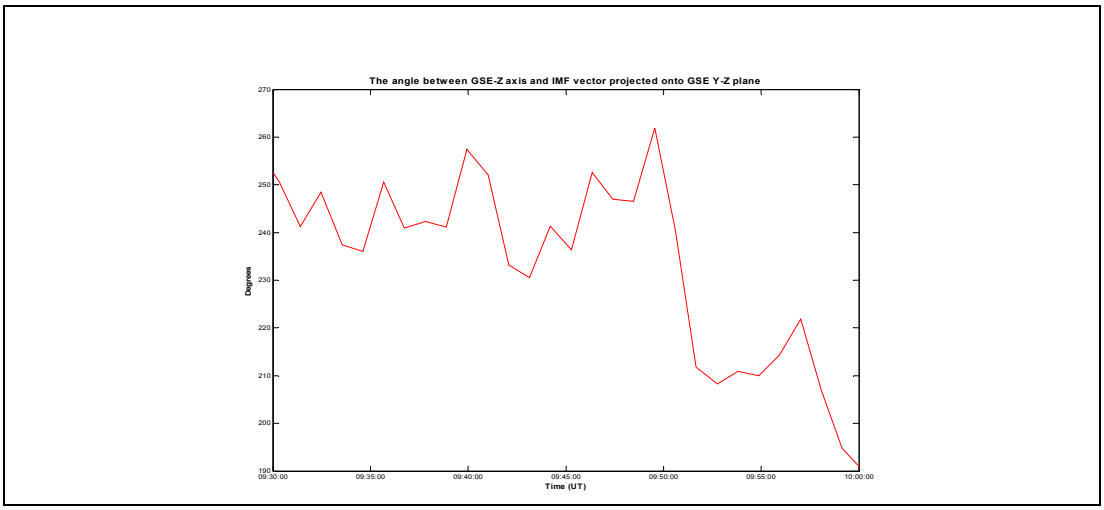

Figure 4.21: *The angle resulting from projecting the IMF vector onto the GSE Y-Z plane.*

Unfortunately, the IMF data apparently were not available in GSM coordinates (see Appendix A.2) at the given interval. But, it will probably still serve to give an estimate of the position of the reconnection site.

If one now project the approximate geomagnetic field at the magnetopause onto the same GSE Y-Z plane as the IMF vector, one can look for the sites where the two fields are anti-parallel. This is done in Figure 4.22.The angle was averaged over the 10 minutes leading up to 09:50 UT, which was 245 degrees. Of course, there are several uncertainties involved, since the IMF coordinates were given in GSE coordinates, and not GSM. This influences the angle of the IMF portrayed in both Figure 4.21 and Figure 4.22 and consequently the magnetic poles in Figure 4.22 should have tilted a few degrees anti-clockwise to the GSE-Z axis. But, it may still give us an image of what we seek, namely the most likely place to search for reconnection.

The two sites in Figure 4.22 are mainly just a guess. There may be enough anti-parallel components other places on the magnetopause which can experience reconnection. But, the site on the lower right side of the figure, could have created a flux tube. Its footprint would then have been on the afternoon side of the ionosphere, where convection was directed sunward and eastwards. The tube which has its footprint in the northern hemisphere will acquire a convection velocity with a positive Z-component, because of the magnetic tension force (can be seen in the ExB-velocity in Figure 4.17). Of course, the Z-component will weaken as the flux tube straightens out, and convects across the polar cap. Its ionospheric footprint would then follow the rest of the convecting plasma across the polar region, while the rest of the tube would be pulled toward the magnetospheric nightside along with the solar wind. This is not a complete description of the event, but the data investigated suggest a development of this manner.

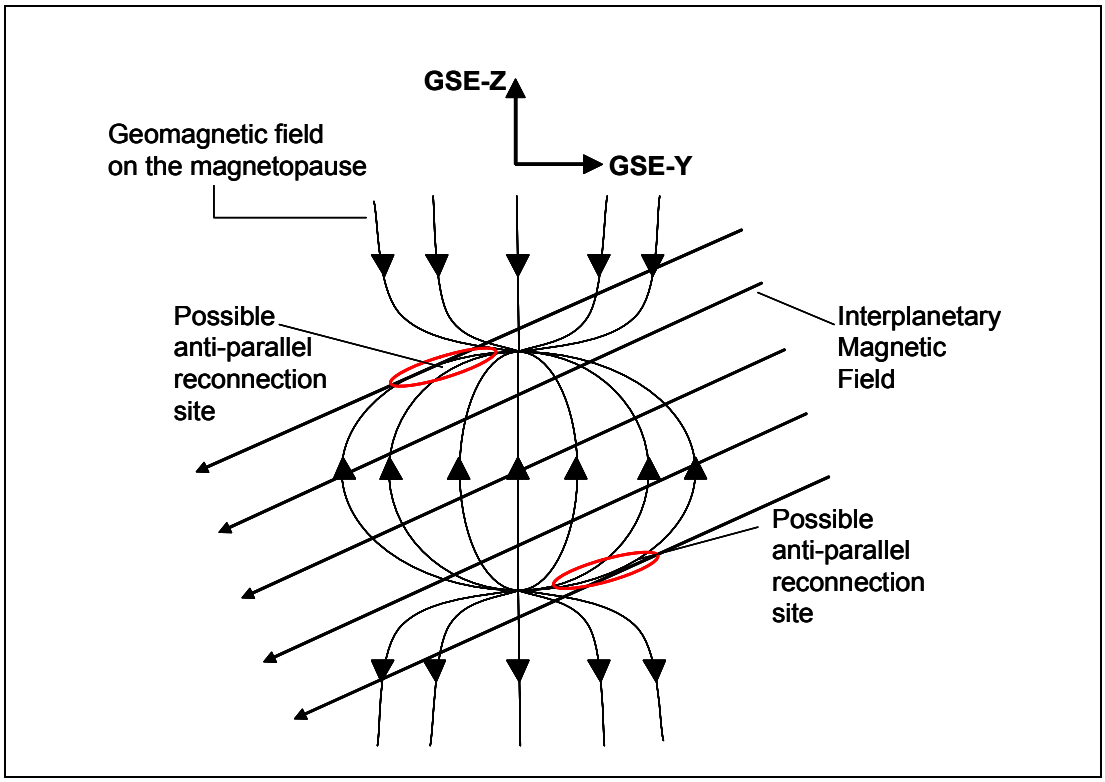

Figure 4.22: *Possible reconnection sites during the 10 minutes before 09:50 UT.*

Finally, investigating Figure 4.5 for this event, reveals that from about 09:45 UT to 10:00 UT there is a period of increased ion density. This can be seen in both the data from the EFW (satellite potential) and the CIS (ion parameters) instruments. However, a small additional increase is seen in the CIS data from both SC1 and SC3 at about 09:51 UT, which indicates that the incident causing the perturbation in the magnetic field is also recognized in other measured parameters.

4. 6. Mapping Factor

In the description of the event in "A possible FTE-passage" on page 53, I referred to the ExB-velocity in the middle of the flux tube and said its direction should be comparable to the convection direction in the ionosphere. But, it could also be interesting to investigate a possible mapping factor, so that one can assume ionospheric ExB-velocities from measurements made by satellites in high-altitude orbits.

In "Frozen-in-Field lines and Drift Velocity (E x B)" on page 7, it is shown that as long as the conductivity is very high, the magnetic flux is constant. Looking at the configuration in Figure 4.23, this can be formulated as: $|B_I| x_I^2 = |B_M| x_M^2$ which leads to:

$$\frac{x_M}{x_I} = \sqrt{\frac{|B_I|}{|B_M|}} \qquad (4.4)$$

where the subscripts M and I refers to the magnetospheric and ionospheric value of the parameter, respectively. The ionospheric magnetic field strength can be calculated with the International Geomagnetic Reference Field (IGRF) model online (see Appendix B). In an altitude of 500 km above Svalbard, the field strength was 44355 nT.

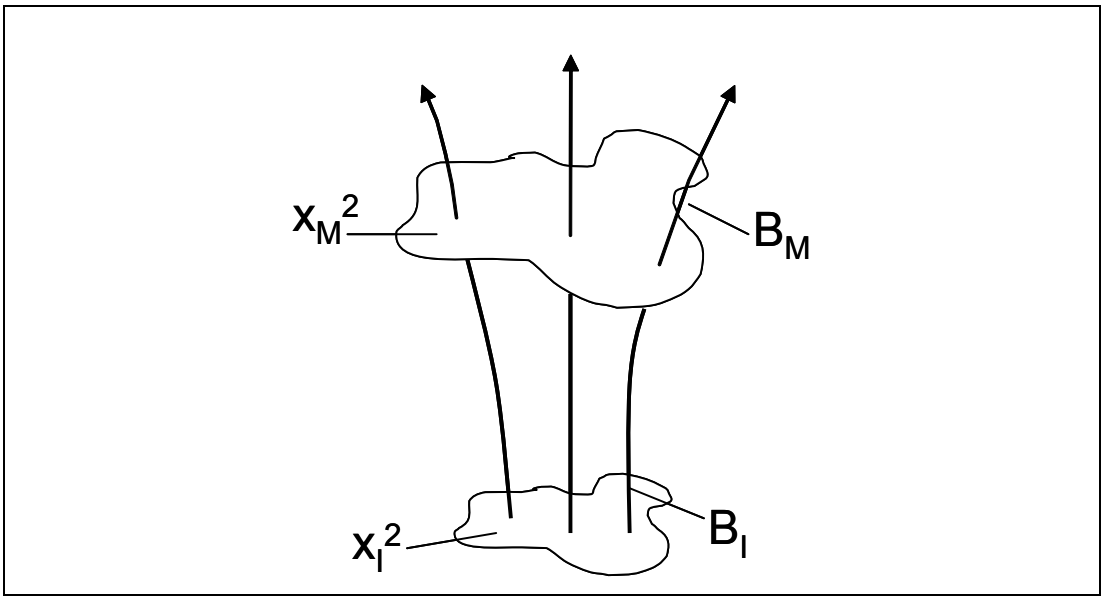

Figure 4.23: *Display of relationship between ionospheric magnetic field strength and typical area size compared with what one should expect further out into the magnetosphere.*

The ratio in Equation (4.4) is called the mapping factor. It can also be found by considering the electric field in the magnetosphere and ionosphere. The only difference is that the electric field multiplied by a typical length scale stays constant, instead of a typical area size. Thus, considering the value of the ExB-velocity in these two regions:

$$\frac{E_M \cdot x_M}{B_M \cdot x_M^{\,2}} = \frac{E_I \cdot x_I}{B_I \cdot x_I^{\,2}} \Rightarrow \frac{E_M}{B_M} = \frac{E_I}{B_I} \cdot \frac{x_M}{x_I} \qquad (4.5)$$

where the magnetic and electric fields are expressed by their absolute values. In Figure 4.24, the mapping factor resulting from Equation (4.4) is displayed. In "A possible FTE-passage" on page 53, the ExB-velocity in the middle of the flux tube was referred to, which was traversed at 09:52:36 UT. The total ExB-velocity was at this time about 53286 m/s, which can also be seen in Figure 4.24. The mapping factor at this time is about 22.5, which leads to an expected ionospheric value of the ExB-velocity of approximately 2368 m/s. In Figure 4.20, one can find the plasma velocity vectors measured by the SuperDARN radars. Looking at the color and length of the vector closest to the magnetic footprint of Cluster, an approximate value can be found to be 700 m/s. This is just a bit more than a factor 3 less than the expected value. In other words, there are processes occurring that modifies the simple assumptions done to reach this result.

Mapping of the electric field with a good accuracy from the equatorial plane to the ionosphere has previously been done [Schmidt et al., 1985]. However, it has been pointed out that treating the magnetic field lines as electric equipotentials, i.e. that the electric field stays constant between neighboring magnetic field lines, may introduce

errors [Mozer, 1970]. This can especially be a problem when having electric fields parallel to the magnetic field lines. The possible FTE-event described above has significant currents running both to and from the ionosphere along magnetic field lines. This might be an explanation why the calculated value of the ExB-velocity in the ionosphere is so much larger than what is observed.

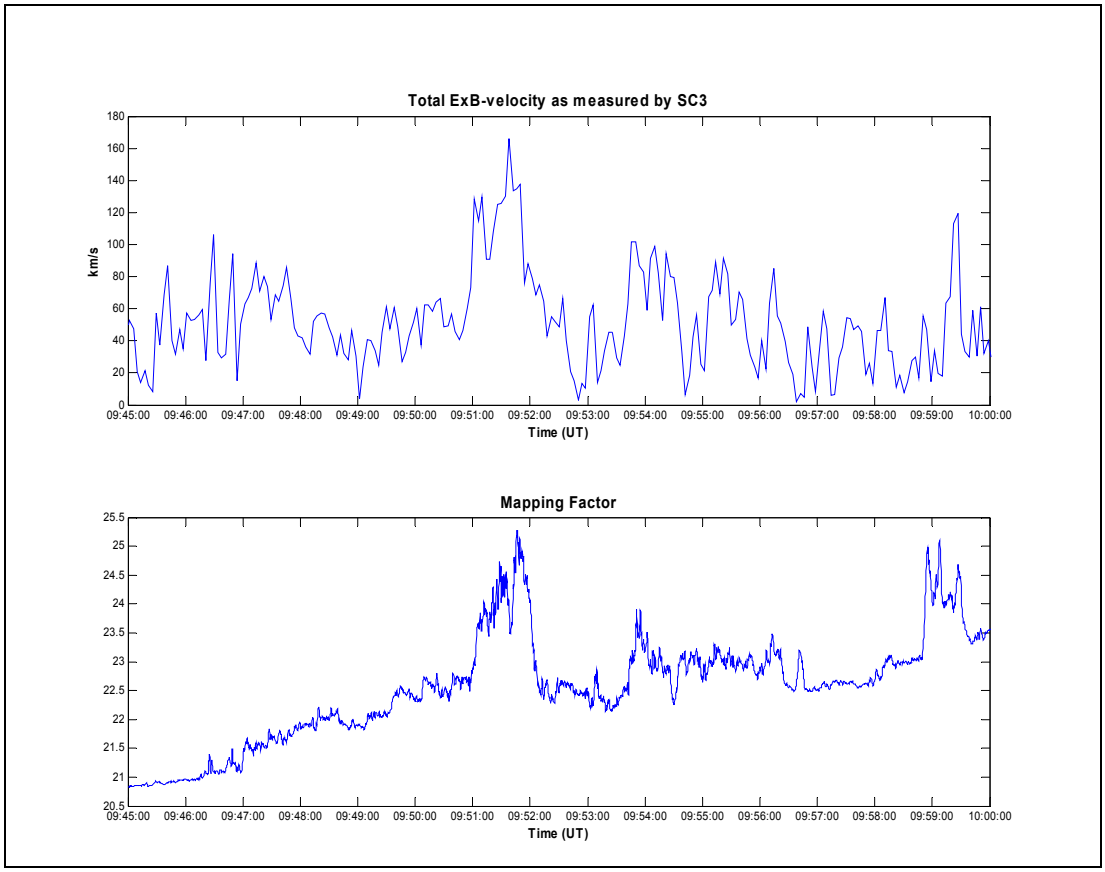

Figure 4.24: *The absolute value of the ExB-velocity measured by SC3, and the mapping factor.*

Using data from the FAST-satellite, which orbited in an altitude of about 4000 km, Pfaff et al. (1998) found, and refers to, several examples of particle acceleration often related to potential drops along magnetic field lines. Thus, having magnetic-field-aligned electric fields is not uncommon in the cusp.

Chapter 5

Summary and Conclusions

On the 11th of February, 2004, Cluster's magnetic footprint passed nearby the ESR's location close to Longyearbyen. During the time interval ~09:04-11:20 UT, both the Cluster spacecraft and the ground-based radars made measurements within the northern polar cusp region. This fact made it possible to compare their data, and investigate cusp dynamics. The initial goal was to try to find events where one could observe the initiation of ion outflow in the EISCAT radar data, and later observe this in the Cluster data. Due to the location of the satellites' magnetic footprint, and the direction of magnetospheric convection, one could not assume that the radar and the satellites were making measurements on exactly conjugated magnetic field lines. However, a phenomenon described in earlier articles as a cause of global outflows, namely a pressure pulse in the solar wind [Cully et al., 2003], was observed. After calculating appropriate time-delays for the propagation of this perturbation, it was found that it was indeed a plausible cause for the upflowing ions in the ionosphere at 10:10 UT, and the outflowing ions at Cluster's location in the magnetosphere at 10:45 UT.

The pre-screening of the data archives with conjunctions between the ESR and Cluster did not leave a large amount of data to be investigated. However, the cusp passage during the 11th of February still had many interesting features. Comparing electric and magnetic fields to those in the ionosphere, required the use of SuperDARN measurements, which spans across larger areas than the EISCAT radar on Svalbard. Although the uncertainties in the mapping of the magnetic footprint of the Cluster satellites, the SuperDARN convection maps assure conjunction between a region of magnetospheric cusp and ionospheric cusp.

In addition to searching for ion outflow, this thesis evolved into including some qualitative analysis based on magnetic and electric field measurements made by Cluster.

The four Cluster satellites entered the cusp region from the mantle between 09:04 UT and 09:05 UT, as was evident from the increase in plasma density and strongly enhanced pulsed injection of magnetosheath type ions and electrons. The configuration of the satellites allowed for an investigation of how the mantle/cusp boundary was oriented and whether it was stationary or not. At the time of passage it was found to be moving, mainly in the anti-sunward direction. The most probable explanation is that the whole cusp region expands and contracts as a consequence of varying solar wind pressure.

On their outbound voyage through the cusp region, the satellites observed a dynamic magnetic field. At about 09:51 UT, there was a clear perturbation which had some characteristics similar to what one would expect from a magnetic flux tube, maybe

resulting from a transient burst of reconnection, i.e. an FTE. Unfortunately, the 32m EISCAT radar on Svalbard was not directed in a favorable direction for observing the ionospheric footprint of such a phenomenon, considering the plasma convection presented in Figure 4.20. However, the dipolar signature in the current density derived from the curlometer technique is consistent with the assumption of a Southwood (1987) type flux transfer event signature. The method described in Appendix A.4 is a tool which is possible to use because of the satellite configuration in 3 dimensions.

When using both ground-based and satellite measurements of plasma parameters, the absolute value of these may differ according to how the magnetic and the electric fields vary. This is evident especially for plasma convection in the ionosphere and magnetosphere. The ExB-velocity was calculated from measurements made by Cluster (SC3), and it was attempted to calculate the ionospheric value of this for the assumed FTE-passage at ~09:52 UT. The calculated ionospheric convection velocity was just a little more than a factor 3 above the measured velocity made by the SuperDARN radars. However, the cusp region is a highly dynamic structure where solar wind plasma is injected. This injection could increase the currents running parallel to the magnetic field lines, and thus making it difficult to predict where the magnetic footprint of Cluster would be. If this position is uncertain, it would complicate the process of comparing radar measurements with the satellite data. Also, as mentioned in Mozer (1970), the assumption of conservation of the electric field between neighboring magnetic field lines may break down if parallel electric fields exist. Pfaff et al. (1998) later reported that this was not uncommon in the cusp region.

As stated in the introduction, this thesis was mainly going to treat ionospheric outflow of particles present in both ground-based (ESR) and satellite (Cluster) data. However, as time passed, it evolved into investigating only one event which contained outflow seen both by the radar and the satellites. There were several incidents where Cluster's magnetic footprint was relatively close to Svalbard, but there was not always much activity to focus on. So, it felt natural to look at some of the other features in the data set, as described above.

One thing that this investigation bear witness of, is that one needs a very accurate model of the geomagnetic field, which also would have to be sensitive to external parameters such as changes in the IMF, to be able to obtain a one-to-one conjunction between a ground-based instrument and a satellite. And, even if this is developed, one would still have to calculate how the ExB-drift and ionospheric convection influences any perturbations or particle trajectories during the time delay between the two measurements. But, utilizing such instruments like SuperDARN, and/or possibly an all-sky camera, would yield vital information about the gathered by the localized Cluster in situ measurements and narrow beam experiments like EISCAT.

5. 1. Some thoughts about future work

Cluster's four spacecraft enables the use of specific techniques such as constructing a 2 dimensional model of the magnetopause, with much higher accuracy than the normal 1 spacecraft missions [Hasegawa et al., 2005]. This can also be applied for the study of FTE's, and their connection to PMAF's [Oksavik et al., 2004]. Tied to the ionospheric

signature of an FTE, is a phenomenon called inverted V-potentials, which signifies electric potential drops parallel to the magnetic field. An inverted V-potential can be seen in ESR data, as it causes ion upflow [Moen et al., 2004]. A coherent measurement set, with data from the ESR, Cluster and a satellite located in the solar wind, may yield information about how FTE's are created and where they are most likely to develop.

So far, the whole process of accelerating ions from the ionosphere and outwards is not fully understood. There have been both 2- and 1-dimensional approaches to this problem [Bouhram et al., 2003]. Cluster, during late winter/early spring, traverses the polar cusp in a high altitude orbit (~6-7 R_e). Thus, if Cluster data is combined with lower altitude orbiting satellites one can develop more accurate models of how the ion outflow events evolve in this rather turbulent region.

One limitation when using conjugated ground-based and Cluster events, is that the Cluster satellites are located in the polar cusp for only about 2.5 hours. Of course, this is a longer time interval than for the lower orbiting satellites, but Cluster's orbital period only allows one pass every 57 hours. Therefore, adding up the constraints of conjunction with ground-based data, presence within the cusp at periods with any significant activity, and favorable orbital configuration (late winter/early spring) does not leave an abundance of data which can be thoroughly investigated. A suggestion of how to increase the relevant amount of data, could be to let the EISCAT radars run for longer time periods before and after Cluster enters and leaves the cusp. This has of course already been done, but there were several satellite passes which at first seemed interesting, but where the radar coverage was either very limited or non-existing. So, the advice is rather to continue to cover conjugated events.

A great tool to combine with the relatively narrow field-of-view of EISCAT, and the in situ measurements made by satellites, is the SuperDARN data, as mentioned above. With its applied convection model across the polar cap, it adds coherent information to the turbulent and dynamic ionospheric cusp. Especially when it comes to events where conjugated measurements are of any significance. As an example, in this thesis it was used for investigating the movement of magnetic field lines compared to the position of Cluster's magnetic footprint and the location of EISCAT. The SuperDARN data was also used to identify the cusp inflow region.

Bibliography

Akasofu S.-I., **(1981)**, Energy coupling between the solar wind and the magnetosphere, *Space Science Reviews*, 28, pp. 121-190

André M. and Yau A., **(1997)**, Theories and observations of ion energization and outflows in the high latitude magnetosphere, *Space Science Reviews*, 80, pp. 27-48

Axford W. I., **(1968)**, The Polar Wind and the Terrestrial Helium Budget, *Journal of Geophysical Research*, 73, No. 21, pp. 6855-6859

Balogh A., Carr C. M., Acuña M. H., Dunlop M. W., Beek T. J., Brown P., Fornacon K.-H., Georgescu E., Glassmeier K.-H., Harris J., Musmann G., Oddy T., Schwingenschuh K., **(2001)**, The Cluster Magnetic Field Investigation: overview of in-flight performance and initial results, *Annales Geophysicae*, 19, pp. 1207-1217

Bouhram M., Malingre M., Jasperse J. R., Dubouloz N., **(2003)**, Modeling transverse heating and outflow of ionospheric ions from the dayside cusp/cleft. 1 A parametric study, *Annales Geohphysicae*, 21, pp. 1753-1771

Bouhram M., Klecker B., Paschmann G., Rème H., Blagau A., Kistler L., Puhl-Quinn P., Sauvaud J.-A., **(2004)**, Multipoint analysis of the spatio-temporal coherence of dayside O+ outflows with Cluster, *Annales Geophysicae*, 22, pp. 2507-2514

Carroll B. W., Ostlie D. A., **(1996)**, An Introduction to Modern Astrophysics, *Addison-Wesley Publishing Company, Inc.*, pp. 394-416

Cowley S. W. H. and Lockwood M., **(1992)**, Excitation and decay of solar wind-driven flows in the magnetosphere-ionosphere system, *Annales Geophysicae*, 10, pp. 103-115

Cully C. M., Donovan E. F., Yau A. W., Arkos G. G., **(2003)**, Akebono/Suprathermal Mass Spectrometer observations of low-energy ion outflow: Dependence on magnetic activity and solar wind conditions, *Journal of Geophysical Research*, 108, No. A2, 1093, doi:10.1029/2001JA009200

Daglis I., Akasofu S.-I., **(2004)**, Aurora - The magnificent northern lights, *The Eggs*, Issue 7, pp. 12-18 (available online at www.the-eggs.org)

Escoubet C. P., Schmidt R., Goldstein M. L., **(1997)**, Cluster-Science and Mission Overview, *Space Science Reviews*, 79, pp. 11-32

Fuselier S. A., Ghielmetti A. G., Moore T. E., Collier M. R., Quinn J. M., Wilson G. R., Wurz P., Mende S. B., Frey H. U., Jamar C., Gerard J.-C., Burch J. L., **(2001)**, Ion outflow observed by IMAGE: Implications for source regions and heating mechanisms, *Geophysical Research Letters*, 28, No. 6, pp. 1163-1166

Fuselier S. A., **(2002)**, Localized ion outflow in response to a solar wind pressure pulse, *Journal of Geophysical Research*, 107, No. A8, 1203, 10.1029/2001JA000297

Fuselier S. A., Mende S. B., Moore T. E., Frey H. U., Petrinec S. M., Claflin E. S., Collier M. R., **(2003)**, Cusp Dynamics and Ionospheric Outflow, *Space Science Reviews*, 109, pp. 285-312

Gardner L.C. and Schunk R.W., **(2004)**, Neutral polar wind, *Journal of Geophysical Research*, 109, A05301, doi:10.1029/2003JA010291

Goldston R. J. and Rutherford P. H., **(1995)**, Single-fluid magnetohydrodynamics, Introduction To Plasma Physics, *Institute of Physics Publishing Bristol and Philadelphia*, pp. 115-128

Gustafsson G., Boström R., Holback B., Holmgren G., Lundgren A., Staciewicz K., Åhlèn L., Mozer F. S., Pankow D., Harvey P., Berg P., Ulrich R., Pedersen A., Schmidt R., Butler A., Fransen A. W. C., Klinge D., Thomsen M., Fälthammar C.-G., Lindqvist P.-A., Christenson S., Holtet J., Lybekk B., Sten T. A., Tanskanen P., Lappalainen K., Wygant J., **(1997)**, The electric field and wave experiment for the Cluster mission, *Space Science Reviews*, 79, pp. 137-156

Gustafsson G., André M., Carozzi T., Eriksson A.I., Fälthammar C.-G., Grard R., Holmgren G., Holtet J. A., Ivchenko N., Karlsson T., Khotyaintsev Y., Klimov S., Laakso H., Lindqvist P.-A., Lybekk B., Marklund G., Mozer F., Mursula K., Pedersen A., Popielawska B., Savin S., Stasiewicz K., Tanskanen P., Vaivads A., Wahlund J.-E., **(2001)**, First results of electric field and density observations by Cluster EFW based on initial months of operation, *Annales Geophysicae*, 19, pp. 1219-1240

Hallinan T., **(1991)**, Auroras, Geomagnetism (vol. 4), edited by J. A. Jacobs, *Academic Press*, London, pp. 741-752

Harvey C. C., **(2000)**, Spatial Gradients and the Volumetric Tensor, Analysis Methods for Multi-Spacecraft Data (electronic edition), edited by G. Paschmann and P. W. Daly, *ESA Publications Division*, pp. 308-310

Hasegawa H., Sonnerup B. U. Ö., Klecker B., Paschmann G., Dunlop M. W., Rème H., **(2005)**, Optimal reconstruction of magnetopause structures from Cluster data, *Annales Geophysicae*, 23, pp. 973-982

Hughes W. J., **(1995)**, The Magnetopause, Magnetotail, and Magnetic Reconnection, Introduction to Space Physics, edited by M. G. Kivelson and C. T. Russell, *Cambridge University Press*, pp. 236-242

Hundhausen A. J., **(1995)**, The Solar Wind, Introduction to Space Physics, edited by M. G. Kivelson and C. T. Russell, *Cambridge University Press*, pp. 96-110

Ishibashi H., Marubashi K., **(2004)**, Structure of interplanetary magnetic cloud on April 16, 1999 and its origin estimated by fitting the torus-shaped flux rope model, *Geophysical Research letters*, 31, L21807, doi:10.1029/2004GL020702

Kivelson M. G., **(1995)**, Physics of Space Plasmas, Introduction to Space Physics, edited by M. G. Kivelson and C. T. Russell, *Cambridge University Press*, pp. 27-50

Landmark B., **(1973)**, Formation of the Ionosphere, Cosmical Geophysics, edited by A. Egeland, Ø. Holter and A. Omholt, *Universitetsforlaget*, pp. 73-74

Lepping R. P., Berdichevsky D., **(2000)**, Interplanetary magnetic clouds: Sources, properties, modeling, and geomagnetic relationship, *Recent Research Developments in Geophysical Research*, 3, pp. 77-96

Lockwood M., Sandholt P. E., Cowley S. W. H., Oguti T., **(1989)**, Interplanetary magnetic field control of dayside auroral activity and the transfer of momentum across the dayside magnetopause, *Planetary and Space Science*, 37, No. 11, pp. 1347-1365

Lockwood M., Hapgood M. A., **(1998)**, On the cause of a magnetospheric flux transfer event, *Journal of Geophysical Research*, 103, A11, pp. 26,453-26,478

Manchester W. B., Gombosi T. I., Roussev I., Ridley A., De Zeeuw D. L., Sokolov I. V., Powell K. G., **(2004)**, Modeling a space weather event from the Sun to the Earth: CME generation and interplanetary propagation, *Journal of Geophysical Research*, 109, A02107, doi:10.1029/2003JA010150

Maszl C., **(2004)**, The Curlometermethod and Cluster II, A student project work in Space Plasma Physics performed at the Swedish institute of Space Physics, Uppsala, [Document last accessed at http://www.space.irfu.se/exjobb/2004_christian_maszl/Documentation/projectwork_maszl.pdf, the 17. of November, 2005], pp. 20-22

McPherron R. L., **(1995)**, Magnetospheric Dynamics, Introduction to Space Physics, edited by M. G. Kivelson and C. T. Russell, *Cambridge University Press*, pp. 406-407 and pp. 456-457

Moen J., Oksavik K., Carlson H. C., **(2004)**, On the relationship between ion upflow events and cusp auroral transients, *Geophysical Research Letters*, 31, L11808, doi:10.1029/2004GL020129

Mozer F. S., **(1970)**, Electric field mapping in the ionosphere at the equatorial plane, *Planetary and Space Science*, 18, pp. 259-263

Ogawa Y. **(2002)**: Generation Mechanisms of Ion Upflow in the Polar Topside Ionosphere, A Dissertation for the Degree of Doctor Scientiarium. Division of Particle and Astrophysical Science, Graduate School of Science, Nagoya University, Japan, pp. 7-8

Oksavik K., Moen J., Carlson H. C., **(2004)**, High-resolution observations of the small-scale flow pattern associated with a poleward moving auroral form in the cusp, *Geophysical Research Letters*, 31, L11807, doi:10.1029/2004GL019838

Parker E. N., **(1958)**, Dynamics of the interplanetary gas and magnetic fields, *Astrophysical Journal*, 128, pp. 664-676

Paschmann G., **(1991)**, The Earth's Magnetopause, Geomagnetism (vol. 4), edited by J. A. Jacobs, *Academic Press*, London, pp. 295-331

Pfaff R., Clemmons J., Carlson C., Ergun R., McFadden J., Mozer F., Temerin M., Klumpar D., Peterson W., Shelley E., Moebius E., Kistler L., Strangeway R., Elphic R., Cattell C., **(1998)**, Initial FAST observations of acceleration processes in the cusp, *Geophysical Research Letters*, 25, No. 12, pp. 2037-2040

Pedersen A., Decreau P., Escoubet C.-P., Gustafsson G., Laakso H., Lindqvist P.-A., Lybekk B., Masson A., Mozer F., Vaivads A., **(2001)**, Four-point high time resolution information on electron densities by the electric field experiments (EFW) on Cluster, *Annales Geophysicae*, 19, pp. 1483-1489

Priest E. R., **(1995)**, The Sun And Its Magnetohydrodynamics, Introduction to Space Physics, edited by M. G. Kivelson and C. T. Russell, *Cambridge University Press*, pp. 65-69

Rosenbauer H., Grünwaldt H., Montgomery M. D., Paschmann G., Sckopke N., **(1975)**, Heos 2 Plasma Observations in the Distant Polar Magnetosphere: The Plasma Mantle, *Journal of Geophysical Research*, 80, No. 19, pp. 2723-2737

Russell C. T., **(2000)**, The Polar Cusp, *Advances in Space Research*, 25, No. 7/8, pp. 1413-1424

Russell C. T., **(2001)**, Solar Wind and Interplanetary Magnetic Field: A Tutorial, Space Weather, Geophysical Monograph 125, edited by P. Song, H. J. Singer, and G. L. Siscoe, *American Geophysical Union*, pp. 73-89

Schmidt R., Nielsen E., Pedersen A., **(1985)**, Comparison of electric fields measured on GEOS-2 and by the STARE radar, *Annales Geophysicae*, 3, pp. 421-428

Schunk R. W., (2000), Theoretical developments on the causes of ionospheric outflow, *Journal of Atmospheric and Solar-Terrestrial Physics*, 62, pp. 399-420

Southwood D. J., **(1987)**, The Ionospheric Signature of Flux Transfer Events, *Journal of Geophysical Research*, 94, A4, pp. 3207-3213

Torkar K., Riedler W., Escoubet C. P., Fehringer M., Schmidt R., Grard R. J. L., Arends H., Rüdenauer F., Steiger W., Narheim B. T., Svenes K., Torbert R., André M., Fazakerley A., Goldstein R., Olsen R. C., Pedersen A., Whipple E., Zhao H., **(2001)**, Active spacecraft potential control for Cluster - implementation and first results, *Annales Geophysicae*, 19, pp. 1289-1302

Walker R. J., Russell C. T., **(1995)**, Solar-Wind Interactions With Magnetized Planets, Introduction to Space Physics, edited by M. G. Kivelson and C. T. Russell, *Cambridge University Press*, pp. 169-172

Weimer D. R., Goertz C. K., Gurnett D. A., Maynard N. C., Burch J. L., **(1985)**, Auroral Zone Electric Fields from DE 1 and 2 at Magnetic Conjunctions, *Journal of Geophysical Research*, 90, A8, pp. 7479-7494

Yau A. W. and André M., **(1997)**, Sources of ion outflow in the high latitude ionosphere, *Space Science Reviews*, 80, pp. 1-25

Zhou X.-W., Russell C. T., Le G., Tsyganenko N., **(1997)**, Comparison of observed and model magnetic fields at high altitudes above the polar cap: POLAR initial results, *Geophysical Research Letters*, 24, No. 12, pp. 1451-1454

Østgaard N., Germany G., Stadsnes J., Vondrak R. R., **(2002)**, Energy analysis of substorms based on remote sensing techniques, solar wind measurements, and geomagnetic indices, *Journal of Geophysical Research*, 107, A9, 1233, doi:10.1029/2001JA002002

Figure References

Figure 1.1: http://www.northern-lights.no/english/science/birkeland.shtml [Accessed the 7. of June, 2005]

Figure 1.2: http://www.northern-lights.no (Northern Lights Photo of the Year 2003) [Accessed the 16. of November, 2005]

Figure 2.2: http://farside.ph.utexas.edu/teaching/plasma/lectures/node21.html [Accessed the 22. of June, 2005]

Figure 2.5: http://sohowww.estec.esa.nl/explore/images/layers.gif [Accessed the 16. of November, 2005]

Figure 2.7: http://www.keelynet.com/spider/magfield.htm [Accessed the 30. of June, 2005]

Figure 2.8: http://spaceweather.com/glossary/coronalholes.html [Accessed the 1. of July, 2005]

Figure 2.10: http://earthobservatory.nasa.gov/Newsroom/NewImages/images.php3?img_id=16345 [Accessed the 1. of July, 2005]

Figure 2.11: http://hesperia.gsfc.nasa.gov/sftheory/cme.htm [Accessed the 1. of July, 2005]

Figure 2.12: http://clusterlaunch.esa.int/science-e-media/img/4b/hires_36939.JPG [Accessed the 2. of July, 2005]

Figure 2.14: http://myweb.cwpost.liu.edu/jstevens/hutton/cowley.pdf

Figure 3.1: http://clusterlaunch.esa.int/science-e/www/object/index.cfm?fobjectid=28661 [Accessed the 19. of August, 2005]

Figure 3.2: http://clusterlaunch.esa.int/science-e/www/object/index.cfm?fobjectid=36664 [Accessed the 19. of August, 2005]

Figure 3.4: http://cluster.irfu.se/efw/ops/dummies/page1.html [Accessed the 30. of August, 2005]

Figure 3.6: http://www.uio.no/studier/emner/matnat/fys/FYS3610/h05/undervisningsmateriale/Compendium/radars.pdf [Accessed the 16. of November, 2005]

Figure 3.7: http://www.eiscat.com/ESR/ [Accessed the 16. of November, 2005]

Abbreviations

ACE - **A**dvanced **C**omposition **E**xplorer

ASPOC - **A**ctive **S**pacecraft **PO**tential **C**ontrol (Cluster)

CIS - **C**luster **I**on **S**pectrometry (Cluster)

CME - **C**oronal **M**ass **E**jection

CODIF - **CO**mposition and **DI**stribution **F**unction analyzer (Cluster)

CPI - **C**omprehensive **P**lasma **I**nstrument (Geotail)

DMSP - **D**efense **M**eteorological **S**atellite **P**rogram

EFW - **E**lectric **F**ield and **W**ave experiment (Cluster)

EISCAT Radar - **E**uropean **I**ncoherent **SCAT**ter Radar

ESA - **E**uropean **S**pace **A**gency

ESR - **E**ISCAT **S**valbard **R**adar

FGM - FluxGate Magnetometer (Cluster)

FTE - **F**lux **T**ransfer **E**vent

GSE - **G**eocentric **S**olar **E**cliptic coordinate system

GSM - **G**eocentric **S**olar **M**agnetic coordinate system

HIA - **H**ot **I**on **A**nalyzer (Cluster)

IMF - **I**nterplanetary **M**agnetic **F**ield

ISTP - **I**nternational **S**olar- **T**errestrial **P**rogram

ISAS - **I**nstitute of **S**pace and **A**eronautical **S**cience

LEP - **L**ow-**E**nergy **P**articles (Geotail)

MGF - **MaG**netic **F**ield (Geotail)

MHD - **M**agneto**H**ydro**D**ynamic

MLT - **M**agnetic **L**ocal **T**ime

MP - **M**agneto**P**ause

NASA - **N**ational **A**eronautics and **S**pace **A**dministration

PMAF - **P**oleward **M**oving **A**uroral **F**orm

SC - **S**pace**C**raft

SuperDARN - **Super D**ual **A**uroral **R**adar **N**etwork

TAI - **T**ransversely **A**ccelerated **I**ons

UHF - **U**ltra **H**igh **F**requency

UT - **U**niversal **T**ime

UWI - **U**p**W**elling **I**ons

VHF - **V**ery **H**igh **F**requency

Appendix A

Coordinates and Analysis Methods

A. 1. Geographic Coordinates (GEO)

This coordinate system rotates along with the Earth, with its X-axis crossing the Greenwich meridian. The Z-axis points north, parallel with the Earth's spin-axis. The Y-axis completes this right-hand system.

This system is useful when defining positions on the Earth's surface. One needs only two parameters, the longitudinal- and the latitudinal angle. The longitude is the angle between the X-axis and the line going through the point's projection into the equatorial plane. The latitude is the angle between the equatorial plane and the line that goes through the point itself (see Figure A.1). The latitude varies from -90^o (90^o S) to 90^o (90^o N). The longitude has value 0^o at the Greenwich meridian. From there it increases toward the east. Its value can vary from 0^o-360^o, or from -180^o-180^o and so on. The longitudinal position can also be expressed as 15^o W (west) for example.

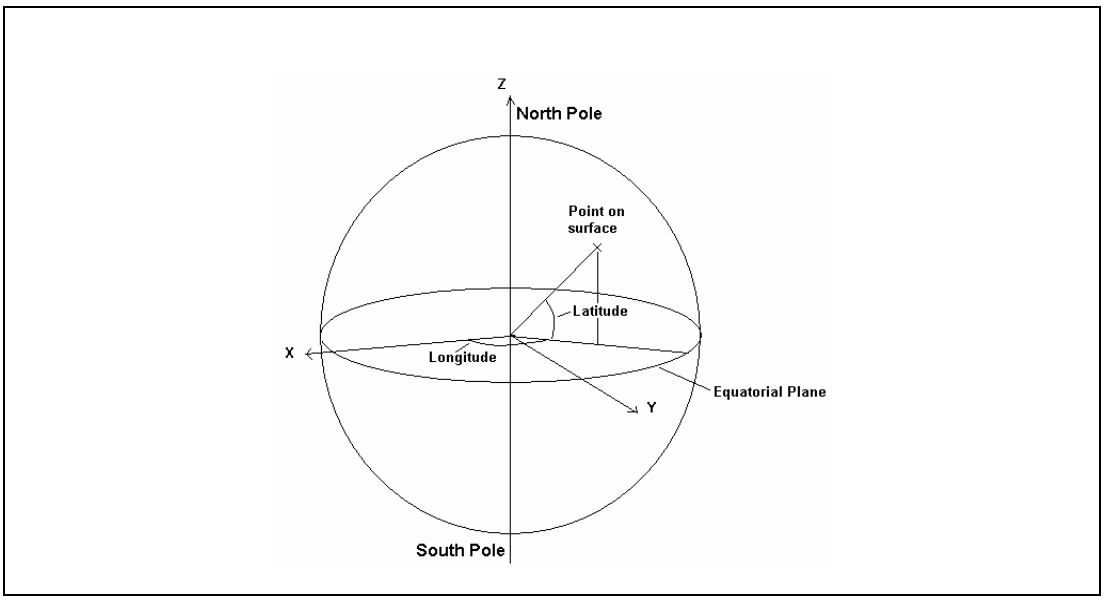

Figure A.1: *The Geographic coordinates*

A. 2. Geocentric Solar Ecliptic System (GSE)

Within this coordinate system, the X-axis always points from the Earth's center toward the Sun, and the Z-axis is perpendicular to the ecliptic (the plane that contains the Earth's orbit around the Sun). The Y-axis completes the right-hand system, and points roughly in the opposite direction with respect to the Earth's trajectory.

This system is convenient to use when considering parameters involving the solar wind, and when describing positions and trajectories of satellites. However, during long periods of time, the effects of the rotation of the X- and Y-axis around the Z-axis must be considered. But, within shorter intervals, where other coordinate systems must include the rotation of Earth, this system has a clear advantage. See Figure A.2 for further details.

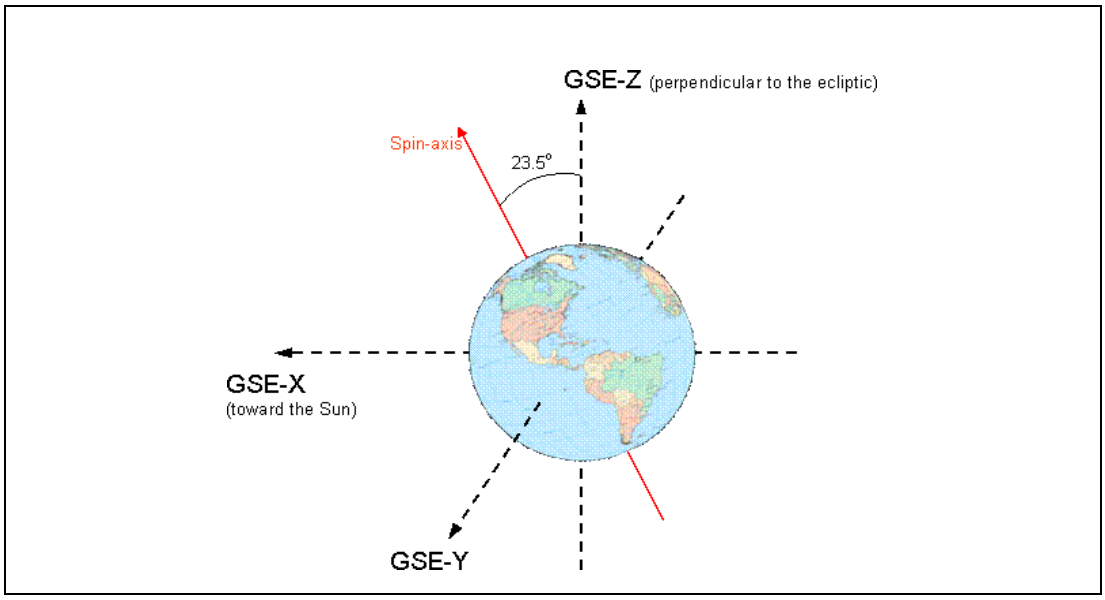

Figure A.2: *The Geocentric Solar Ecliptic coordinates*

It is also worth mentioning the Geocentric Solar Magnetic (GSM) coordinates, which have the same X-axis, but where the Z-axis run from the Earth's center through the magnetic pole closest to the geographic north pole, and then projected onto the GSE Y-Z plane. The GSM Y-axis will then also lie in the GSE Y-Z plane to complete the system.

A. 3. Magnetic Local Time (MLT)

When looking down at the northern hemisphere, one can divide it into MLT-sectors as shown in Figure A.3. These are oriented according to where the Sun's position is, so they do not rotate along with the Earth. However, during a whole year, they will rotate 360 degrees. Also, it's worth noting that the line from 12 MLT through 24 MLT is parallel to the GSE X-line.

The southern hemisphere can also be divided into these sectors, but then the morning side and the afternoon side will switch places (see Figure A.3), since the Earth in that case will rotate clockwise.

Another common terminology for the morning- and afternoon sector, is the dawn- and duskside, respectively.

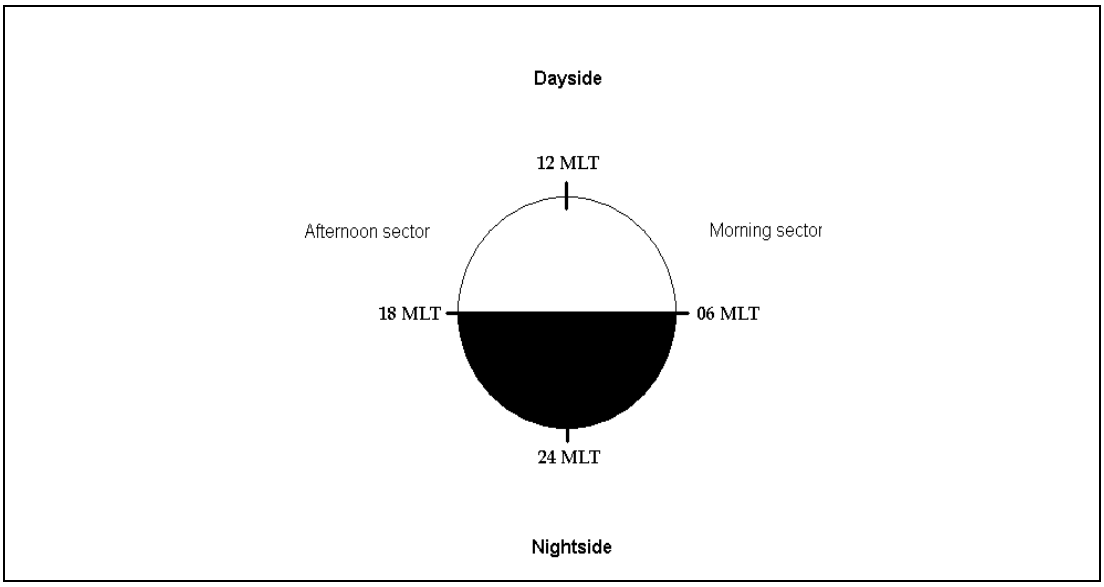

Figure A.3: *The position of the MLT-sectors.*

A. 4. The Curlometer Technique applied with Cluster

As stated in "Magnetic Reynolds Number and Reconnection of magnetic field lines" on page 11, the modified Ampére's law can be expressed as:

$$\mu_0 \vec{J}_{av} = \nabla \times \vec{B} \qquad (A.1)$$

With a few assumptions, this can be applied to the measurements made by the FGM-instrument onboard the Cluster satellites. To make fairly accurate calculations of the current density, $\vec{J}_{av}$, one assumes that it is constant across the volume defined by the four satellites and that the magnetic field varies linearly [Maszl, 2004].

Following the method described in Maszl (2004), one applies Stoke's theorem to Equation (A.1):

$$\mu_0 \vec{J}_{av} \int_A \vec{da} = \int_L \vec{dl} \bullet \vec{B} \qquad (A.2)$$

If the separation between the satellites is small enough to assume that the magnetic field does not change dramatically when moving from one satellite to another, one can express the magnetic field and position vectors as:

$$\vec{B}_{12} = \frac{\vec{B}_1 + \vec{B}_2}{2} \qquad \vec{r}_{12} = \vec{r}_1 - \vec{r}_2 \qquad (A.3)$$

$$\vec{B}_{23} = \frac{\vec{B}_2 + \vec{B}_3}{2} \qquad \vec{r}_{23} = \vec{r}_2 - \vec{r}_3 \tag{A.4}$$

$$\vec{B}_{13} = \frac{\vec{B}_1 + \vec{B}_3}{2} \qquad \vec{r}_{13} = \vec{r}_1 - \vec{r}_3 \tag{A.5}$$

SC1 has been set as the reference satellite (see Figure A.4).

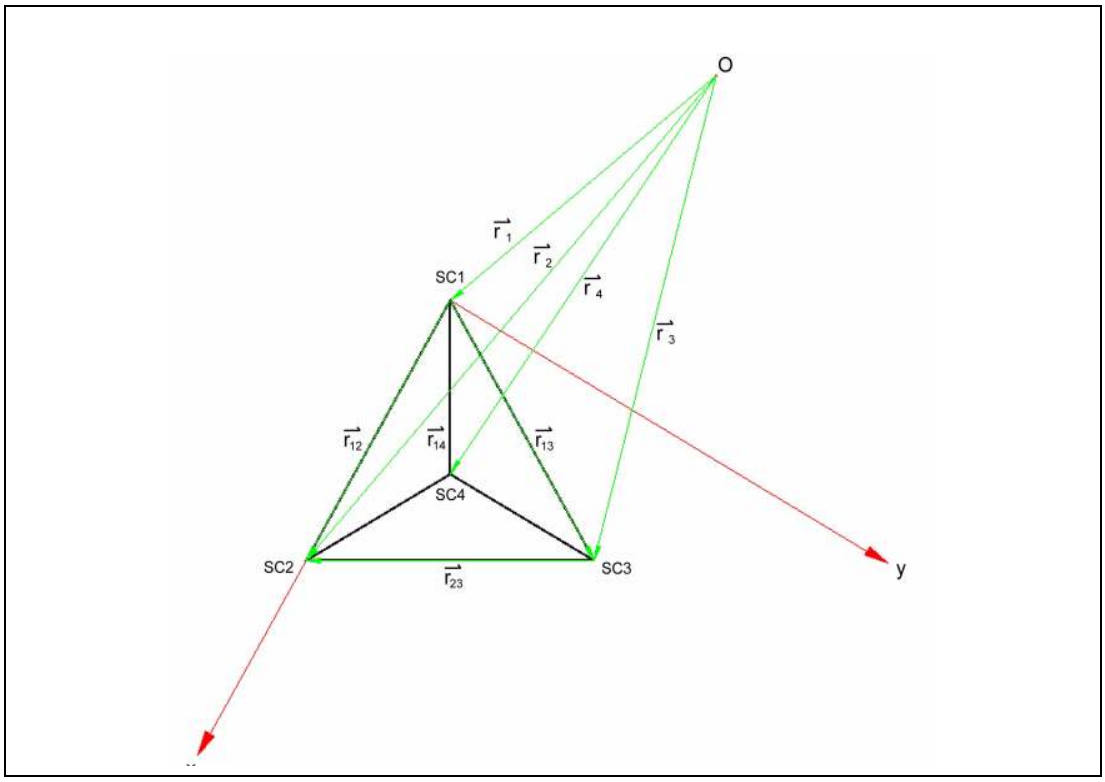

Figure A.4: *The position vectors of the four Cluster space crafts, with SC1 as the reference satellite. [Maszl, 2004]*

One can further express $\int_A \overrightarrow{da} \Rightarrow \frac{1}{2}(\vec{r}_{13} \times \vec{r}_{12})$. The next step is to project the magnetic field onto the edges of the tetrahedron defined by the satellites. This yields:

$$\frac{1}{2}\mu_0 \vec{J}_{av} \bullet (\vec{r}_{13} \times \vec{r}_{12}) = \vec{B}_{12} \bullet \vec{r}_{12} - \vec{B}_{23} \bullet \vec{r}_{23} - \vec{B}_{13} \bullet \vec{r}_{13} \tag{A.6}$$

Now, transforming Equation (A.6) further, using $\Delta\vec{B}_{13} = \vec{B}_1 - \vec{B}_3$ and $\Delta\vec{B}_{12} = \vec{B}_1 - \vec{B}_2$ with equations (A.3) through (A.5), one can finally express the current density in a fairly simple form:

$$\mu_0 \vec{J}_{av} \bullet (\vec{r}_{13} \times \vec{r}_{12}) = \Delta\vec{B}_{13} \bullet \vec{r}_{12} - \Delta\vec{B}_{12} \bullet \vec{r}_{13} \tag{A.7}$$

In many cases it might be interesting to investigate the current density vector in comparison to the magnetic field vector. So, the parallel and perpendicular components of $\vec{J}_{av}$ to $\vec{B}$ can be expressed as [Maszl, 2004]:

$$\vec{J}_{av||} = \frac{\vec{B} \bullet \vec{J}_{av}}{\left|\vec{B}\right|} \qquad (A.8)$$

$$\vec{J}_{av\perp} = \left|\vec{J}_{av}\right| \sqrt{1 - \left(\frac{\vec{B} \bullet \vec{J}_{av}}{\left|\vec{B}\right| \cdot \left|\vec{J}_{av}\right|} \right)^2} \qquad (A.9)$$

A MatLab program code calculating $\vec{J}_{av}$ was given in Maszl (2004).

A. 5. A simple method for analyzing boundary crossings

A great advantage when using four space crafts, as with the Cluster mission, is that one can investigate the position and movement of any discontinuities or boundaries that the satellites may encounter in three dimensions. If a satellite moves across a boundary, this may appear as an increase or decrease in density, or a fluctuation in the magnetic field. Regarding the Cluster instruments, one can use either the FGM, EFW or CIS to detect this. However, EFW has on a regular basis the best time resolution, but on the date investigated in this paper ASPOC is running on SC3 and SC4. Therefore, this only leaves us with two satellites with reliable EFW-data. Luckily, FGM was running in burst mode for most of the interesting time period, which means that one has access to 4 measurements per second of magnetic field vectors in three dimensions.

In Harvey (2000), a non-complicated method which yields the boundary normal vector, $\hat{n}$, and the velocity, V, assumed to be in the direction of $\hat{n}$. We have that the discontinuity is observed at time t_α by spacecraft α, which then is positioned at $\vec{r}_\alpha$. This method is applied to the Cluster satellites, so $1 \le \alpha \le 4$. We assume that during a time interval, $t_\alpha - t_3$, the discontinuity plane moves a distance along its normal, $V(t_\alpha - t_3)$, where V is the discontinuity's velocity in the rest frame of the satellites. This distance equals the satellite separation projected onto $\hat{n}$. This gives us:

$$(\vec{r}_\alpha - \vec{r}_3) \bullet \hat{n} = V(t_\alpha - t_3) \qquad (A.10)$$

Here, SC3 is used as a reference satellite. Now we can introduce the vector $\vec{m} = \frac{\hat{n}}{V}$ and rewrite Equation (A.10) as:

$$D\vec{m} = \boldsymbol{T} \qquad (A.11)$$

where D is a 3x3-matrix $D = \begin{bmatrix} r_1 - r_3 \\ r_2 - r_3 \\ r_4 - r_3 \end{bmatrix}$ and $\boldsymbol{T}$ is a linear array $\boldsymbol{T} = \begin{pmatrix} t_1 - t_3 \\ t_2 - t_3 \\ t_4 - t_3 \end{pmatrix}$. If one now finds the inverse matrix of D, which satisfies $D^{-1}D = I = \delta_{jk}$, one can also calculate:

$$\vec{m} = D^{-1}\boldsymbol{T} \qquad (A.12)$$

This method's accuracy depends on the determination of the position vectors and the time differences. It cannot be applied to applied to situations with more than four space crafts however [Harvey, 2000]. But, for the Cluster satellites it works quite well.

The velocity, $\vec{V'}$, one can acquire by multiplying V with $\hat{n}$, is given in the rest frame of the four satellites. Therefore, in the case where one seeks the plane's velocity vector in regular GSE-coordinates, one must add the velocity vector of the satellites, or of the reference satellite which in Cluster's case is SC3. This is illustrated in Figure A.5.

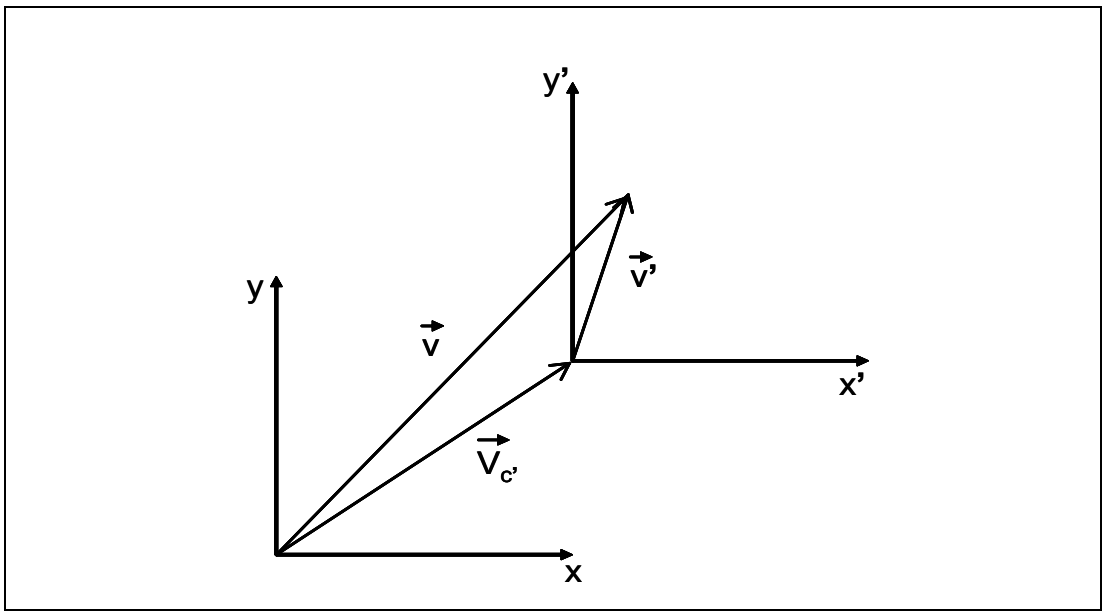

Figure A.5: *Coordinate relations*

Thus, to acquire the velocity vector in the main coordinate system, in this case GSE-coordinates, one must add the calculated velocity vector with the velocity vector of the moving coordinate system:

$$\vec{V}_{plane} = \vec{V}_C + \vec{V'} \qquad (A.13)$$

When investigating discontinuities that are more or less stationary, for example the magnetopause, other methods are usually applied. One often uses the magnetic field parameters, but more statistical treatment is necessary when defining the normal vector component of the boundary plane for example. A program code which yields the parameter $\vec{V'}$ and $\vec{n}$ written in Perl, was provided by Anette L. Borg, PhD-student at the Plasma and Space Physics research group at the University in Oslo.

Appendix B

Internet Resource Pages

ACE- and Geotail-data acquisition site:

- http://cdaweb.gsfc.nasa.gov/cdaweb/istp_public/

Cluster Quicklook Plots:

- http://www.cluster.rl.ac.uk/csdsweb/

Data archive site for SuperDARN:

- http://superdarn.jhuapl.edu/

Dst-index for February, 2004 (at the Kyoto World Data Center) [last accessed the 17. of November, 2005**]:**

- http://swdcdb.kugi.kyoto-u.ac.jp/dstdir/dst1/p/dstprov200402.html

EISCAT data listing at Madrigal Experiment Selector:

- http://www.eiscat.se/madrigal/cgi-bin/madInvent.cgi

ESA's Cluster Page:

- http://clusterlaunch.esa.int/science-e/www/area/index.cfm?fareaid=8

Geotail Project Overview:

- http://pwg.gsfc.nasa.gov/geotail_overview.shtml

IGRF query form:

- http://nssdc.gsfc.nasa.gov/space/cgm/cgm.html

Theory and background material for the ESR and incoherent scatter radars:

- http://www.eiscat.se/ESR/

- http://www.eiscat.se/hardware-UHF.html
- http://hyperion.haystack.edu/midas/inscal.html